MODEL–BASED DESIGN OF CANCER CHEMOTHERAPY TREATMENT SCHEDULES

by

John M. Harrold

B.S. Chemical Engineering, University of Arkansas, 1998

M.S. Chemical Engineering, University of Arkansas, 2000

Submitted to the Graduate Faculty of

the School of Engineering in partial fulfillment

of the requirements for the degree of

Doctor of Philosophy

University of Pittsburgh

2005

UNIVERSITY OF PITTSBURGH

SCHOOL OF ENGINEERING

This dissertation was presented

by

John M. Harrold

It was defended on

July 21st 2005

and approved by

Robert S. Parker, Assistant Professor, Chemical and Petroleum Engineering Department

Julie L. Eiseman, Research Associate Professor, Pharmacology Department

William J. Federspiel, Associate Professor, Chemical and Petroleum Engineering Department

Joseph J. McCarthy, Professor, Chemical and Petroleum Engineering Department

Dissertation Director: Robert S. Parker, Assistant Professor, Chemical and Petroleum Engineering Department

MODEL–BASED DESIGN OF CANCER CHEMOTHERAPY TREATMENT SCHEDULES

John M. Harrold, PhD

University of Pittsburgh, 2005

Cancer is the name given to a class of diseases characterized by an imbalance in cell proliferation and apoptosis, or programmed cell death. Once cancer has reached detectable sizes (10^6 cells or 1 mm^3), it is assumed to have spread throughout the body, and a systemic form of treatment is needed. Chemotherapy is commonly used, and it affects both healthy and diseased tissue. This creates a dichotomy for clinicians who need to develop treatment schedules which balance toxic side effects with treatment efficacy. The optimal treatment schedule — where schedule is defined as the amount and frequency of drug delivered — is the most efficacious schedule evaluated during clinical trials. In this work, a model–based approach for drug treatment schedule design was developed. Cancer chemotherapy modeling is typically segregated into drug pharmacokinetics (PK), describing drug absorption, distribution throughout an organism, and metabolism and pharmacodynamics (PD), which delineates cellular proliferation, and drug effects on the organism. This work considers two case studies: (i) a preclinical study of the oral administration of the antitumor agent 9-nitrocamptothecin (9NC) to severe combined immunodeficient (SCID) mice bearing subcutaneously implanted HT29 human colon xenografts; and (ii) a theoretical study of intravenous chemotherapy from the engineering literature.

Metabolism of 9NC yields the active metabolite 9-aminocamptothecin (9AC). Four different PK model structures were constructed to describe the plasma concentration versus time profiles of 9NC and 9AC: three linear models at a single dose level (0.67 mg/kg 9NC); and a nonlinear model for the dosing range 0.44 – 1.0 mg/kg 9NC. Untreated tumor growth

was modeled using two approaches: (i) exponential growth; and (ii) a switched exponential model transitioning between two different rates of exponential growth at a critical size. All of the PK/PD models considered here have bilinear kill terms which decrease tumor sizes at rates proportional to the effective drug concentration and the current tumor size. The PK/PD model combining the best linear PK model with exponential tumor growth accurately characterized tumor responses in ten experimental mice administered 0.67 mg/kg of 9NC QD×5×2 (Monday-Friday for two weeks) repeated every four weeks. The nonlinear PK model of 9NC coupled to the switched exponential PD model accurately captured the tumor response data at multiple dose levels. Each dosing problem was formulated as a mixed–integer linear programming problem (MILP), which guarantees globally optimal solutions. When minimizing the tumor volume at a specified final time, the MILP algorithm delivered as much drug as possible at the end of the treatment window (up to the cumulative toxicity constraint). While numerically optimal, it was found that an exponentially growing tumor, with bilinear kill driven by linear PK, would experience the same decrease in tumor volume at a final time regardless of when the drug was administered as long as the *same amount* was administered. An alternate objective function was selected to minimize tumor volume along a trajectory. This is more clinically relevant in that it better represents the objective of the clinician (eliminate the diseased tissue as rapidly as possible). This resulted in a treatment schedule which eliminated the tumor burden more rapidly, and this schedule can be evaluated recursively at the end of each cycle for efficacy and toxicity, as per current clinical practice.

The second case study consists of an intravenously administered drug with first order elimination treating a tumor under Gompertzian growth. This system was also formulated as a MILP, and the different objectives were considered. The first objective was minimizing the tumor volume at a final time — the objective the original authors considered. The MILP solution was qualitatively similar to the solutions originally found using control vector parameterization techniques; as much drug as possible was administered at the end of the treatment interval. The problem was then reposed as a receding horizon trajectory tracking problem. Once again, a more clinically relevant objective returned promising results; the

tumor burden was rapidly decreased. This technique could be generalized to arbitrary drug/tumor concentrations provided a PK/PD model exists or could be derived.

TABLE OF CONTENTS

LIST OF TABLES

LIST OF FIGURES

PREFACE

Several years have past and much has been accomplished. While my name is on the front of this document, the work presented here represents the beginning of what I would consider to be a very successful collaborative effort. Many people have helped me along the way, and I would like to take this space to acknowledge them. While the work presented here is theoretical, it is driven by experimental data. The animal data used here was produced by Julie Eiseman and Erin Joseph, and the samples were analyzed in the laboratory of Merrill Egorin — these data were essential for a bulk of the work presented here. I also benefited heavily from the weekly interactions at pharmacokinetics (PK) lunch which brought together people from several disciplines focusing on the analysis of PK data. I began my stay here new to the concept of pharmacokinetic and pharmacodynamic (PD) modeling. My interactions at PK lunch, specifically with Robert Bies, and my experiences at the Biomedical Simulations Resource workshops, organized by David D'Argenio, provided a firm basis and support in my efforts to better understand the different aspects of PK/PD modeling. Julie, Erin, Merrill, and the others at PK lunch were also very helpful in providing critical analysis of my written and presented work. I would also like to acknowledge the support of my adviser, Robert Parker. He has been an excellent mentor and friend throughout my stay here at Pittsburgh.

Of course, all work and no play makes Jack a dull boy. I have been fortunate to share an office with a diverse and interesting group of people. For those few moments away from school every month, we managed to maintain each others sanity.

have algorithm will travel...

1.0 INTRODUCTION

1.1 BACKGROUND

In the United States, cancer is currently the leading cause of death for persons under 85 and accounts for ten percent of the monetary resources devoted to disease treatment [1]. There are over 1.3 million new cases and 570,000 deaths predicted in 2005, and the economic cost to the United States was approximately $189 billion in 2004 [1]. This result is a societal dilemma in terms of human mortality and financial burden.

Cancer refers to a class of diseases characterized by an imbalance in apoptosis, or programmed cell death, and the rate of cellular proliferation [2]. As the tumor mass increases, cancer cells will induce secretion of metallo–proteases which will degrade the extracellular matrix and encourage the creation of new vascular growth through angiogenesis [3]. While competing with the host organism and surrounding tissues for resources, cancer cells may invade local tissue or move about the host via the circulatory system. A tumor is said to have metastasized when cells have successfully relocated to new tissues within the host [3, 4]. The invasive nature of cancer will eventually lead to organ failure and the death of the host organism if left untreated.

Cancerous masses which can be reached through surgery are removed. There are several forms of cancer in which surgery is not an option because of the location of the cancer (*e.g.*, some brain tumors) or because the disease is not localized (*e.g.*, hematological malignancies like leukemia). Radiation therapy, which can target specific tissues, is an option for inoperable forms of cancer. However, once cancer has reached detectable levels it is probable that metastases exist. For this reason a more systemic method of treatment may provide more efficacious results.

Cancer cells proliferate more rapidly than cells from healthy tissues and spend more time actively cycling in the cell–cycle (growth, DNA synthesis, mitosis, etc.) [2]. Chemotherapy is a commonly employed systemic form of treatment which attempts to take advantage of the rapidly proliferating nature of cancer cells. While selectivity of treatment toward diseased over healthy tissues is desired, this objective is not always achieved. Healthy tissues, such as white blood cells and the cells of the intestinal mucosa, also proliferate rapidly and are affected by chemotherapeutic treatment. This creates a dichotomy for clinicians who must balance the need to eliminate the disease with the toxic side effects of treatment. The treatment schedule, defined as dose amount and frequency, used clinically is derived from an empirical process which begins with preclinical evidence found during the drug development process. Later refinement of the treatment schedule takes place throughout clinical testing and patient treatment.

1.2 DRUG DEVELOPMENT PROCESS

The development of chemotherapeutic drug schedules is an empirical process. Information from preclinical research as well as clinical trials in humans is used to determine drug dosing schedules. Possible anticancer compounds are first tested *in vitro* in cell culture. Promising results lead to *in vivo* preclinical trials, which are performed in species expected to respond similarly to humans. Preclinical trials are used to establish optimal dosing route (*e.g.*, intravenous, oral, etc.), and metrics for evaluating toxicity. This is followed by animal studies that establish the efficacy of the drug against different forms of cancer. Efficacious drugs with manageable toxic effects in animal models are then tested in clinical trials.

Phase I clinical trials are used to establish toxicity constraints for humans. A common approach is to consider the species most sensitive to the drug in preclinical testing. Administration of the drug to humans begins at one tenth the lethal dose in 10% of the most sensitive species $\left(\frac{1}{10}\mathrm{LD}_{10}\right)$. Dose levels are then escalated until the dose–limiting toxicity (DLT) is reached. One level below the DLT dose is set as the maximum tolerated dose (MTD). A common method is to increase the dose levels according to a modified Fibonacci series [5].

Phase II studies are then performed to establish efficacy of the anticancer compound against specific types of cancer — most often those cancers identified as being susceptible in preclinical trials. One third of the dose causing DLT is used as a basis for initial dose levels, and empirical evidence is used to guide the efficacy evaluation. Since it is not possible to evaluate every conceivable administration schedule, previous knowledge of similar compounds, known toxicities, and logistical issues are used to establish when the drug should be administered. The objective is to find the drug schedule which will yield the maximum response, typically measured in terms of exposure, without violating the above constraints [6]. Statistically significant responses, such as increased survival times, are used as indications that the compound is clinically effective.

Based on the toxicity limits from Phase I trials and demonstrable efficacy from Phase II trials, a successful compound will then enter Phase III trials. The purpose of Phase III trials is to evaluate a drug and corresponding schedule against the current standard of practice for treating specific forms of cancer. This can involve a single new agent or, more often, the new agent in combination with an approved form of chemotherapy. A successful drug/schedule combination will be statistically more efficacious (based on disease response, toxicity reduction, etc.) than the current gold standard.

Ultimately, the schedule on which anticancer drugs are administered is the schedule from Phase II and Phase III trials which yields the most statistically significant results. These schedules, derived from empirical evidence and heuristics, are considered optimal because they were more efficacious than the others considered. However, it may be possible to employ the data generated during the drug development process to more rigorously define an optimal drug schedule.

1.3 MODEL–BASED CONTROL

Model–based control is currently considered the state–of–the–art in the field of process control [7, 8, 9]. This form of control makes explicit use of system model predictions in order to determine how manipulated variables should be changed to achieve a desired objective.

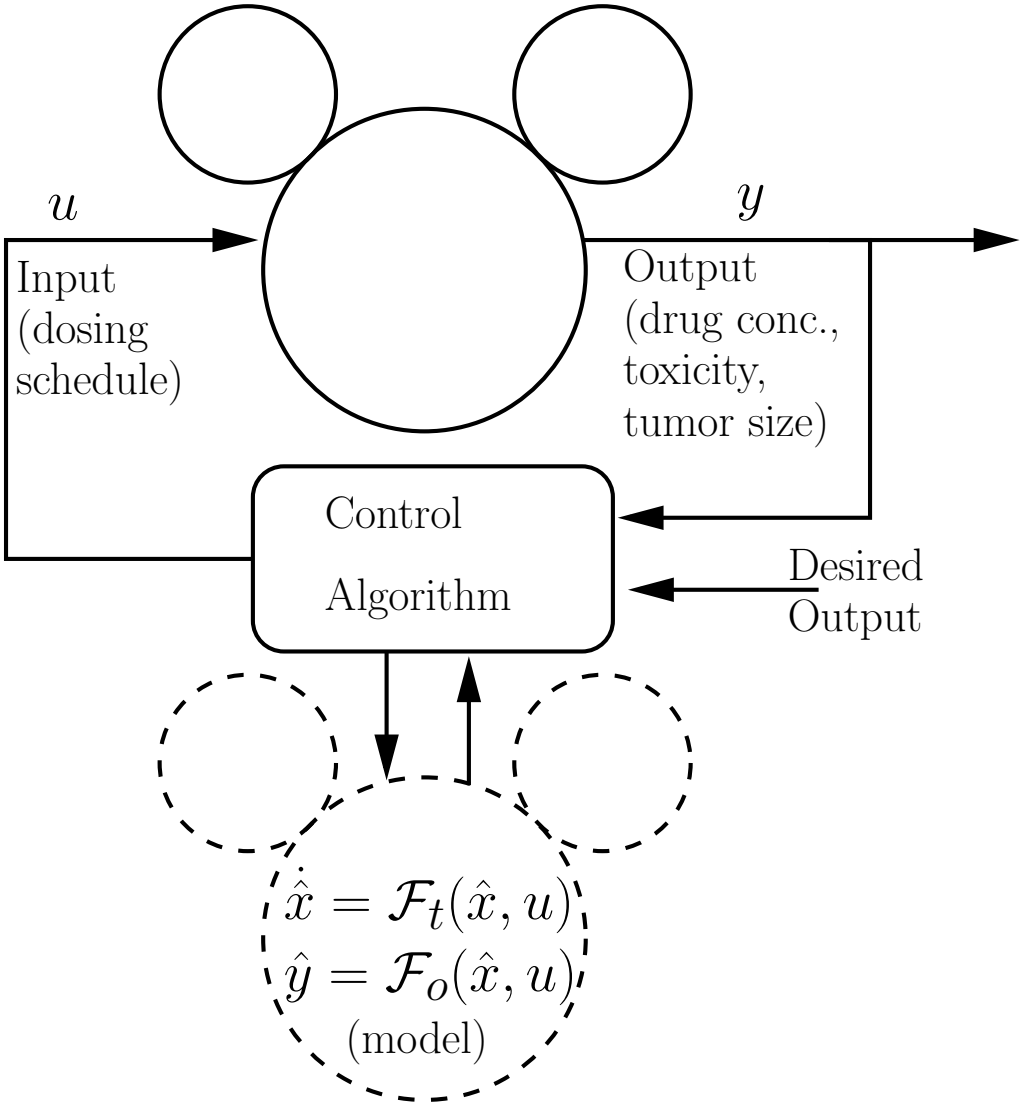

Figure 1: Model–based control algorithm which determines input changes, u, based on estimates of internal states, $\hat{x}$ described by $\mathcal{F}_t(\hat{x}, u)$, output estimates, $\hat{y}$, given $\mathcal{F}_o(\hat{x}, u)$, and actual output measurements y.

This methodology is illustrated in Figure 1 for the treatment of experimental or simulated mice. Data collected during an experiment, either real or simulated, provide the current state of the mouse system. These measurements can include the current drug concentration, information about toxicity (*e.g.*, reductions in white blood cell count or body weight), the current size of the tumor, etc. The desired response may include reductions in tumor volume or a target body weight. The system state and desired response are provided to the controller which utilizes a model of the system to determine the manipulated variable changes required to obtain the desired response. When considering cancer treatment, manipulated variables can include dose levels and the times at which the treatment should be applied. This process operates in a closed–loop fashion, where feedback is used for altering drug administration. Classical feedback control relies on frequent measurements to control the process in real time. However, chemotherapy is given in cycles with periodic updates (every two weeks to two months) with treatment alterations based on evaluations of toxicity and patient response. The current *standard of practice* or *gold standard* of treatment is based on empirical evidence gathered from preclinical and clinical trials carried out during the drug development process.

1.4 OVERVIEW OF MODELING APPROACHES

In the context of model–based control, useful models must be both descriptive and predictive. However, a balance must generally be made between model complexity and predictive accuracy. Simple models (linear relationships, cubic splines, etc.) can be developed which characterize the current dataset but have limited predictive capacity. Depending on the measurements available, detailed models can be constructed that offer excellent predictive capacity [10]. For many processes, physiologically based model structures contain many differential equations often with complex nonlinearities. Such models can prove to be prohibitively complex from a computational perspective when the desired result is the development of an optimal control algorithm. The goal of the present work was to develop models of drug pharmacokinetics (PK) and pharmacodynamics (PD) which are predictive and at the same time suitable for controller synthesis.

1.4.1 Tumor Growth Models

Modeling for cancer systems requires two components. The first is an understanding of the system in the absence of treatment and the second is a description of the effects of treatment. A nominal understanding of how cancer progresses is necessary for model construction in the case of the untreated system. Initially, cancer cells typically proliferate in an exponential fashion. The size of the cancerous mass is measured experimentally as a volume, though this mass is often referred to in terms of the number of cells (10^6cells $\approx$ 1mm^3) [11]. As the cancerous mass increases in size, stochastic recruitment of blood vessels leads to scarcity in nutrients [3]. In response to decreased availability of nutrients, the rate of proliferation slows, and the population of cancer cells asymptotically approach a plateau population [4]. Cancerous masses reaching this stage of growth are typically considered to be under Gompertzian growth [11]. Other models have been developed in order to incorporate reductions in proliferation rates as tumor sizes increase. These include the saturating Logistic model [12] and the Verhulst–Perl equation [13]. Simeoni *et al.* demonstrated a model which grows exponentially when tumor volumes are low and linearly as tumor volumes increase [14].

Cell–cycle models have also been proposed [15, 16] to characterize the proliferative nature of cancer. A schematic is shown in Figure 2. These models explicitly represent the transition of cells between the different phases of the cell–cycle [2]. Many anticancer drugs are cycle–specific, which means their primary effect occurs during a specific phase of the cell–cycle. While understanding cellular proliferation at this level is ideal, acquiring data characterizing the fraction of cells in the different phases is nontrivial. In order to determine the fraction of cells at different phases of the cell–cycle, samples must be obtained and stained for DNA and RNA content at different points in time [17]. Based on the amount of DNA or RNA in different cells, the fraction of cells in a specific phase can be determined [17]. However, using only macroscopic volumes to identify parameters in a cell–cycle model can lead to identifiability problems. For example, consider the transition rates k_S and k_{G1}. Estimating these parameters from tumor volume measurements could lead to two different sets of parameters such that $k_S > k_{G1}$ or $k_S < k_{G1}$ that predict the same macroscopic behavior

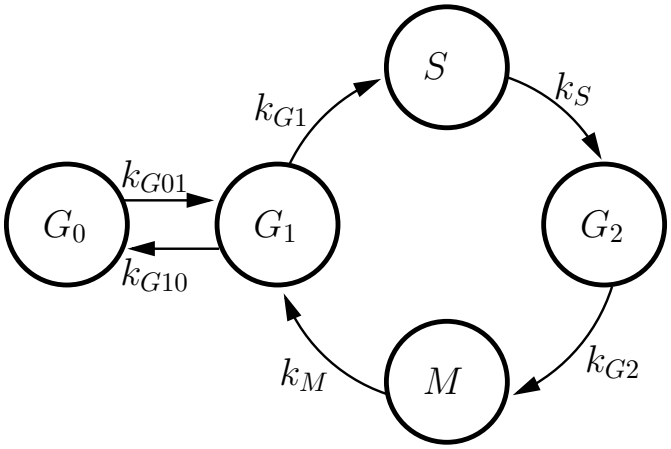

Figure 2: Typical five phase representation of the cell–cycle [2]. Cell–cycle phases are: growth (G_1), DNA synthesis (S), secondary growth (G_2), mitosis (M), and quiescent (G_0). Transition rates between phases are given by k_i.

[18]. However the former would predict fewer cells in S than the latter. This can lead to problems when considering a drug which is S–phase specific. Because the macroscopic preclinical experimental data used in this work does not adequately inform a cell–cycle description of tumor growth, macroscopic growth models were used exclusively.

1.4.2 Pharmacokinetic Modeling

PK models describe the effects organisms have on the drug. These effects typically include the absorption, distribution, metabolism, and elimination of the compound [19, 20]. The study of drug PK was first introduced by Teorell where he suggested that the major tissues in the body could be modeled such that chemical substances were distributed throughout the body based on the physiological construction of the organism [19, 20]. Models of this nature are now commonly called physiologically–based pharmacokinetic (PB/PK) models [21]. This is illustrated in the left half of Figure 3. The individual organs are treated as well–mixed compartments where a drug is distributed homogeneously throughout the organ. Organs with nonuniform drug distribution can be better described by partitioning the tissue into subcompartments. Construction of these types of models can prove problematic as the data requirements are extensive and tissue–specific data may be very difficult or impossible to obtain clinically. For example, to obtain the average drug concentration in the kidneys of an experimental animal, the animal is euthanized, the kidneys are removed and homogenized, and the concentration is determined using analytical techniques (*e.g.*, HPLC). Performing this type of analysis is expensive and time consuming and it is simply not possible to analyze human patients in this fashion. To reduce model complexity and better represent available data, Teorell suggested using a more simplified model structure [19, 20]. This resulted in the traditional compartmental model, an example of which is shown on the right side of Figure 3. This simplified representation is used because plasma concentrations can be obtained more easily than organ tissue concentrations. A remote compartment here is shown to account for any higher–ordered dynamics that are observed experimentally.

The model structure of compartmental models — number of compartments, connectivity, and the rate of transition between compartments — will depend primarily on the dynamics of

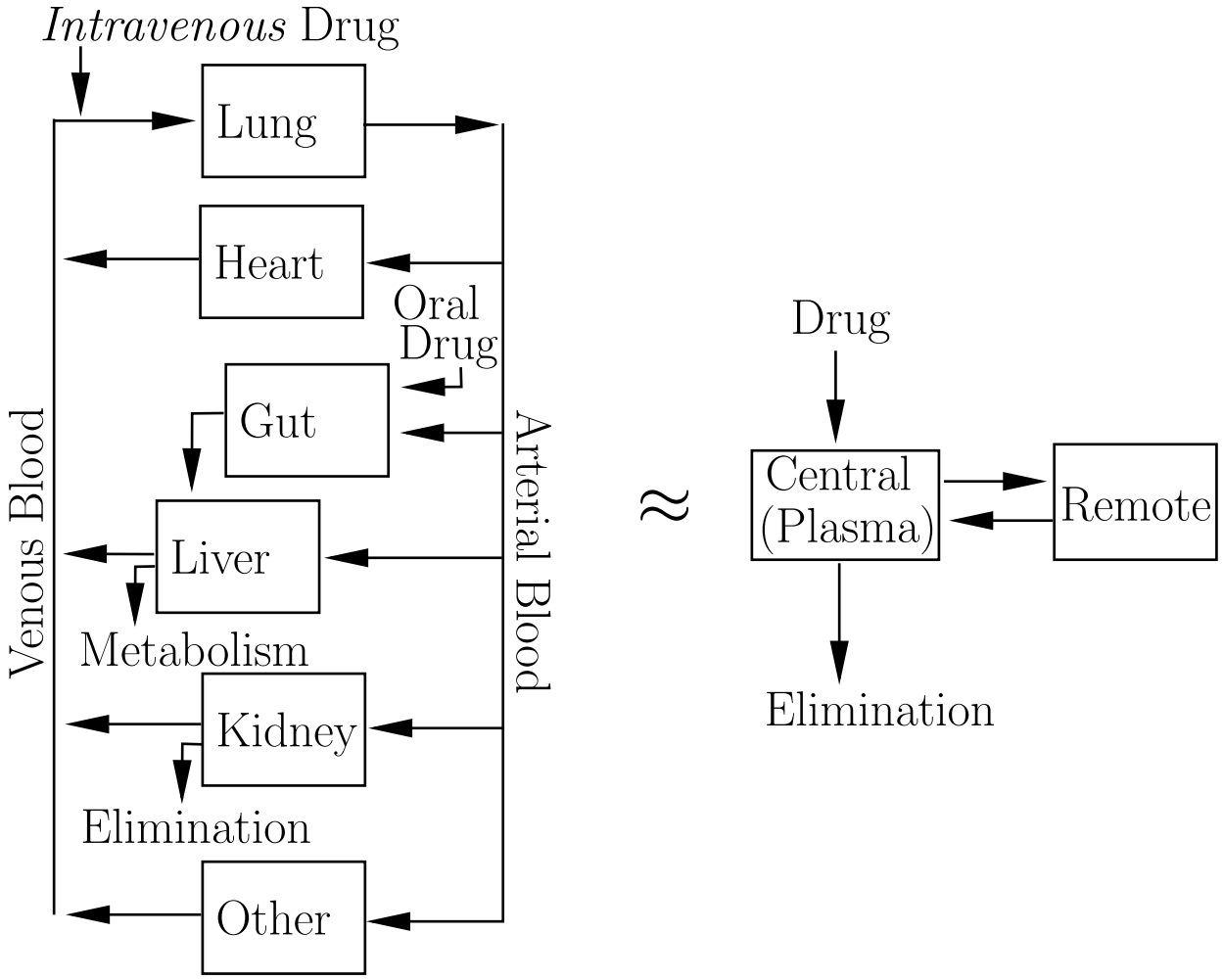

Figure 3: PB/PK representation of drug distribution for an orally or intravenously administered drug (left), and compartmental approximation (right).

the data being fit. It is common to assign physiological significance to parameters in compartmental models. For example, a pharmacokineticist might model an orally administered drug by adding a compartment between the "Drug" input and "Plasma" compartment on the right side of Figure 3. The rate of drug leaving this new compartment and entering the "Plasma" compartment might be taken as the rate of absorption from the gut into the plasma. This may or may not be the case and cannot be established without a measurement of drug concentration in the gut. Hence, physiological interpretations of simplified compartmental model parameters are more often a psychological construct than a rigorous understanding of the underlying physiology. Regardless, the class of compartmental models is widely accepted and employed in drug development [22, 23, 24].

The necessary complexity of compartmental models is largely dictated by the PK response found in experimental data. Linear PK models, models in which each of the rates of transition between compartments is linear in the system state, can be used to describe many systems. The volume of work done in this area is too numerous to enumerate here, using the query *'cancer PK PD'* in pubmed returns 19,162 results, but a number of software packages provide modeling and simulation capability for a variety of model structures (*e.g.* ADAPT II [25], NONMEM [23], etc.). From a control perspective, linear PK models are typically preferred because they are more easily implemented in controller synthesis [26, 27]. However, many biological systems exhibit nonlinear behavior [21]. Modified compartmental model structures have been developed to account for many types of nonlinearities, such as saturable pathways. Cyclophosphamide, for example, exhibits saturable elimination, and Michaelis–Menten kinetics have been employed to describe these effects [28]. This and other nonlinear effects are commonly accounted for by incorporating nonlinear functionality into transition rates between compartments. These structure selections can be simple if the data exhibit easily identifiable characteristics (*e.g.*, first–order response). Otherwise, there exist few methods for rigorous determination of PK model structure. One empirical method is the use of genetic algorithms to determine the optimal model structure based on a set of possible structures [29]. Stepwise forward model construction begins with a simple model structure. Elements are randomly added to the model and tested to determine if they improve accuracy. Model contributions that improve accuracy are retained. Addition of terms is halted when

a stopping criterion specific by the user is met (*e.g.* upper bound on model complexity, fit accuracy, etc). Stepwise term elimination often follows the model construction step. The element whose removal has the least effect on the quality of fit is removed completely if changes in the quality of fit are below a specified threshold. This process is repeated iteratively until no further improvement in the quality of fit can be obtained.

Compartmental models are common because they are intuitive to construct and many tools have been developed to aid in estimation of their parameters [21, 23, 25]. They are also popular because they answer many of the questions which concern clinicians. These include determining the exposure of a drug, quantified as the area under the plasma concentration versus time curve. The rate of drug clearance is another characteristic important to clinicians because it provides an indirect measure of drug exposure. Clearance and exposure are parameters which can be used to characterize individuals, which is important given the disparate nature of the patent population. In this regard, individual behavior can be identified (patient–specific parameters) while also explicitly accounting for the interindividual variability (population parameter distribution). This is accomplished by performing a population analysis provided measurements are available from a statistically significant number of individuals. A population analysis provides an average PK response as well as an estimate for the variability found in the population. Classically, statistical parameter information has been determined in one of two ways. The first method obtains parameter estimates for all of the data simultaneously. This is referred to as the naïve pooled data approach [23]. The other option evaluates individual parameter estimates for each data set. Individual estimates are then used to calculate average parameter estimates. This is referred to as the two–stage approach [23]. The naïve pooled data approach is known to give poor estimates, and the two-stage approach is considered to introduce bias [23]. A relatively new development combines the two aforementioned methods to eliminate some of the shortcomings related to bias and estimation. This is referred to as mixed effects modeling [30, 31] and is most commonly associated with the Nonlinear Mixed–Effects Modeling (NONMEM) software package [23].

1.4.3 Pharmacodynamic Modeling

1.4.3.1 General PD Modeling While PK models describe the action of the body on the drug, PD models describe the effect of the drug on the body. In the field of oncology, these effects can be positive (elimination of disease) or negative (elimination of the white blood cells or other toxicity). Since the effects of drugs on organisms are being studied, one approach uses PK models to *drive* a PD model [12, 32]. This means that predictions of drug concentrations from PK models are used within the PD model. The precise use of PK predictions will depend on how well the mechanism of drug action has been characterized and the relationship between that mechanism and the PK predictions available.

Due to the complexity of biological systems, detailed mechanistic models can become prohibitively complex for the same reasons found when dealing with PK models [19, 20]. For this reason, a more simplified approach assumes a causal relationship between the concentration of a drug in the plasma, or another compartment, and the PD effect [12]. When correlating drug PK with PD, the presence of the drug as predicted by the PK model occurs over a specified interval of time, and the duration of the effect can be similar. Alternatively, the PD effect may occur for a fraction of the time the drug is present or can persist for a duration much longer than that which the PK alone would predict. PD effects can also be characterized as responding somewhat immediately to drug PK or an appreciable time after the drug is assumed to have been eliminated. These two aspects of correlative drug effects are shown in Figure 4.

Drugs effects occurring on the same timescale as drug PK with an immediate response to modeled drug concentrations are the easiest to characterize. For example, intravenous injection of insulin has a rapid effect on the level of glucose in the blood [33]. The simplest model effect is one which is directly proportional to the concentration of the drug/plasma concentration and can be addressed by most simulation packages capable of performing numerical integration.

Another PD effect is one which begins at drug administration but persists for an appreciable time after the drug has been eliminated. For example, this can occur when a small amount of drug binds tightly to and saturates a receptor. Some drug can still be bound

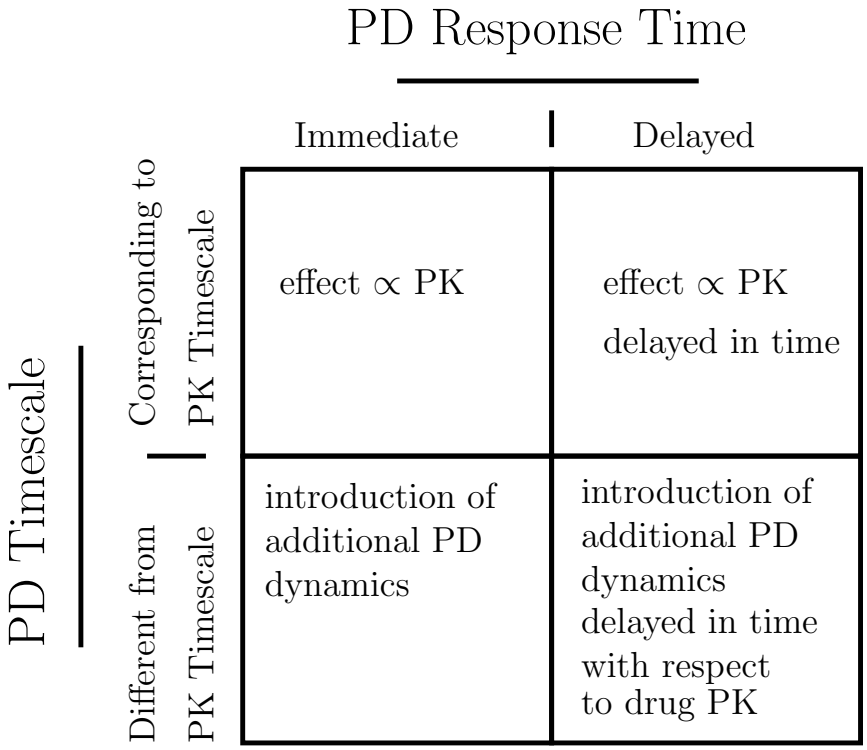

Figure 4: Pharmacodynamic effect matrix characterizing different aspects of PK driven PD response (where $\propto$ indicates proportionality to).

to the receptor even though the remaining unbound drug circulating through the body has been eliminated. This can be accounted for by adding additional dynamics between the PK prediction of plasma concentration and the PD effect. This leads to a prolonged exposure at the site of action with respect to the concentration in the plasma. This adds to model complexity, but does not affect the simulation techniques.

On the other end of the spectrum, the time between administration and effect can be quite disparate. Consider the effects of smoking, where an individual can be exposed to chemicals (tar, nicotine, etc.) for many years before exhibiting the more extreme negative side effects such as cancer and emphysema. While the effects are not strictly quantifiable, few people would dispute the correlation between smoking and the negative effects on the health of individuals [34]. These effects could occur for the duration of exposure shifted in time or at a different rate all together. This is an extreme example of what the pharmacological community refers to as indirect response models [35], and one method for capturing these effects is to place several compartments in series between the PK and PD models. An alternative method to model such lagged effects is to account for them directly as time delays [26].

1.4.3.2 Chemotherapeutic Effects Modeling the PD effects of chemotherapy represents a deviation from the normal growth pattern of cancer. At the most detailed level, the interaction between the drug and the diseased tissue can be accounted for by understanding the transport properties of the drug and it's mechanism of action (*i.e.*, inhibition of signal pathways [36], anti–angiogenic effects [37], etc.). Cancer cells, like other cells, are robust complex systems which are capable of compensating for many molecular changes introduced by chemotherapy. Consequently, modeling a system at the intracellular level requires large amounts of data and a clear understanding of the pathways, interactions and molecular targets that are being affected.

Detailed physiologically–based models of chemotherapy lie on one end of a continuum. On the other end is a correlative approach which utilizes statistical inference to associate causal relationships between drug administration and effect. This may seem like a simplistic approach, but it may be the only credible means of evaluating data when lacking a more

detailed understanding of chemotherapeutic effects is unavailable. This approach focuses on using the available data to develop mathematical descriptions of chemotherapy.

In the engineering literature, mathematical descriptions typically begin with a PK model. To account for drug effects, plasma drug concentration predictions are usually used as approximations for drug concentrations at the site of the tumor. This is based on the rationale that tumors are well–perfused and have permeable capillaries [3]. The PD response is then represented mathematically by incorporating a bilinear term proportional to both the current size of the tumor and the concentration of the drug [12, 15, 38].

1.4.4 Camptothecin Analogs

In this work we consider the anticancer effects of 9-nitrocamptothecin (9NC). 9NC is a member of the camptothecin family, a class of drugs derived from the camptotheca tree [39]. 9NC exists in both the active lactone and inactive carboxylate forms shown in Figure 5 [39, 40]. After passing through the liver, 9NC readily converts to 9-aminocamptothecin (9AC) which also exists in the same active and inactive forms in plasma. The camptothecin family is characterized by the five ring structure shown in Figure 5. Camptothecins have been investigated because of their ability to inhibit topoisomerase-I [41], thereby blocking DNA synthesis and inhibiting tumor growth in the S phase of the cell–cycle.

Purified camptothecin is not water soluble, so it was initially given in a salt form. This resulted in most of the drug being converted into the inactive carboxylate form and little exposure of the active lactone form to the diseased tissues. As a result, different analogs and delivery methods were sought to maintain stability of the lactone ring as long as possible in plasma. Common analogs include topotecan, and irinotecan. A search of pubmed for *'camptothecin PK PD'* returns 697 results. Several are discussed below to highlight the types of information obtained from PK/PD analysis of camptothecins.

Topotecan was one of the first approved camptothecin analogs. This water–soluble derivative has a lactone ring with a 2.9 hour half life in plasma after intravenous infusion [39]. Topotecan plasma concentration versus time data was modeled using a two–compartment structure [39, 42]. More recently, Gallo *et al.* developed a PK model to describe the

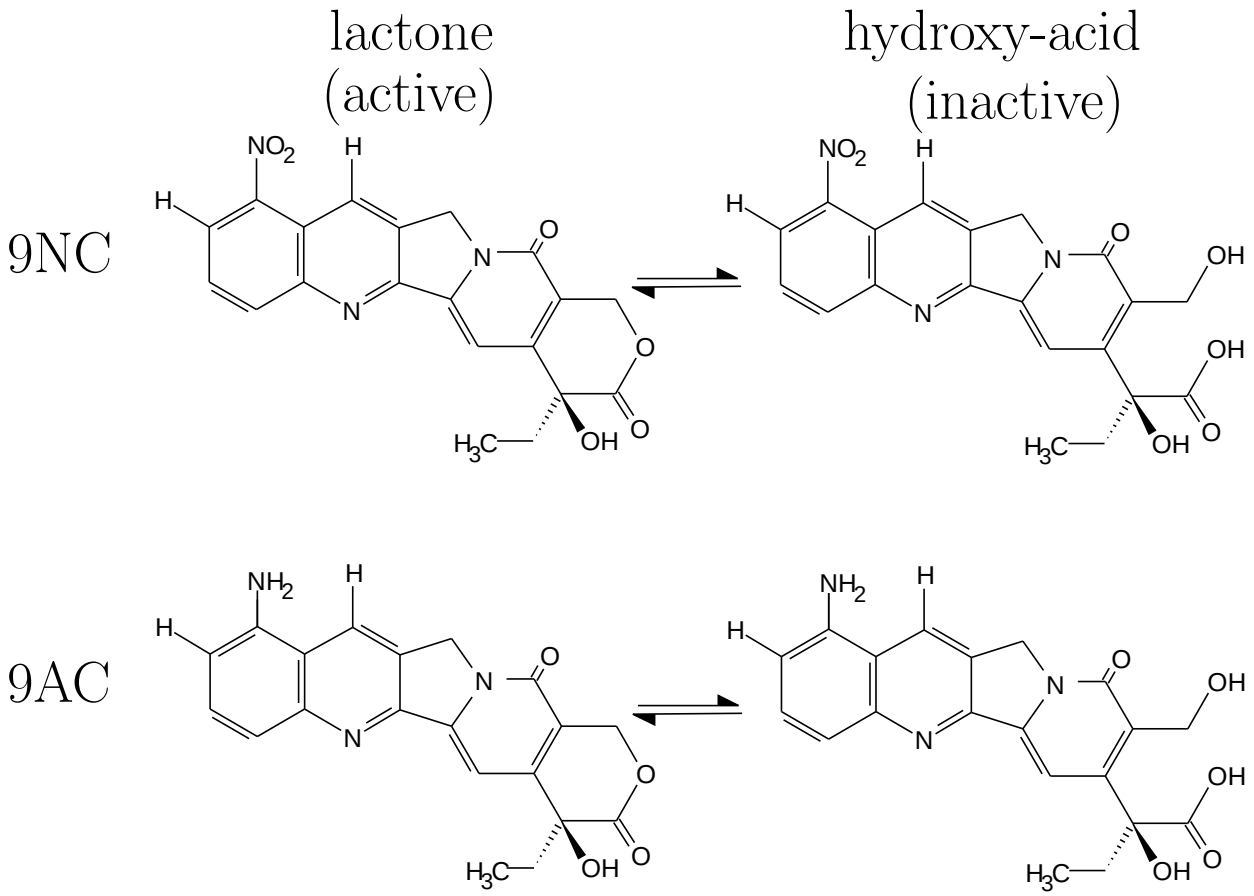

Figure 5: Chemical structures for the lactone and carboxylate forms of 9NC and 9AC.

disposition of topotecan in plasma and tumor [43]. They developed a *hybrid* model which used a compartmental model of plasma PK to drive a compartmental model of the tumor PK. The plasma portion of the model was a standard two compartment model [25] — drug input into a central compartment which has exchange with a peripheral compartment. The plasma PK predictions were then used as inputs into the tumor PK model which was three subcompartments in series: a vascular compartment, connected to an interestitial compartment, in contact with an intracellular compartment [43]. This model to characterized drug disposition in tumors and aided Gallo *et al.* in drug regimen design.

Simeoni and coworkers recently presented a series of PK driven PD models [14]. The drugs under consideration included irinotecan, paclitaxel, and 5-florouracil. Compartmental PK models were developed for each compound (two compartment model with a central plasma and remote peripheral compartment was used for irinotecan) and used to drive the PD model. Both A2780 human ovarian carcinoma and HCT116 colon carcinoma xenografts were studied in female, athymic nude mice. The PD model consisted of a growth term which slowed as the tumor volume increased; a bilinear kill term was added that decreased the rate of proliferation in response to the presence of the drug as predicted by the PK model. The cells exiting the proliferating phase in response to the drug entered subsequent *damaged* cell compartments (three in series) eventually leading to the death of the cells. The authors accurately predicted both untreated and treated tumor growth in animals. They further presented this as a tool which could be used in preclinical and clinical trials.

The study of drug disposition (PK) and effects (PD) are common in the field of oncology (over 19,000 results when searching for *'cancer PK PD'* in pubmed) . These studies are not generic; most focus on specific drug/tumor combinations. These combinations are dealt with individually because the PK and PD can vary significantly depending on the chemotherapeutic agent(s), tumor line, and host organism. Examples presented here dealt specifically with camptothecin analogs. As suggested by Simeoni [14] and Gallo [43], PK and PD models can be exploited to inform clinical decisions and to aid in the development of dose schedules.

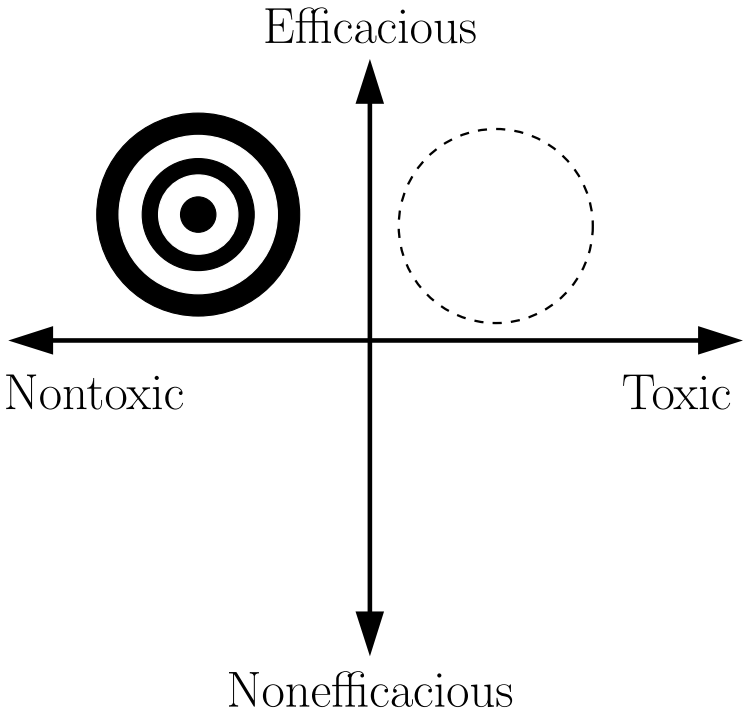

Figure 6: Drug continuum for treatment efficacy and toxicity indicating the location of most current anticancer agents (dashed region).

1.5 CONTROL: DOSE SCHEDULING

Anticancer drugs can be conceptually thought to lie on the two continua shown in Figure 6. One continuum characterizes the efficacy of the drug while the other describes toxicity. Ideally, drugs would be found which reside in the upper left quadrant of Figure 6 (target). However, existing drugs are more often located in the quadrant containing the dashed circle. Consequently, the objective of a clinician in prescribing chemotherapy is to determine the amount and frequency of drug administration that balance the competing drug effects of efficacy and toxicity. The methods currently used to determine such schedules are well established in the clinic, and they are also highly empirical. While these methods currently yield positive results, it is appropriate to inquire if a more rigorous method could be applied, not as a substitute for, but in tandem with, the current process.

1.5.1 Literature Approaches

The dose scheduling problem has been considered by several authors in the literature [12, 13, 16, 18, 38, 38, 44, 45, 46, 47, 48]. Like many problems in process control, this was formulated as a constrained optimization. An objective function is constructed such that the changes in the input which yield the minimum possible objective function value are considered the optimum set of inputs. The objective is to minimize the number of cancerous cells, or the volume of a tumor, at a final time. This is accomplished while satisfying the dynamic constraints defined by the PK and PD of the drug [38, 45]. Also, inequality and equality constraints could be included to limit toxicity and account for logistical concerns.

One of the first mathematical approaches applied to optimizing cancer chemotherapy was described by Swan [13]. A logistic growth model was used to describe macroscopic tumor proliferation, and chemotherapeutic effects were considered to be bilinear (proportional to drug concentration and tumor size) and saturable with respect to drug concentration. The objective was to achieve homeostasis by continuously delivering an intravenous drug. While this type of treatment is possible, it can lead to toxicity and become prohibitively expensive. Hence, most drugs are developed to be delivered intravenously over short periods of time (*e.g.*,

one hour infusions) or more ideally to be administered orally. The methodology developed in this document can readily deal with these constraints.

A chemotherapy dosing problem was posed in 1990 by Pereira *et al.* [16] where a cell–cycle model was used to describe the proliferation of cancer in the presence of multi–drug chemotherapy. The PK of the drugs were described generically as linear ODEs. An algorithm utilizing a gradient based approach to solve the nonlinear programming problem for generic drug/tumor combinations. This method of solution provides no guarantee of optimality and ignores the fact that most drug/tumor combinations require specific consideration.

Panetta considered a similar theoretical problem using a simplified cell–cycle model [15], represented by two populations of cells, resting and proliferating. The chemotherapeutic effect occurred in the proliferation phase. The effects of pulsed chemotherapy were analyzed to categorize the regimens between those that would and would not eliminate tumor masses. Panetta identified the optimal treatment period and dose in the absence of constraints addressing toxicity. By ignoring toxicity, Panetta ignores one of the primary concerns of clinicians [49, 50] and thus a critical aspect of the dosing problem.

In 1990, Martin *et al.* studied an intravenously administered drug with first–order elimination acting on a tumor undergoing Gompertzian growth [51]. In contrast to the work by Swan, the drug here was considered to be administered weekly — a more relevant treatment methodology based on current clinical practice. The objective was to determine the amount of drug to administer on a weekly basis over a treatment horizon of one year to minimize the final tumor volume without violating toxicity constraints. This is a topic that Martin detailed in 1992 [45] and eventually expanded into a book with Teo [12]. The dosing problem was formulated as a utilized optimal control and used control vector parameterization to determine the solutions. The "parameters" here refer to the magnitude of the doses given weekly. The solutions developed by Martin were mathematically optimal, however clinically irrelevant, as the algorithm suggested withholding treatment until the last half of the treatment window for highly effective drugs. At this point, as much drug as possible would be given such that toxicity constraints were not violated. Manipulation of the manipulated variable at the end of the prediction horizon is a common characteristic found in optimal control problems when optimizing states at the end of the horizon [52]. This

type of solution completely ignores clinical practice where toxicity and efficacy are what drive treatment. In the absence of further compelling evidence, it would be unethical for a clinician to withhold treatment for six months based on the suggestion of an engineering algorithm. One of the primary focuses of this dissertation is to develop methodologies which can address clinical concerns.

Costa *et al.* considered a deviation of the final time problem previously mentioned [53]. PD models were altered to contain a population of both drug susceptible and a uniform population of drug resistant cells. Drug effect was described by a bilinear kill term, and the objective was a variant of the final time objective considered by Martin and Teo [12]. This work utilized optimal control as a solution methodology and found optimal dosing profiles when considering cells in the rapidly proliferating phase of growth. However, the dosing profiles found by Costa *et al.* for cells at slower rates of proliferation were suboptimal.

Similar to the work by Costa *et al.* [53], Swierniak *et al.* also considered a PD model in which cancer cells were segregated into both drug susceptible and drug resistant cells [46]. The drug resistant cells contained a range of drug resistances. A gradient–based approach was utilized to find solutions dosing solutions The final time selected was short and solved for successively to develop a periodic treatment. Toxicity was not explicitly considered. A maximum value was placed on each dose and the total amount of drug administered was included as a term in the objective function. While the solutions found were mathematically suboptimal, their periodic nature is more realistic in a clinical sense.

Afenya considered a minimum time problem [47]; using an optimal control formulation. This methodology places the control variable at one extreme (maximum possible dose) and the objective is to determine the optimum time to switch to the other extreme (no drug administered) such that the objective is achieved in the minimum possible time. The PD model selected consisted of two cell populations: abnormal, or cancerous, tissues comprised one population while healthy cells were modeled with the second. While the minimum time analysis may apply to other engineering processes, it is an inherently poor choice for the development of cancer chemotherapy schedules. It results in applying the maximum possible dose of drug for an extended duration. In a clinical setting, this would likely lead to fatal

drug–induced toxicity. Constraints to prevent this type of toxicity are easily implemented using the framework discussed in this dissertation.

Ledzewicz and Schättler also approached cancer treatment as a final time problem [38, 44]. A cell–cycle model of cancer proliferation was used in conjunction with cycle specific drugs. The PK of the drug was ignored; it was assumed that drug administration directly inhibited proliferation. In order to achieve solution optimality, *bang-bang* solutions were considered. This involves determining the times to switch between the maximum value of drug input and the minimum amount of drug input. The objective consisted of two components: the amount of diseased tissue at a final time and the total amount of drug administered. Again, no explicit consideration of toxicity was made. These solutions are mathematically optimal; however, they are myopic in that continuous infusion of chemotherapeutics at their maximum tolerable level is not clinically realizable.

1.5.2 Toward Clinical Relevance

The clinical final treatment time (as employed by Martin and Teo) is not generally defined *a priori*. Toxicity and efficacy drive treatment decisions [49, 50], and endpoints such as disease remission are not easily predicted. High variability in patient response can make it difficult for clinicians to predict treatment outcomes in terms of efficacy and toxicity. For this reason, treatment is typically given in cycles which allow clinicians to evaluate the response of patients and use information feedback to alter treatment accordingly.

The studies discussed in subsection 1.5.1 drug dosing for cancer treatment in the abstract as a single problem with a generic drug/tumor combination. While there are many situations in engineering where such abstraction is possible, the problem of determining cancer chemotherapy dosing schedules does not allow such generalizations. Unlike many chemical processes, biological systems are very complex. It is not uncommon for organisms to exhibit significant variability in response to disease treatment [54]. As a result, drug/tumor combinations may have to be treated independently from a modeling perspective and patient specific parameters may have to be derived when trying to obtain an optimal treatment schedule.

1.6 DISSERTATION OVERVIEW

It should be possible to determine a clinically relevant chemotherapy schedule that optimizes the trade-off between treatment efficacy and patient quality of life based on a prescribed objective and a mathematical characterization of drug pharmacokinetics, efficacy, and toxicity. It is proposed that a method for developing optimal cancer chemotherapy schedules can be accomplished in two steps: (1) model development and (2) control algorithm synthesis and analysis.

Chapter 2 develops a linear PK model of 9-nitrocamptothecin (9NC), and its major active metabolite 9-aminocamptothecin (9AC), in the plasma of severe combined immunodeficient (SCID) mice at a single dose level. A revised model is then developed based on additional PK data to describe the nonlinear plasma disposition of 9NC and 9AC over a range of dose levels. The PK models are then used in chapter 3 to derive PD models that characterize the effects of 9NC administration on HT29 human colon carcinoma xenografts implanted subcutaneously in SCID mice. Two PK/PD models are presented: the first is driven by the linear PK model and the second forced by the nonlinear PK model.

Chapter 4 focuses on step 2, the synthesis of model–based control algorithms. Instead of employing optimal control techniques, this chapter addresses these control problems from a mathematical programming perspective. Optimal dosing problems for the linearly driven PK/PD model from chapters 2 and 3 and the system studied by Martin [12] are addressed. These problems are transformed and the dosing profiles are determined by solving a mixed–integer linear programming problems (MILP). The optimal dosing profile for the nonlinear PK/PD system from Chapters 2 and 3 is also determined using an MILP. Finally, in Chapter 5, conclusions drawn from the modeling and treatment design studies, and recommendations for extending and improving upon the results are provided.

2.0 PHARMACOKINETIC MODELING

After administration, a drug will distribute throughout an organism. At different locations within the organism, the drug can also be metabolized or eliminated. PK models are utilized to describe these processes and provide researchers with an *in silico* means of estimating physiological phenomena such as drug clearance and exposure. To facilitate model construction of tools such as ADAPT II® [25] and NONMEM®[23] have been employed by the medical and pharmacological communities. Novel model structures can also be developed in simulation packages such as MATLAB (© 2005, The Mathworks, Nantick, MA). In addition to describing drug concentrations as a function of time, PK models in this work are used to drive the PD models developed in Chapter 3.

2.1 9-NITROCAMPTOTHECIN

The drug 9-nitrocamptothecin (9NC) is an orally administered camptothecin analog that is being evaluated in clinical trials [55]. Preclinical PK data were obtained from SCID mice (some bearing subcutaneously implanted human HT29 colon carcinoma xenografts) after oral 9NC administration. Following oral administration, 9NC is absorbed into the bloodstream through the gastrointestinal tract. In plasma, 9NC quickly equilibrates between its active lactone and inactive carboxylate forms [55]. Further, the nitro group on 9NC is readily reduced to form the active primary metabolite 9-aminocamptothecin (9AC) [56]. 9AC also exists in both the active lactone and inactive carboxylate forms [55] (see Figure 5). The parent, 9NC, and metabolites then distribute to the tumor and normal tissues [40].

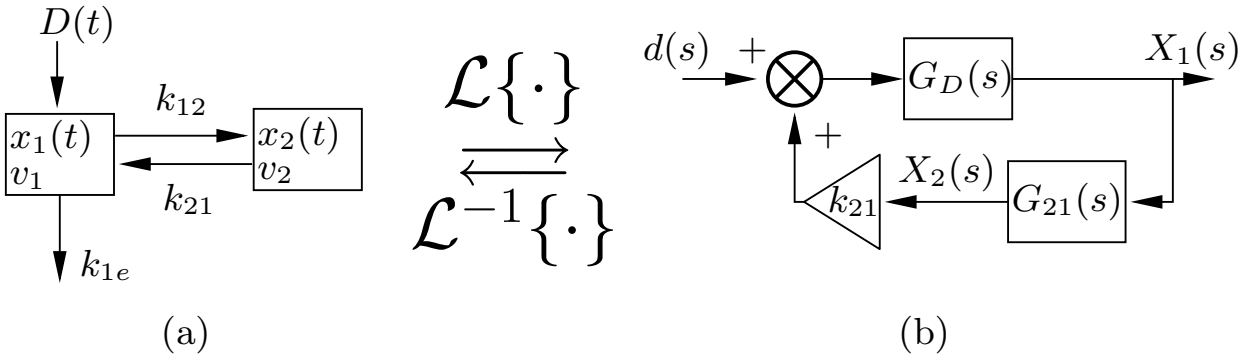

Figure 7: Two state compartmental model of intravenous drug disposition: (a) compartmental description, (b) equivalent Laplace domain representation. $\mathcal{L}\{\cdot\}$ is the Laplace transform operation and $\mathcal{L}^{-1}\{\cdot\}$ is the inverse Laplace transform.

2.2 MODELING METHODOLOGIES

2.2.1 Compartmental Models

Figure 7(a) shows an example of a compartmental model which could be used to represent the intravenous administration of a drug, $D(t)$, to a central compartment (*e.g.* plasma) with drug mass $x_1(t)$ and volume of distribution $v_1(t)$. This model assumes that the drug is being eliminated from the central compartment at a rate k_{1e} and can be distributed to and released from a peripheral tissue at rates k_{12} and k_{21}, respectively. The peripheral tissue contains a mass of drug $x_2(t)$ distributed homogeneously throughout the volume $v_2(t)$. The system shown in Figure 7(a) can be represented mathematically by performing mass balances over each compartment:

$$\begin{aligned} \dot{x}_1(t) &= D(t) - k_{12}x_1(t) - k_{1e}x_1(t) + k_{21}x_2(t) \\ \dot{x}_2(t) &= k_{12}x_1(t) - k_{21}x_2(t) \\ C(t) &= \tfrac{x_1(t)}{v_1} \end{aligned} \tag{2.1}$$

Here $C(t)$ is the concentration of the drug with respect to time and the dot operator ($\dot{}$) indicates a rate of change—the first derivative with respect to time.

2.2.2 Laplace Domain Representation

The system from equation (2.1) is referred to as a time domain representation. Another common way to conceptualize this system is in the Laplace domain. The Laplace domain provides a useful framework for dynamic analysis of linear systems. Equation (2.1) is comprised of linear ODEs, and it is possible to transform equation (2.1) into the Laplace domain. Assuming both the the initial concentration of the drug ($x_1(t = 0)$) and that the amount of drug administered before time zero ($D(t = 0^-)$) are zero, the individual elements

for the state equation describing x_1 are transformed in the following way:

$$\begin{aligned}
\mathcal{L}\{\dot{x}_1(t)\} &= sX_1(s) \\
\mathcal{L}\{D(t)\} &= d(s) \\
\mathcal{L}\{-k_{12}x_1(t)\} &= -k_{12}X_1(s) \\
\mathcal{L}\{-k_{1e}x_1(t)\} &= -k_{1e}X_1(s) \\
\mathcal{L}\{k_{21}x_2(t)\} &= k_{21}X_2(s)
\end{aligned} \tag{2.2}$$

Where $\mathcal{L}\{\cdot\}$ is the Laplace transform operator and the variable s is the independent variable in the Laplace domain. For clarity, states in the Laplace domain are identified by capital letters as a function of s with the exception of dose which is represented in the Laplace domain by $d(s)$. The state equations from (2.1) can be transformed and solved for their respective states in the Laplace domain to yield:

$$X_1(s) = \frac{\frac{1}{(k_{12}+k_{1e})}}{\frac{1}{(k_{12}+k_{1e})}s+1}d(s) + \frac{\frac{(k_{21})}{(k_{12}+k_{1e})}}{\frac{1}{(k_{12}+k_{1e})}s+1}X_2(s) \tag{2.3a}$$

$$= (d(s) + k_{21}X_2(s)) \underbrace{\frac{\frac{1}{(k_{12}+k_{1e})}}{\frac{1}{(k_{12}+k_{1e})}s+1}}_{G_D(s)} \tag{2.3b}$$

$$X_2(s) = \underbrace{\frac{\frac{k_{12}}{k_{21}}}{\frac{1}{k_{21}}s+1}}_{G_{21}(s)} X_1(s) \tag{2.3c}$$

The functions G_D and G_{21} are first–order transfer functions. The term transfer function is used because it translates, or transforms, effects of changes in one state or input onto another. For example, G_{21} translates changes in X_1 on to X_2. The order of the transfer function refers to the highest power of s in the denominator. A transfer function is said to be in standard form when the coefficients of s^0 are equal to one in both the numerator and denominator. Transforming the system into the Laplace domain and placing it in standard form provides a system of equations which are unique from an analysis standpoint. Consider $G_{21}(s)$: the coefficient $\frac{k_{12}}{k_{21}}$ is referred to as the system *gain* and the coefficient of s in the denominator, $\frac{1}{k_{21}}$, is the *time constant* of the system. These are typically referred to by the symbols K_i and τ_i, respectively, and the index i is used to distinguish between transfer functions. The gain translates the magnitude of changes in X_1 in to proportional magnitude

changes in X_2, and the time constant determines the rate at which this occurs. This form is unique because it effectively decouples steady–state and dynamic effects into two separate parameters.

The system of equations from equation (2.3) can be represented in block diagram from as shown in Figure 7(b). Arrows represent the values of the states and the blocks contain the transfer functions. The operators shown in Figure 7, $\mathcal{L}\{\cdot\}$ and $\mathcal{L}^{-1}\{\cdot\}$, represent the Laplace transform and inverse Laplace transform operations, respectively.

The method of transforming linear ODEs into the Laplace domain was shown in equation (2.2). This example encompasses some important concepts in discussing dynamic systems. However, it does not address the concept of delayed systems. This issue was introduced in subsection 1.4.3 when delayed PD effects were discussed. Delay systems are common in both chemical processes and biological systems. Mathematically, delayed states are represented by the Heaviside function, $\mathcal{H}(\cdot)$, in the time domain. The Heaviside function acts as a switch and is defined in the following way:

$$\mathcal{H}(t) = \begin{cases} 0 & t < 0 \\ 1 & t \geq 0 \end{cases}$$

A state, x, delayed by 5 time units would be represented by $x(t-5)\mathcal{H}(t-5)$ in the time domain. The Laplace domain representation would be given by:

$$\mathcal{L}\{x(t-5)\mathcal{H}(t-5)\} = X(s)e^{-5s}$$

A natural question arises: if both domains (*i.e.*, time and Laplace) describe the same phenomenon, why should one be selected over the other? The distinction between the two methods becomes important when trying to regress model parameters.

2.2.3 Parameter Estimation

The objective of parameter estimation is to determine the set of parameters which will best fit the data—this presupposes that a model structure has been selected. The parameter estimation problem from a given model structure is formulated as an optimization problem where values for the set of parameters, $\mathcal{P}$, are determined such that the prediction error — the difference between the actual values, $\mathcal{Y}(k)$, and the predicted values, $\hat{\mathcal{Y}}(k, \mathcal{P})$ — is minimized. Mathematically, this is written as follows:

$$\min_{\mathcal{P}} \quad \text{SSE} = \sum_{k=1}^{n_{data}} \Gamma_{\mathcal{Y}}^2(k,k) \left(\mathcal{Y}(k) - \hat{\mathcal{Y}}(k,\mathcal{P})\right)^2 = \left|\left|\Gamma_{\mathcal{Y}} \left(\mathcal{Y}(k) - \hat{\mathcal{Y}}(k,\mathcal{P})\right)\right|\right|_2^2 \tag{2.4}$$

Equation (2.4) minimizes the sum squared error, SSE, between actual and predicted. This is commonly referred to using the notation at the far right of equation 2.4, called the squared two–norm. This increases the penalty for prediction errors as the deviation from experimental data increases. One side effect of this optimization is that parameters which satisfy (2.4) are assumed to be part of a Gaussian distribution [57]. The parameter, $\Gamma_{\mathcal{Y}}$, is a weighting parameter to increase or decrease the penalty associated with individual data points. One possible weighting uses the inverse of the variability associated with individual measurement points; this increases the importance of fitting data points associated with smaller standard deviations.

All of the parameter estimation techniques previously mentioned require an optimization of some kind. While the models may consist of linear ordinary differential equations (ODEs), meaning they are linear in the states, x, the optimization may not be linear with respect to the parameters. It can be advantageous to transform the system such that nonlinearities are eliminated, the number of parameters are reduced, or nonlinear structures more amenable to regression are used. However, it can be difficult to eliminate all of the nonlinearities and parameter couplings when estimating parameters.

Hence, it is often necessary to solve nonlinear programming problems (NLP) [58, 59]. While efficient algorithms exist for specific types of nonlinearities [60], gradient-based methods provide a general technique for solving a NLP [59]. Gradient-based minimization utilizes the partial derivatives of the objective function with respect to the parameters to determine

the parameter adjustments necessary to minimize the objective function. This is an iterative process that depends on initial guesses for parameter estimates; based on the quality of the initial guess, the algorithm may converge to either a local or global minimum [58]. In order to reduce the probability of finding a local minimum, the algorithm may be started at different points in the parameter space. Parameter estimates in this work were determined using the *fmincon* function from the optimization toolbox in MATLAB® Release 14 (©2005, The MathWorks, Natick, MA) on x86-based computers.

2.2.4 Selecting from Competing Model Structures

Situations arise where different model structures can be developed to describe the same system. The intended use of a model may contribute to structure selection decisions (*e.g.*, linear structures are typically more amenable to controller synthesis than nonlinear models). When no *a priori* preference or justification for a particular model structure exists, other metrics are considered. Since the purpose of a model is to act as a surrogate for an actual system, it is necessary to determine which model structure *best* estimates the data. One method of comparing different model structures is to employ Akaike's Information Criterion (AIC) [61]:

$$\text{AIC} = (\text{number of points}) \ln\left(\frac{\text{SSE}}{(\text{number of points})}\right) + 2(\text{number of parameters}) \qquad (2.5)$$

The AIC is a metric that balances between adding parameters and improving model quality (lowering SSE). The model structure which provides the lowest AIC is preferred based on the parsimony principle.

2.3 LINEAR PK MODELING OF 9NC AND 9AC LACTONE

2.3.1 Five Compartment Model

The first step in modeling this system was to characterize the PK of 9NC. Since an orally administered drug with a metabolite of interest was being considered, the compartmental

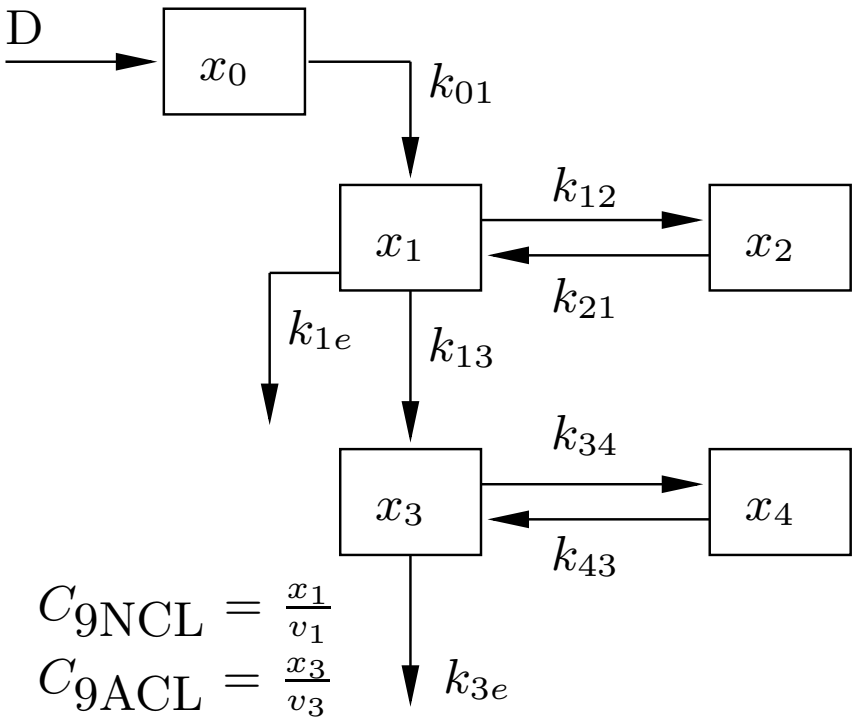

Figure 8: Five compartment pharmacokinetic model for the disposition of 9NC and 9AC lactone after oral dosing of 9NC.

model shown in Figure 8 was used. Compartments x_2 and x_4 were included to capture the dynamics (in this case slowed elimination) of 9NC and 9AC in compartments x_1 and x_3 respectively. Parallels can be drawn between the underlying physiology and the model structure, given in differential form in equation (2.6):

$$\dot{x}_0(t) = D(t) - k_{01}x_0(t) \tag{2.6a}$$

$$\dot{x}_1(t) = k_{01}x_0(t) + k_{21}x_2(t) - (k_{12} + k_{13} + k_{1e})x_1(t) \tag{2.6b}$$

$$\dot{x}_2(t) = k_{12}x_1(t) - k_{21}x_2(t) \tag{2.6c}$$

$$\dot{x}_3(t) = k_{13}x_1(t) + k_{43}x_4(t) - (k_{34} + k_{3e})x_3(t) \tag{2.6d}$$

$$\dot{x}_4(t) = k_{34}x_3(t) - k_{43}x_4(t) \tag{2.6e}$$

$$C_{\text{9NCL}} = \frac{x_1(t)}{v_1} \tag{2.6f}$$

$$C_{\text{9ACL}} = \frac{x_3(t)}{v_3} \tag{2.6g}$$

Here the states are represented by x_i and parameters are given by k_i and v_i. The mass of the drug, D, enters the compartment x_0 as a bolus. This compartment can be interpreted as describing the kinetics of drug absorption and first-pass liver effects after oral administration. The drug is absorbed from the gut into the plasma at a rate k_{01}. Transport from the plasma central compartment (x_1) to the remote peripheral compartment (x_2), and vice versa, takes place at the respective rates k_{12} and k_{21}. The lactone form of 9NC is either eliminated from the plasma at a rate of k_{1e} or metabolized to 9AC lactone at a rate of k_{13}. Similar interaction with the peripheral tissues (x_4) is possible for 9AC lactone at the rates of k_{34} and k_{43}, respectively. Lastly, 9AC lactone is eliminated at a rate of k_{3e}.

Major shifts in the equilibrium between the active lactone and inactive carboxylate forms of 9NC and 9AC occur in the presence of binding proteins [55, 62]. While these are commonly found in humans, they do not affect 9NC or 9AC dynamics in mice (*i.e.*, no human serum albumin is present) [62]. It was assumed that equilibrium between lactone and carboxylate forms of 9NC and 9AC in the plasma was achieved rapidly [55], and no attempt was made to model equilibrium shifts because 9NC lactone was measured, albeit indirectly.

For parameter estimation purposes, the ten parameters for this model were all estimated independently. Two sets of parameters were found for two separate sets of 9NC and 9AC

Table 1: Mean, standard deviation, and individual estimates for the compartmental model parameters.

	Mean	Std. Dev.	tumor–bearing	non–tumor–bearing	
k_{01}	2.15×10^{-2}	6.97×10^{-3}	1.656×10^{-3}	2.642×10^{-3}	min^{-1}
k_{12}	3.11	3.01	0.984	5.242	min^{-1}
k_{13}	0.643	8.22×10^{-2}	0.585	0.701	min^{-1}
k_{1e}	1.016	0.301	0.803	1.229	min^{-1}
k_{21}	0.471	0.248	0.295	0.646	min^{-1}
k_{34}	2.030	1.012	2.746	1.314	min^{-1}
k_{3e}	2.575	1.023	1.856	3.298	min^{-1}
k_{43}	0.966	0.227	0.806	1.127	min^{-1}
v_1	3.888	0.169	3.768	4.008	ml
v_3	9.639	0.462	9.966	9.313	ml

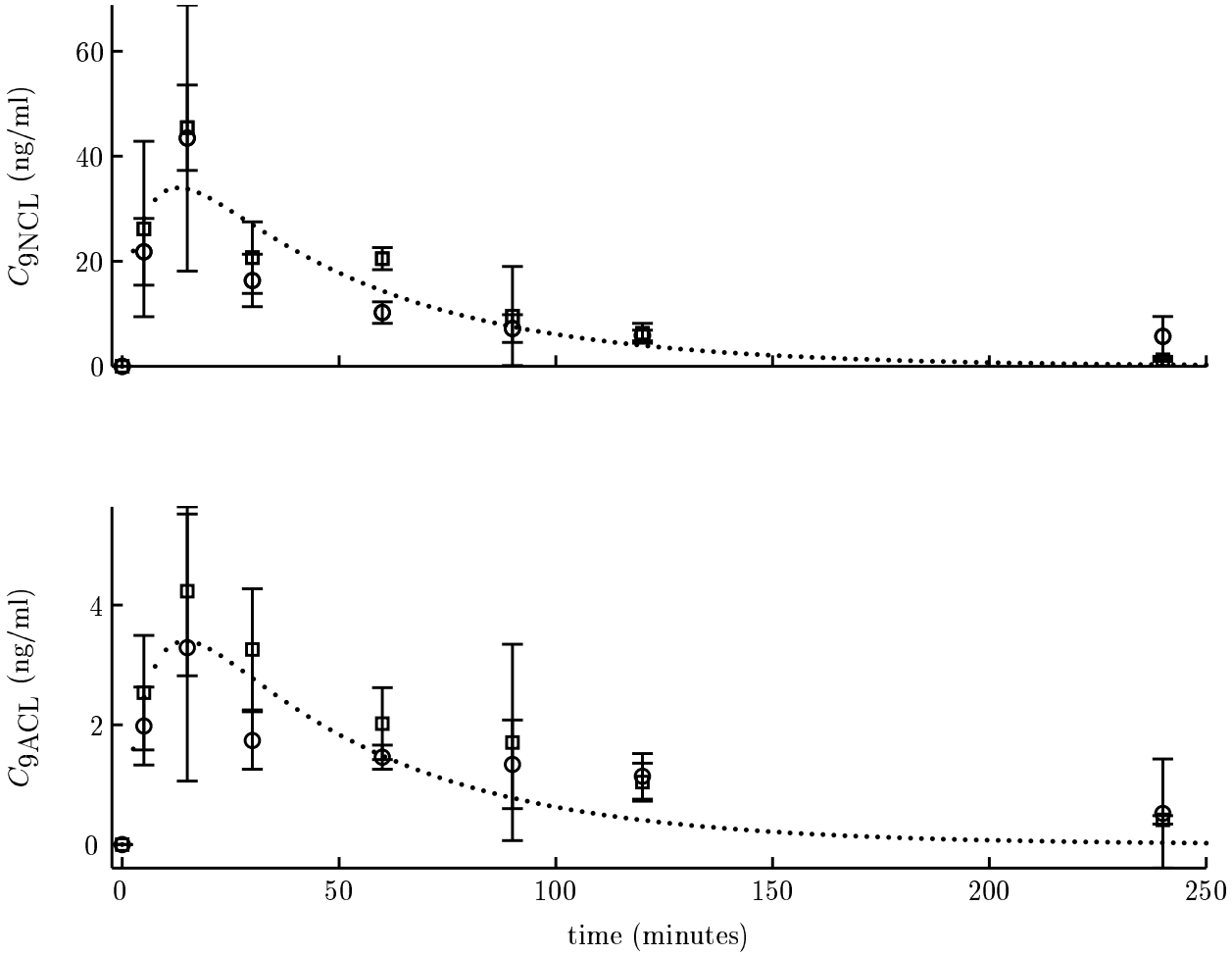

Figure 9: Experimental 9NC lactone (top pane) and 9AC lactone (bottom pane) concentrations from two studies: (□) - tumor-bearing animals and (○) - non-tumor-bearing animals. Data shown ± are 1 standard deviation. Compartmental model predictions using the model from Figure 8 (···) and mean PK parameter values.

plasma data: one experiment used tumor-bearing animals and the other using non-tumor-bearing animals. These parameters are shown in Table 1. These parameters will be discussed in detail in section 2.3.3. These data are shown in Figure 9 along with one standard deviation in the measurement, for each experimental point in time—each datum point represents the average value for three mice. From these data it can be seen that there is no statistical difference between the two studies. The two sets of parameters were averaged and the "average" model was simulated in response to the same 0.67 mg/kg dose to produce the model prediction shown in Figure 9. The data shown in Figure 9 exhibit a quick increase in 9NC concentration followed by a slow decrease. Consider the 9NC lactone concentrations. The compartmental model underestimates the peak concentration to better approximate the data points which follow. In fact, this model does a poor job of capturing the dynamic behavior seen in the data. This is particularly true between $t = 15$ min and $t = 60$ min.

2.3.2 Two Timescale Model

To better capture the dynamic response, an alternative PK model for 9NC and 9AC lactone dynamics is shown in the Laplace domain in Figure 10. This model is referred to as a two timescale model because the dynamics are governed by two distinctly different pathways. This model is governed by the following equations:

$$\dot{x}_1(t) = \mathcal{H}(t-\theta)D(t-\theta)\frac{\beta_1}{\tau_1} - \frac{x_1(t)}{\tau_1} \tag{2.7a}$$

$$\dot{x}_2(t) = \frac{\alpha_1}{\tau_2}D(t) - \frac{x_4(t)}{\tau_4} \tag{2.7b}$$

$$\dot{x}_3(t) = \frac{x_1(t)+x_2(t)}{\tau_3} - \frac{x_2(t)}{\tau_3} \tag{2.7c}$$

$$\dot{x}_4(t) = \frac{\alpha_2}{\tau_4}x_3(t) - \frac{x_4(t)}{\tau_4} \tag{2.7d}$$

$$C_{9\text{NCL}} = K_1 x_3(t) \tag{2.7e}$$

$$C_{9\text{ACL}} = K_2(x_3(t)+x_4(t)) \tag{2.7f}$$

A fraction, α_1, of the dose D enters the system as a mass through the right pathway in Figure 10 and experiences the dynamics governed by G_2. The remainder of the dose, β_1, takes the left pathway and is delayed by θ time units before passing through G_1. The states

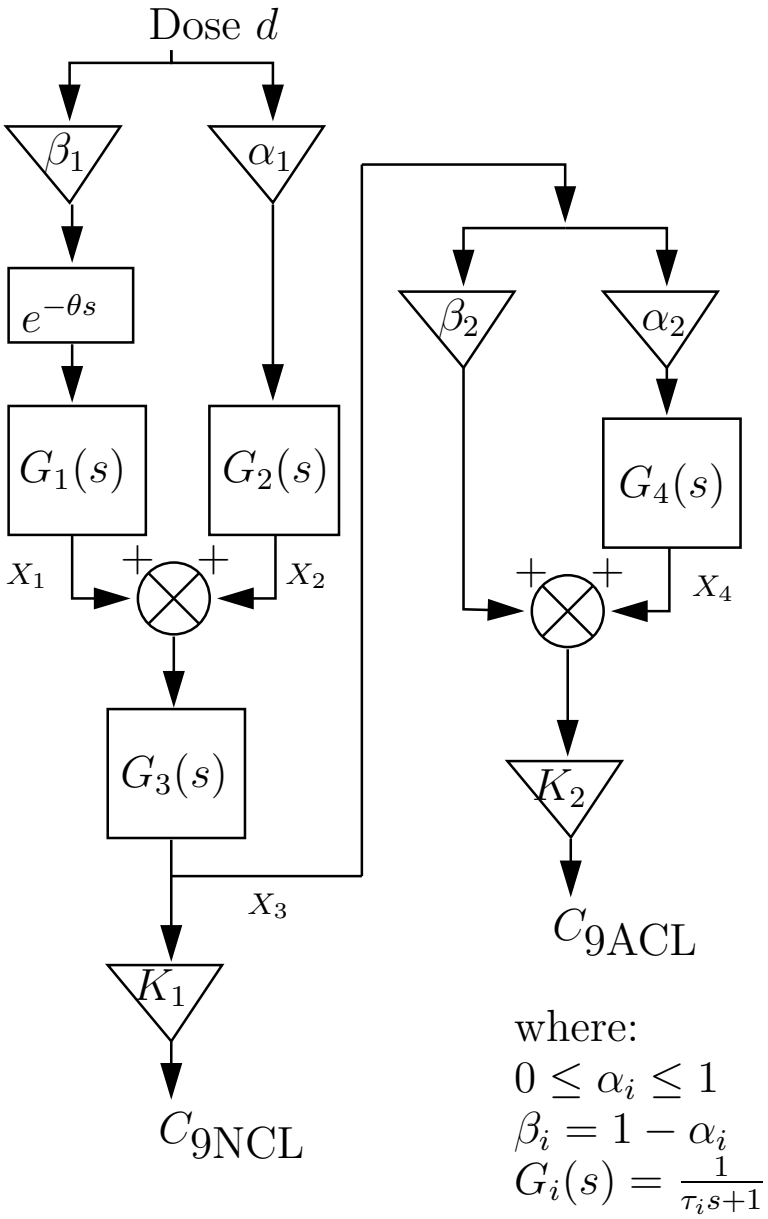

Figure 10: Two timescale pharmacokinetic model for the disposition of 9NC and 9AC lactone after oral dosing shown in the Laplace Domain. Transfer functions, G_i, have unity gain and β_i and α_i are complementary fractions. The gains, K_1 and K_2, convert the respective signals representing the masses of 9NC and 9AC lactone to concentrations, and θ is a time delay.

Table 2: Mean, standard deviation, and individual estimates for the two time scale model parameters.

	Mean	Std. Dev.	tumor–bearing	non–tumor–bearing	
τ_1	389	469.5	57.06	721.0	min
τ_2	11.87	0.134	11.97	11.776	min
τ_3	11.65	6.252×10^{-2}	11.70	11.609	min
τ_4	38.07	44.97	6.275	69.865	min
K_1	0.327	0.177	0.201	.45187e-01	ml^{-1}
K_2	3.84×10^{-2}	2.33×10^{-2}	2.192×10^{-2}	5.48×10^{-2}	ml^{-1}
α_1	0.343	0.208	.489	.19581e-01	—
α_2	0.442	0.166	.325	.55939e-01	—
θ	29.97	3.812×10^{-3}	29.98	29.97	min

x_1 and x_2 are combined to form the input into G_3 whose output x_3 represents the mass of 9NC lactone in the plasma. The two pathways can be biologically interpreted as different areas of adsorption in the digestive tract of the mouse. A fraction, β_2, of the 9NC lactone in plasma is converted directly into 9AC, and the remaining 9NC, α_2, is converted to 9AC after passing through G_4.

This model contains nine parameters, and these were regressed independently to the tumor–bearing and non–tumor–bearing mouse data sets. For each dataset, parameters were estimated by first finding the parameters describing 9NC dynamics. These parameters (α_1, θ, τ_1, τ_2, τ_3, and K_1) were fixed, and the parameters associated with 9AC (α_2, τ_4 and K_2) were regressed. The parameter estimates are given in Table 2 and will be discussed in detail later. The mean parameter values for the two studies were used to develop the model predictions shown in Figure 11. These model predictions are plotted along with those of the compartmental model previously discussed. By comparing the two model predictions from Figure 11, the two timescale model appears to be superior to the compartmental model. The two timescale model is able to capture the rapid increase in 9NC plasma concentrations

Table 3: AIC and SSE results for compartmental, and two timescale (indicated by the subscripts c, and t, respectively) for both tumor–bearing and non-tumor-bearing animals. Mean values represent AIC and SSE calculated by considering deviations of mean model predictions from both datasets.

	tumor-bearing	non-tumor-bearing	mean parameters
AIC_c	62.4	64.7	105.8
AIC_t	33.4	45.2	106.1
SSE_c	225.9	262	529.7
SSE_t	41.9	87.6	503.2

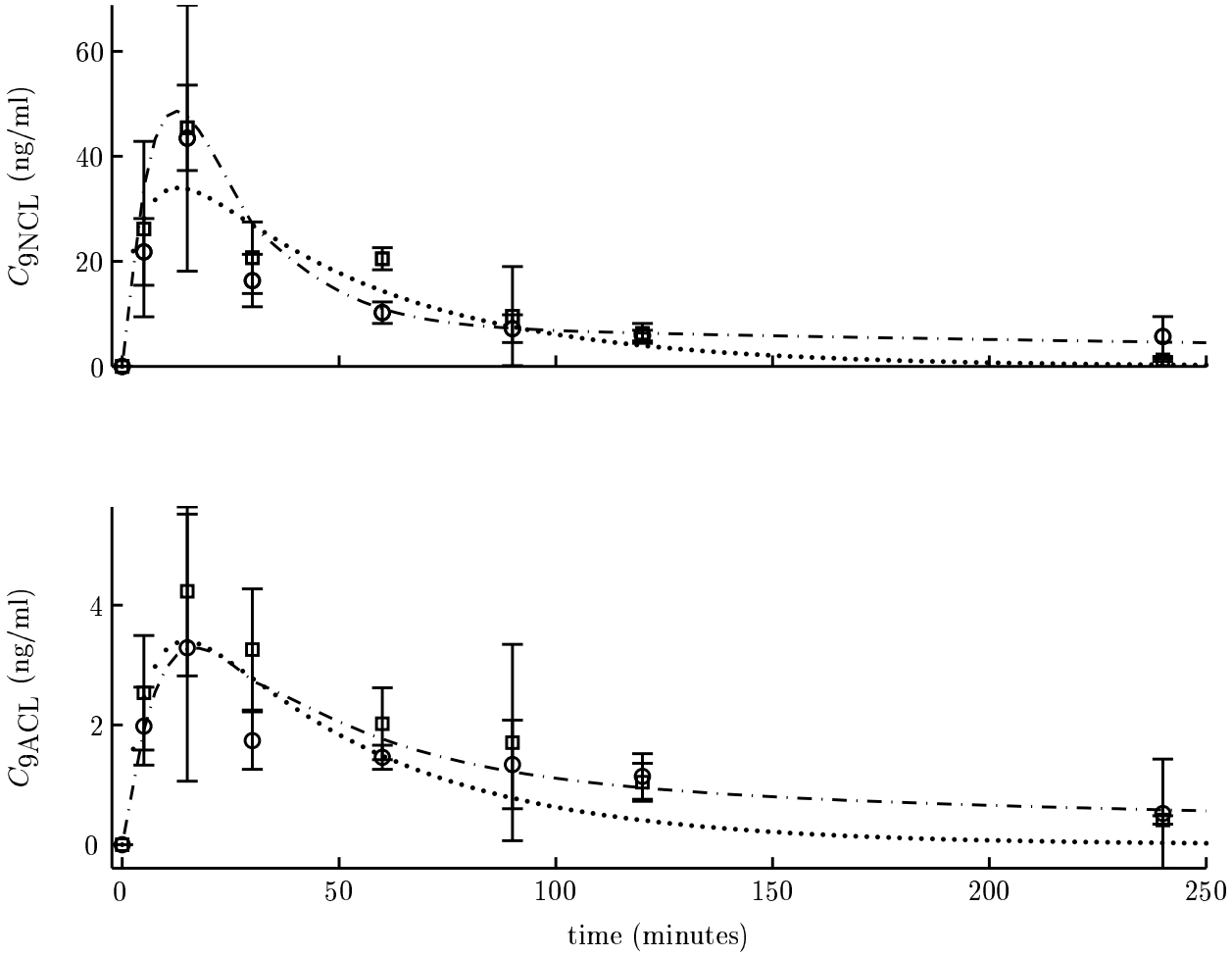

Figure 11: Experimental 9NC lactone (top pane) and 9AC lactone (bottom pane) concentrations from two studies: (□) - tumor–bearing animals and (○) - non–tumor–bearing animals. Data shown are ± 1 standard deviation. Model predictions use the compartmental from Figure 8 (· · ·) and the two timescale model from Figure 10 (- - -) with mean PK parameter values.

as well as the slowed elimination seen at later times. Similar dynamics are seen for 9AC as well. To quantitatively compare the compartmental and two timescale model structures, the AIC was calculated and is shown in Table 3. The AICs for the individual data sets are significantly lower for the two timescale model. To determine an *average* AIC, sum-squared errors were calculated based on the differences between the average model predictions and the individual data points — this doubled the number of data points in the AIC calculation. While the average AIC for the two timescale model is still lower, the effect is less dramatic. The two timescale model provides better predictions for the individual data sets, but this improvement is not as apparent when all of the data is considered simultaneously.

2.3.3 Recycle Model

An alternative PK model for 9NC and 9AC lactone dynamics is shown in the Laplace domain in Figure 12 and has the following differential equation representation:

$$\dot{x}_0(t) = -\frac{x_0(t)}{\tau_0} + \frac{D(t)}{\tau_0} \tag{2.8a}$$

$$\dot{x}_1(t) = \frac{x_0(t)}{\tau_1} - \frac{x_1(t)}{\tau_1} + \frac{x_3(t)}{\tau_1} \tag{2.8b}$$

$$\dot{x}_2(t) = \frac{\beta_1\alpha_2}{\tau_2}x_1(t) - \frac{x_2(t)}{\tau_2} + \frac{x_4(t)}{\tau_2} \tag{2.8c}$$

$$\dot{x}_3(t) = \mathcal{H}(t-\theta)x_1(t-\theta)\frac{\alpha_1}{\tau_r} - \frac{x_3(t)}{\tau_r} \tag{2.8d}$$

$$\dot{x}_4(t) = \mathcal{H}(t-\theta)x_2(t-\theta)\frac{\alpha_1}{\tau_r} - \frac{x_4(t)}{\tau_r} \tag{2.8e}$$

$$C_{\text{9NCL}} = \beta_1 K_p x_1(t) \tag{2.8f}$$

$$C_{\text{9ACL}} = \beta_1 K_p x_2(t) \tag{2.8g}$$

The recycle structure model given by equation (2.8) also captures plateau dynamics observed in the experimental PK data, around $t = 35$ min. The dose, D, enters as a bolus (in mass units) and undergoes first-order dynamics described by equation (2.8a). This can be physiologically interpreted as absorption from the gastrointestinal tract. Next, the rate of appearance of 9NC lactone is dictated by equation (2.8b). A fraction, β_1, of the mass of 9NC lactone appears in the plasma with the remainder, α_1, recycled. Recycling can be loosely

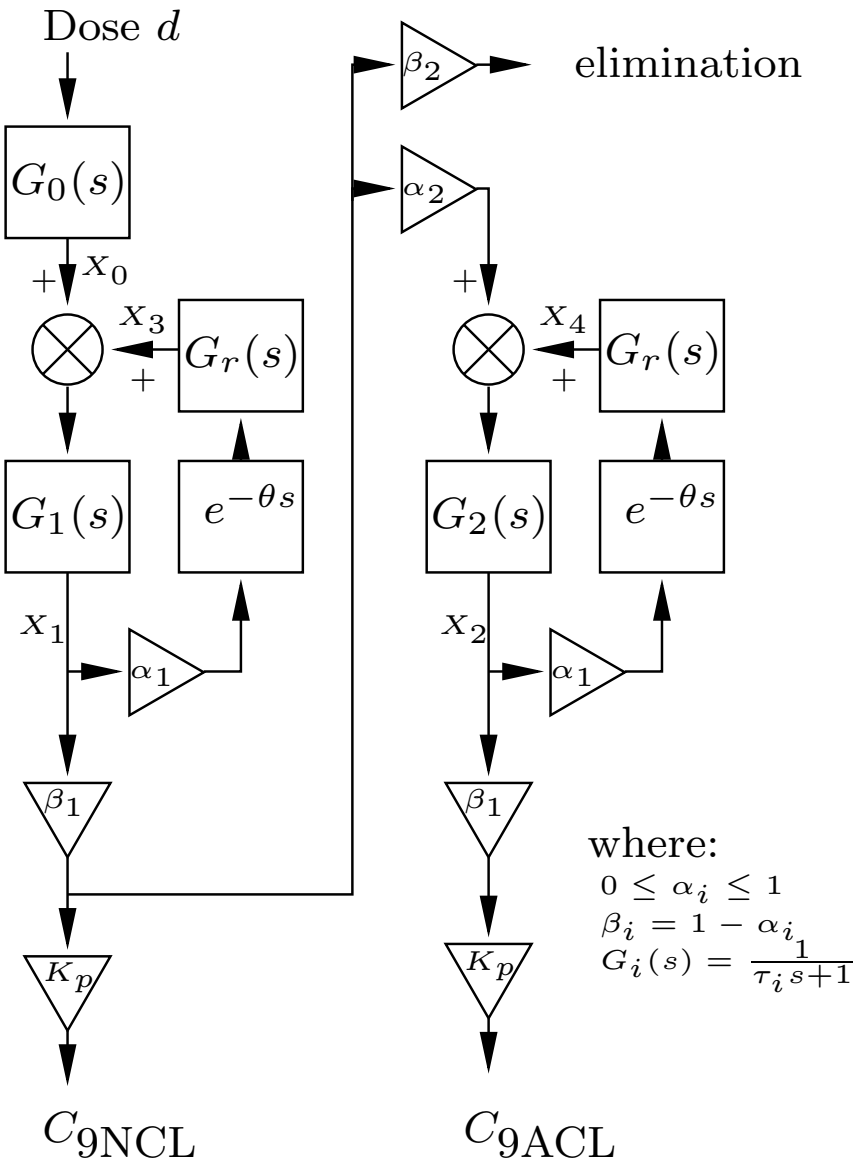

Figure 12: Recycle-based pharmacokinetic model for the disposition of 9NC lactone and 9AC lactone after oral dosing shown in the Laplace domain. The transfer functions, G_i, have unity gain, β_1 and α_1 are complementary fractions, the gain, K_p, converts the signals representing the masses of 9NC lactone and 9AC lactone to concentrations, and θ is a time delay.

Table 4: Mean, standard deviation, and individual estimates for the recycle model parameters.

	Mean	Std. Dev.	tumor–bearing	non–tumor–bearing	
τ_0	11.4	0.465	11.05	11.71	min
τ_1	12.5	1.49	13.52	11.42	min
τ_2	0.492	0.681	1.0×10^{-2}	0.974	min
τ_r	16.1	6.92	11.169	20.95	min
K_p	0.173	1.82×10^{-2}	0.186	0.160	ml^{-1}
α_1	0.447	1.74×10^{-2}	0.434	0.460	—
α_2	0.157	3.76×10^{-4}	0.156	0.157	—
θ	28	8.81	21.76	34.22	min

interpreted as representing the sluggish dynamics associated with storage in a remote non-plasma tissue, for eventual return to the plasma; this is similar in concept to Figure 8. The recycled mass, $\alpha_1 x_1$, is then delayed by θ minutes and undergoes the dynamics described by equation (2.8e) before being recombined with x_0 (the mass leaving G_0 from Figure 12). A fraction, β_2, of the 9NC lactone mass found in the plasma, $\beta_1 x_1$, is eliminated; the remainder, α_2, appears as 9AC lactone. The dynamics of conversion of 9NC lactone to 9AC lactone are described by equation (2.8c). A fraction of 9AC lactone, $\beta_1 x_2$, appears immediately in the plasma and the remainder, $\alpha_1 x_2$, is recycled in a manner similar to the 9NC lactone recycle loop.

All eight parameters (τ_0, τ_1, τ_2, τ_r, K_p, α_1, α_2, andθ) for the recycle model were estimated simultaneously for each dataset: tumor–bearing and non–tumor–bearing and are given in Table 4. Using the average parameters, the recycle model predictions shown in Figure 13 were simulated. The quick initial increase in plasma concentrations of 9NC lactone and 9AC lactone, as well as the relatively slow elimination at later times are captured well by the recycle model structure. The AIC and quality of fit criteria for all three linear PK models are shown in Table 5. When the individual studies were modeled, the two timescale model

Table 5: AIC and SSE results for compartmental, two timescale, and recycle models (indicated by the subscripts c, t, and r, respectively) for both tumor–bearing and non-tumor-bearing animals. Mean values represent AIC and SSE calculated from deviations of mean model predictions from both datasets combined.

	tumor-bearing	non-tumor-bearing	mean
AIC_c	62.4	64.7	105.8
AIC_t	33.4	45.2	106.1
AIC_r	42.1	46.6	80.19
SSE_c	225.9	262	529.7
SSE_t	41.9	87.6	503.2
SSE_r	81.5	108.3	237.84

had lower AIC values. However when the AIC was calculated using the data and the average model predictions, the recycle model was shown to better represent the average behavior. Parameter estimates for each model structure were obtained for each of the two studies, and the average values of the parameters for the two model structures along with parameter standard deviations, are shown in Table 6.

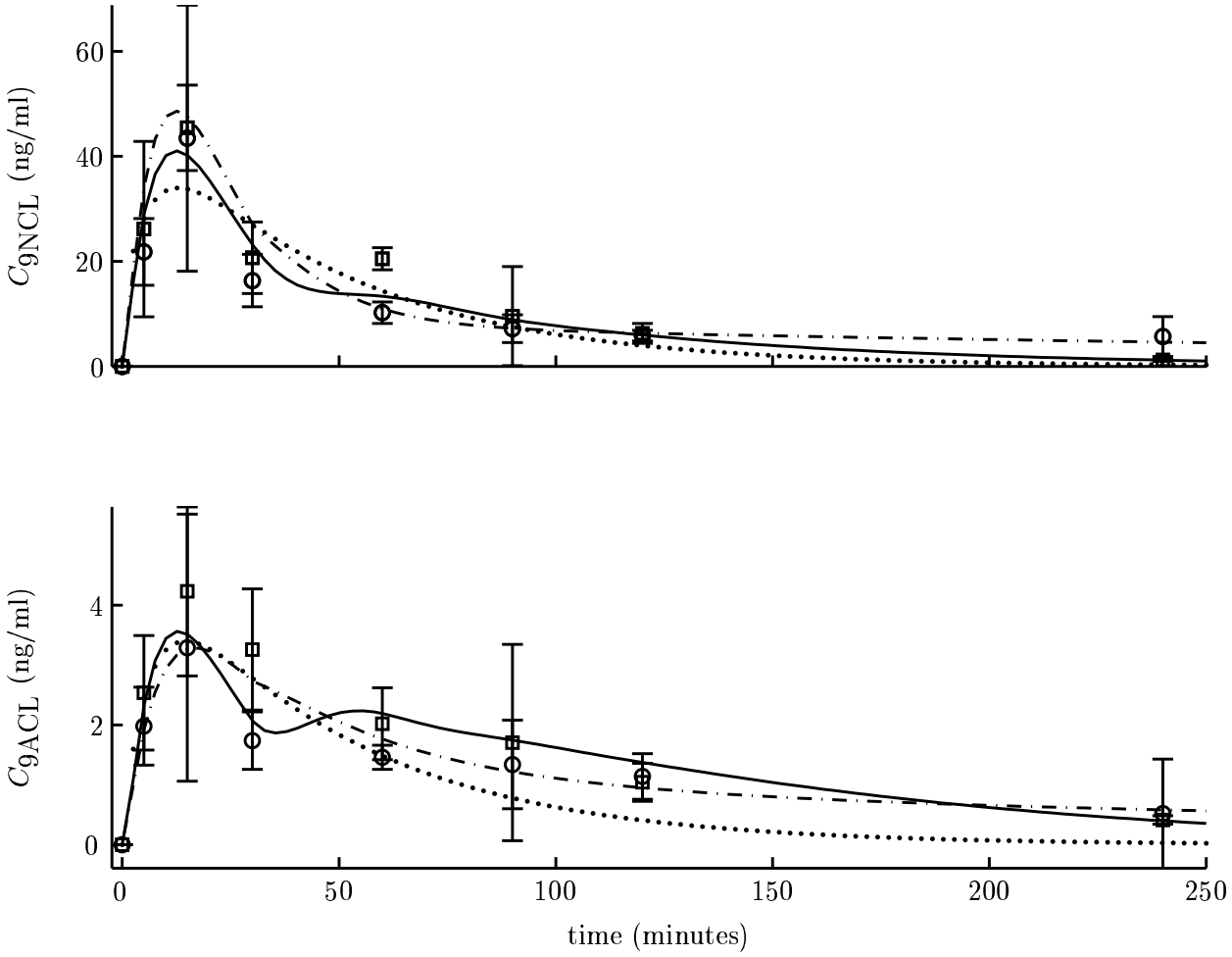

Figure 13: Experimental 9NC lactone (top pane) and 9AC lactone (bottom pane) concentrations from two studies: (□) - tumor–bearing animals and (○) - non–tumor–bearing animals. Data shown are ± 1 standard deviation. Model predictions use the compartmental from Figure 8 (···), the two timescale model from Figure 10 (-·-), and the recycle model from Figure 12 (—) with mean PK parameter values.

Table 6: Average PK parameters for linear models.

5-Compartment				Two Timescale				Recycle			
	Mean	Std. Dev.			Mean	Std. Dev.			Mean	Std. Dev.	
$\bar{k}_{01}$	2.15×10^{-2}	6.97×10^{-3}	min^{-1}	$\bar{\tau}_1$	389	469.5	min	$\bar{\tau}_0$	11.4	0.465	min
$\bar{k}_{12}$	3.11	3.01	min^{-1}	$\bar{\tau}_2$	11.87	0.134	min	$\bar{\tau}_1$	12.5	1.49	min
$\bar{k}_{13}$	0.643	8.22×10^{-2}	min^{-1}	$\bar{\tau}_3$	11.65	6.252×10^{-2}	min	$\bar{\tau}_2$	0.492	0.681	min
$\bar{k}_{1e}$	1.016	0.301	min^{-1}	$\bar{\tau}_4$	38.07	44.97	min	$\bar{\tau}_r$	16.1	6.92	min
$\bar{k}_{21}$	0.471	0.248	min^{-1}	$\bar{K}_1$	0.327	0.177	ml^{-1}	$\bar{K}_p$	0.173	1.82×10^{-2}	ml^{-1}
$\bar{k}_{34}$	2.030	1.012	min^{-1}	$\bar{K}_2$	3.84×10^{-2}	2.33×10^{-2}	ml^{-1}	$\bar{\alpha}_1$	0.447	1.74×10^{-2}	—
$\bar{k}_{3e}$	2.575	1.023	min^{-1}	$\bar{\alpha}_1$	0.343	0.208	—	$\bar{\alpha}_2$	0.157	3.76×10^{-4}	—
$\bar{k}_{43}$	0.966	0.227	min^{-1}	$\bar{\alpha}_2$	0.442	0.166	—	$\bar{\theta}$	28	8.81	min
$\bar{v}_1$	3.888	0.169	ml	$\bar{\theta}$	29.97	3.812×10^{-3}	min				
$\bar{v}_3$	9.639	0.462	ml								

To evaluate model confidence, the variability in the parameters was considered. A lower overall variability in model parameters would indicate that the model structure is more amenable to representing the experimental data. Many of the parameters in both the compartmental and two timescale models exhibited significant variability (standard deviations greater than half of the mean). Values such as k_{12} from the compartmental model and τ_1 and τ_4 from the two timescale model would be cause for concern — τ_1 and τ_4 have standard deviations greater than the mean. However, this is not so for the majority of the recycle model parameters. There is significant variability (standard deviating greater than the mean) for the parameter τ_2 in the recycle model which is a direct result of the variability observed in the mean values in the 9AC data. Referring specifically to the variance in the mean values in the third and fourth time points for 9AC lactone in Figure 13, the parameter τ_2 is the only adjustable parameter which affects *only* the 9AC lactone concentration profile. This would lead to an expectation of high variability in τ_2.

Of the three models presented here, the recycle model provides the best fit of the overall system response. The average AIC values are lower, and this is related to decreased parametric variability. More robust model predictions can be made when the bounds on parameter variability are tighter. The recycle model had fewer parameters than the other two models; this reduces parameter identifiability problems which may be encountered in the nonlinear optimization.

The model structures studied above assume that the PK of 9NC lactone and 9AC lactone are linear with respect to dose. A series of experiments were carried out to determine the disposition of 9NC and 9AC total (lactone + carboxylate) at 0.44, 0.67 and 1.0 mg/kg to support or invalidate the claim of linear PK.

2.4 NONLINEAR PK MODEL OF TOTAL DRUG

The experiments investigating nonlinearity of 9NC and 9AC PK utilized the analysis method described in subsection B.5 of Appendix B. Because all 9NC and 9AC present in plasma was converted to their respective lactone forms prior to analysis only total 9NC and 9AC

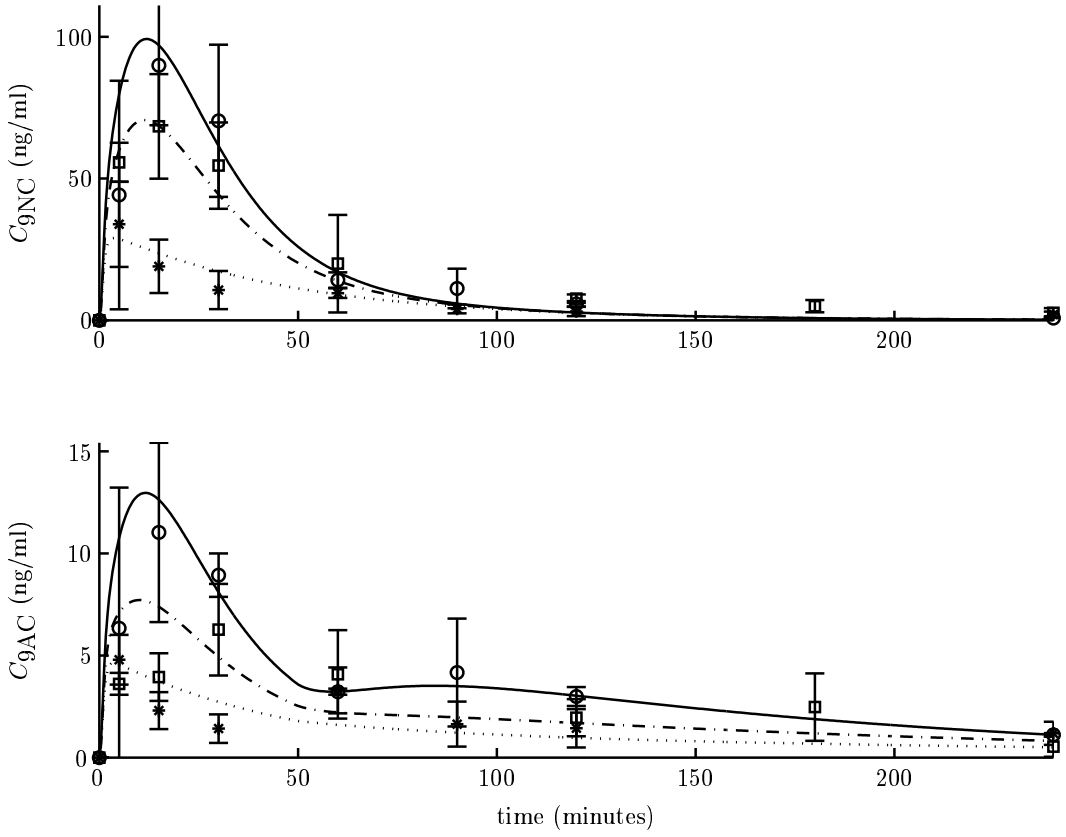

Figure 14: Total plasma concentrations measurements/model predictions of 9NC (top) and 9AC (bottom) in response to oral administration of 9NC at dose levels of 0.44 ($\ast$/$\cdots$), 0.67 (□/-·-), and 1.0 (○/—) mg/kg. Error bars indicate ± one standard deviation in the measured data.

levels were modeled. The plasma PK data after oral administration of 0.44, 0.67, and 1.0 mg/kg 9NC are shown in Figure 14. The data obtained after a dose of 0.44 mg/kg are characteristically different than those data obtained in response to doses of 0.67 and 1.0 mg/kg. The peak plasma concentration after a 0.44 mg/kg dose occurs at the second time point (5 min), whereas the peak plasma concentration for the higher dose levels appears to occur at the third time point (15 min). In the context of linear systems, changing peak time indicates a nonlinear in the time constant. Furthermore, the ratio of peak 9NC concentrations after doses of 1.0 to 0.67 mg/kg is 1.24 whereas for a linear system it should be 1.49. This violation of the scaling property of linear systems indicates a nonlinearity in the gain of the system. The model structure shown in Figure 15 was developed to address these issues. Because of the characteristic difference between plasm a concentration versus time profiles after a low doses (0.44 mg/kg) and after higher doses (0.67 and 1.0 mg/kg), a two pathway approach was considered. The drug mass below a threshold takes one pathway and the mass of drug above that threshold takes another. The portion of the model in Figure 15 bounded by the dotted line was developed in order to characterize the response after a dose of 0.44 mg/kg. The mass of 9NC administered below the Threshold, d_l, pases through two identical first order systems characterized by τ_l. A fraction, β_1, of the mass in X_3 is recycled as an input to G_r. The remainder, α_1, of X_3 is present in the plasma. This portion of the model is linear and characterized by four parameters (τ_l, α_1, τ_r, and K_l). These parameters were estimated and fixed, and the portion of the model bounded by the dashed line was added. This additional model contribution characterized the disposition of 9NC after higher doses (0.67 and 1.0 mg/kg). The mass of 9NC above the threshold, d_u, undergoes dynamics governed by two first order systems in series. These systems, G_u, were characterized by τ_u, and the mass X_1 was converted into concentration using K_u. There was one nonlinear component in this portion of the model — the inverse relationship between the gain, K_u, and the most recent dose administered, D_{last}. The nonlinear gain was defined as:

$$K_{nl} = \frac{K_u}{D_{last}}$$

The two portions of the model discussed above represent the dynamics of 9NC. The remainder of the model characterized the dynamics of 9AC. The total mass of 9NC, $\alpha_1 X_3$

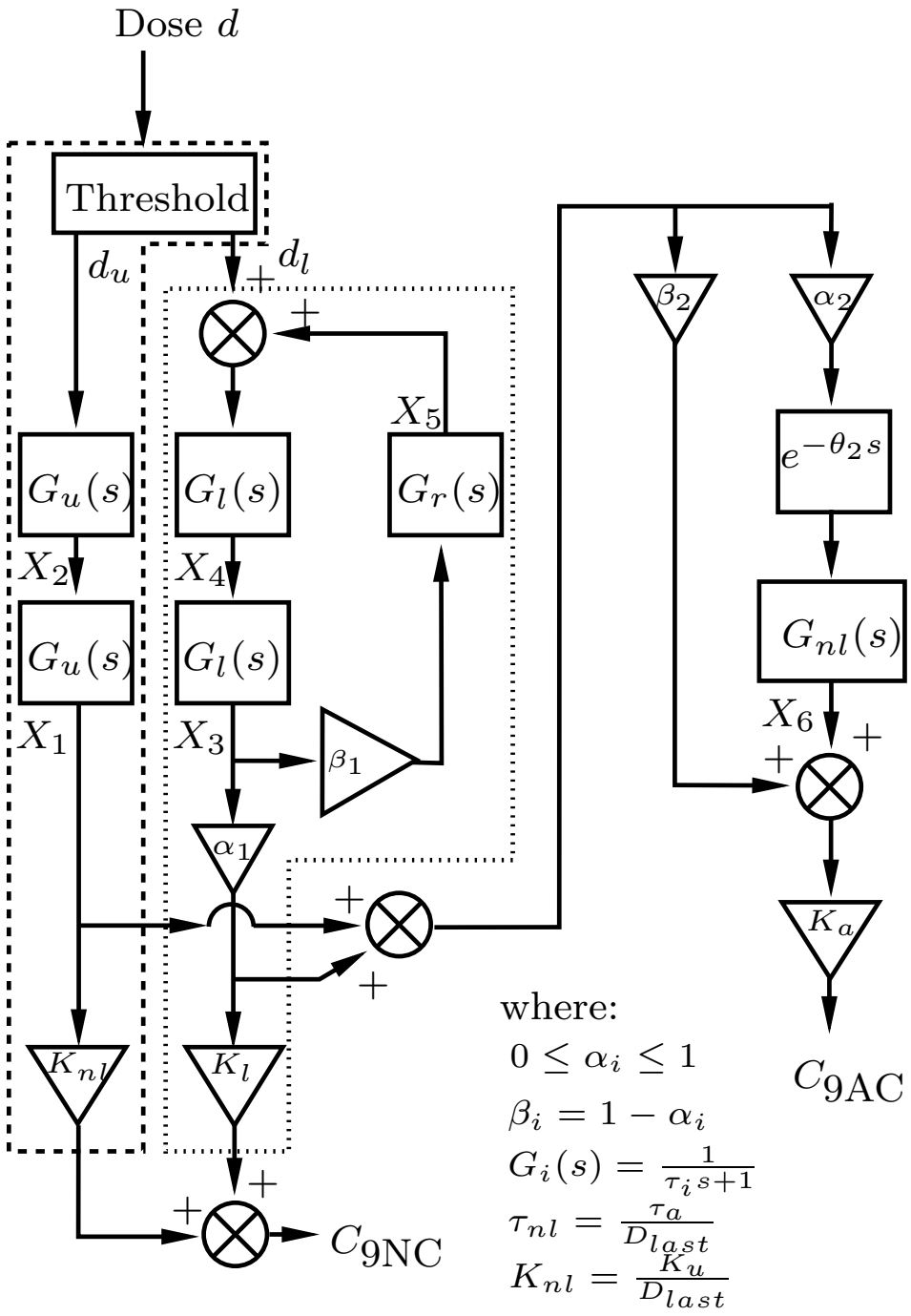

Figure 15: Nonlinear PK model for the total forms of 9NC and 9AC. Both the gain K_{nl} and time constant τ_{nl} are nonlinear in the most recent dose applied D_{last}.

and X_1 resulting from dose masses below and above the threshold, respectively, is split into two pathways. A fraction of 9NC, β_2, is converted directly to 9AC. The remaining fraction, α_2, experienced a time delay of length θ_2 and the dynamics G_{nl} before being converted to 9AC. The portion of the model which describes the conversion of 9NC to 9AC is linear with the exception of the nonlinear time constant, τ_{nl}, which is inversely proportional to the dose. This was done to account for the more rapid elimination of 9AC observed at higher doses (Figure 14). The ODE representation of Figure 15 is given as:

$$\dot{x}_1(t) = \frac{x_2(t)}{\tau_u} - \frac{x_1(t)}{\tau_u} \tag{2.9a}$$

$$\dot{x}_2(t) = \frac{D_u(t)}{\tau_u} - \frac{x_2(t)}{\tau_u} \tag{2.9b}$$

$$\dot{x}_3(t) = \frac{x_4(t)}{\tau_l} - \frac{x_3(t)}{\tau_l} \tag{2.9c}$$

$$\dot{x}_4(t) = \frac{D_l(t) + x_5(t)}{\tau_l} - \frac{x_4(t)}{\tau_l} \tag{2.9d}$$

$$\dot{x}_5(t) = \beta_1 \frac{x_3(t)}{\tau_r} - \frac{x_5(t)}{\tau_r} \tag{2.9e}$$

$$\dot{x}_6(t) = \alpha_2(x_1(t-\theta_2) + \alpha_1 x_3(t-\theta_2))\mathcal{H}(t-\theta_2)\frac{D_{last}}{\tau_{nl}} - x_6(t)\frac{D_{last}}{\tau_{nl}} \tag{2.9f}$$

$$C_{\text{NC}} = x_1(t)\frac{K_u}{D_{last}} + K_l\alpha_1 x_3(t) \tag{2.9g}$$

$$C_{\text{AC}} = (x_1(t) + x_3(t)\alpha_1)\beta_2 K_a + x_6(t)K_a \tag{2.9h}$$

Here D_{last} is the value of the last nonzero dose in mg/kg. The values of $D_l(t)$ and $D_u(t)$ are defined in terms of $D(t)$ and the Threshold as follows:

$$D_l(t) = \begin{cases} D(t) & D(t) \leq \text{Threshold} \\ \text{Threshold} & D(t) > \text{Threshold} \end{cases} \tag{2.10}$$

$$D_u(t) = \begin{cases} 0 & D(t) \leq \text{Threshold} \\ D(t) - \text{Threshold} & D(t) > \text{Threshold} \end{cases} \tag{2.11}$$

Here $D(t)$, $D_l(t)$, $D_u(t)$ and Threshold are all defined in terms of drug mass. The parameters for the model (2.9) are shown in Table 7. The predicted responses from the model are also shown in Figure 14 for each of the three dose levels. The model captures the characteristic shape of the 9NC responses well. The 9AC responses for 1.0 and 0.44 mg/kg are also also

Table 7: PK parameters for the nonlinear model of the total forms of 9NC and 9AC.

Threshold	9.078×10^3	ng–9NC
τ_u	12.36	min
τ_l	1.482	min
τ_r	0.184	min
τ_{nl}	107.98	min
α_1	0.64	—
α_2	0.468	—
K_{nl}	0.216	ml^{-1}
K_l	0.162	ml^{-1}
K_a	0.0491	ml^{-1}
θ_2	49.20	min

described by the model. The 9AC data for 0.67 mg/kg at 15 and 30 min exhibit behavior which this model structure is unable to capture. The key shortcoming of the nonlinear PK model is its inability to capture the dynamics of the delayed peak in 9AC ($15 \leq t \leq 30$ min) for a dose of 0.67 mg/kg. The analytical methods used to determine the total concentrations of 9NC and 9AC in response to 0.44 and 1.0 mg/kg are considered to be more reliable. Consequently, greater importance was placed on these data for modeling purposes. Given the relative concentrations of 9NC and 9AC, however, the overall performance is quite good.

2.5 SUMMARY OF PK MODELS

In this chapter several different model structures were presented to describe the PK of 9NC in SCID mice. Linear models were developed using two datasets of plasma lactone concentrations of 9NC and 9AC obtained from tumor–bearing and normal SCID mice after oral administration of 0.67 mg/kg of 9NC. The compartmental model structure lacked

predictive accuracy A two timescale model was developed which reduced the number of parameters from ten to nine and improved the model fit of the individual datasets. A recycle model was developed which further reduced the number of parameters to eight. Although the two timescale model better represented the individual data sets, the recycle model provided superior fit to the combined data as measured by AIC. Experimental data were obtained for the total concentrations of 9NC and 9AC after oral administration of 9NC at 0.44, 0.67 and 1.0 mg/kg. Analysis of the average response of these data showed the existence of nonlinear behavior dependent on the dose levels. A nonlinear PK model was developed to capture the nonlinear dynamics. Both the lactone and total PK models exhibit novel structures. By developing these models in the Laplace domain, structures were selected such that parameters were associated with specific behavior. Using this methodology, time points associated with significant variability could be associated with specific parameters. This was demonstrated in the description of the parametric variability of the recycle model.

The objective of this work is to utilize mathematical descriptions of cancer chemotherapy to derive treatment schedules. The PK models developed in this chapter were constructed to drive PD models of toxicity and efficacy. Much effort was made to accurately describe the dynamic PK response under the assumption that model quality limits achievable controller performance [8]. The structures were also selected with the objective of controller synthesis in mind. Linear PK models were selected because control methodologies for linear systems are well understood. Of the linear PK models presented, the recycle model structure was found to be superior based on AIC values as well as being the model structure with the fewest parameters. However, if the linear descriptions are unable to achieve desired results (in a control sense), the nonlinear PK model can be utilized. The nonlinear PK model was found to accurately describe the plasma concentrations of 9NC and 9AC total in response to a range of doses. From a PK/PD modeling perspective, linear PK models will first be considered and nonlinear models will be investigated for their ability to predict a broader range of PK responses.

3.0 PHARMACODYNAMIC MODELING

Drugs are administered to elicit an effect; however, side effects are common. In cancer chemotherapy, the desired effect is the reduction of tumor burden. Chemotherapy is a systemic form of treatment with side effects including the reduction of the patient's immune system performance, neurotoxicity, and loss of body weight, among others. PD models are mathematical representations of the various effects of the drug. In this chapter the progression of the disease in the absence of treatment is characterized first. For the SCID mouse case study, growth of the HT29 human colon carcinoma xenografts is modeled in the absence of treatment. The untreated tumor growth model is then combined with an average PK model and data from mice treated with 9NC is used to develop a PK/PD description of drug effect. This combined PK/PD representation was further used to develop a model of drug toxicity using body weight reductions as an indicator since mice receiving 9NC develop diarrhea leading to loss of body weight.

3.1 TUMOR GROWTH MODELING

3.1.1 Cell–Cycle

Figure 2 in Chapter 1 shows the five phases of the cell–cycle with the rate of transition between states given by the various k_i parameters. The quiescent, or resting, state of a cell is given by G_0. When cells are actively proliferating, they readily move through the other phases of the cell–cycle. The S and M phases represent the phases in which DNA is synthesized and mitosis occurs, respectively, and they are separated by the growth phases

G_1 and G_2 [2]. Most cells of healthy tissues in adults spend a majority of their time in the quiescent G_0 phase [2]. However, this is not so for cancer cells. Conceptually, cancerous cells can be thought of to have a combination of higher values of k's within the cell–cycle and a higher ratio of k_{G01} to k_{G10} than normal tissues. Treating the phases of the cell–cycle as compartments, the cell–cycle can be modeled in the following manner:

$$\dot{G}_0(t) = k_{G10}G_1(t) - k_{G01}G_0(t) \tag{3.1a}$$

$$\dot{G}_1(t) = k_{G01}G_0(t) - k_{G10}G_1(t)\boxed{+2k_M M(t)} - k_{G1}G_1(t) \tag{3.1b}$$

$$\dot{S}(t) = k_{G1}G_1(t) - k_S S(t) \tag{3.1c}$$

$$\dot{G}_2(t) = k_S S(t) - k_{G2}G_2(t) \tag{3.1d}$$

$$\dot{M}(t) = k_{G2}G_2(t)\boxed{-k_M M(t)} \tag{3.1e}$$

$$N(t) = G_0(t) + G_1(t) + S(t) + G_2(t) + M(t) \tag{3.1f}$$

The total number of cancer cells is given by N. Tumor size can be either a volume (as measured experimentally) or a total number of cancerous cells as mentioned above. The volume of a tumor is considered to be proportional to the number of tumor cells. The constant of proportionality is 1000π μm^3, which assumes cells of spherical shape and a radius of 10 μm. The description in equation (3.1) is linear and mitotic proliferation is highlighted by the boxed terms in (3.1b) and (3.1e) — for every cell leaving M two cells enter G_1. While the transition rates in (3.1) are written as constants, they can just as easily be functions of time, average cell age, or the number of cells in a particular phase. Using transition rates which are not constants will result in a set of nonlinear equations. A major drawback of cell–cycle models is that identification of the parameters in (3.1) requires measurements of the different phases of the cell–cycle at different points in time. At present this is not an obtainable measurement for solid tumors in a clinical setting.

3.1.2 Macroscopic Growth Models

HT29 tumor growth data, like much experimental data, was macroscopic in nature. Detailed tumor growth models, like the cell–cycle model above, become over–parameterized in the

context of available preclinical data. Hence, lumped-parameter growth models were used in this work.

3.1.3 Exponential Growth Model

Exponential growth is described in terms of a doubling time, τ_e, and the following first–order linear ODE [63]:

$$\dot{N}_e = \frac{\ln(2)}{\tau_e} N_e \tag{3.2}$$

Here N_e represents the size of the tumor. Well–nourished tumor cells will proliferate exponentially, and empirical evidence suggests that tumors initially undergo an exponential growth phase [11].

3.1.4 Gompertz Growth Model

As tumor size increases, the tumor growth slows as the mass approaches a plateau population [11]. This type of growth is normally described using the Gompertz equation [12, 32]:

$$\dot{N}_g = \frac{1}{\tau_g} \ln\left[\frac{\ln(\rho_g/N_0)}{\ln(\rho_g/2N_0)}\right] N_g \ln\left(\frac{\rho_g}{N_g}\right) \tag{3.3}$$

Here ρ_g is the plateau population, N_0 is the initial number of tumor cells, and τ_g is the doubling time of the tumor during exponential growth [12].

3.1.5 Switched Exponential Growth Model

To characterize the Gompertz equation (3.3), data from the plateau region of growth must be obtained. However, many animals would succumb to the tumor burden and die before entering this region of growth [32]. In the xenograft model evaluated here, the tumor-bearing animals were euthanized for ethical reasons before their tumors approached the plateau population. Hence, data from these animals encompasses the exponential phase of growth and a portion of the transition from exponential to Gompertzian growth, but ρ_g is not

uniquely identifiable. To fit the data in the transition between exponential and Gompertzian growth, a modification was made to the exponential growth model (3.2):

$$\dot{N}_s = \frac{\ln 2}{\tau_e(N_s)} N_s \tag{3.4a}$$

$$\tau_e(N_s) = \begin{cases} \tau_{e,f}, & N_s < N_{th} \\ \tau_{e,s}, & N_s > N_{th} \end{cases} \tag{3.4b}$$

Equation (3.4) is referred to as a switched exponential model, and it is a modification of the model presented by Simeoni *et al.* which used a nonlinear continuous function to describe the transition from exponential to Gompertzian growth [14]. In the present study, a piecewise continuous function was used here because the discontinuity is more amenable to controller design in a mixed–integer programming framework. The model in (3.4) is structurally similar to the exponential model (3.2); however, τ_e is dependent on the current size of the tumor. The cancerous mass increases at a rate $\tau_{e,f}$ until the tumor size reaches the threshold size, N_{th}. At this point, the rate of proliferation slows to $\tau_{e,s}$.

3.1.6 Model Comparison

The models from equations (3.2),(3.3), and (3.4) assume a homogeneous population of cells. Each of these model structures are shown for comparison in Figure 16. All model predictions are essentially identical for the first doubling time (τ time units). At this point the cells under Gompertzian growth begin to proliferate less rapidly due to the nonlinear growth dynamics. The switched exponential model is capable of tracking the Gompertzian growth curve over a longer period of time when compared to the exponential model — approximately 3.5τ and 1τ, respectively. Hence, the switched exponential model is expected to provide a superior fit to tumor growth data that grows sub–exponentially but cannot fully inform a Gompertzian plateau population estimate.

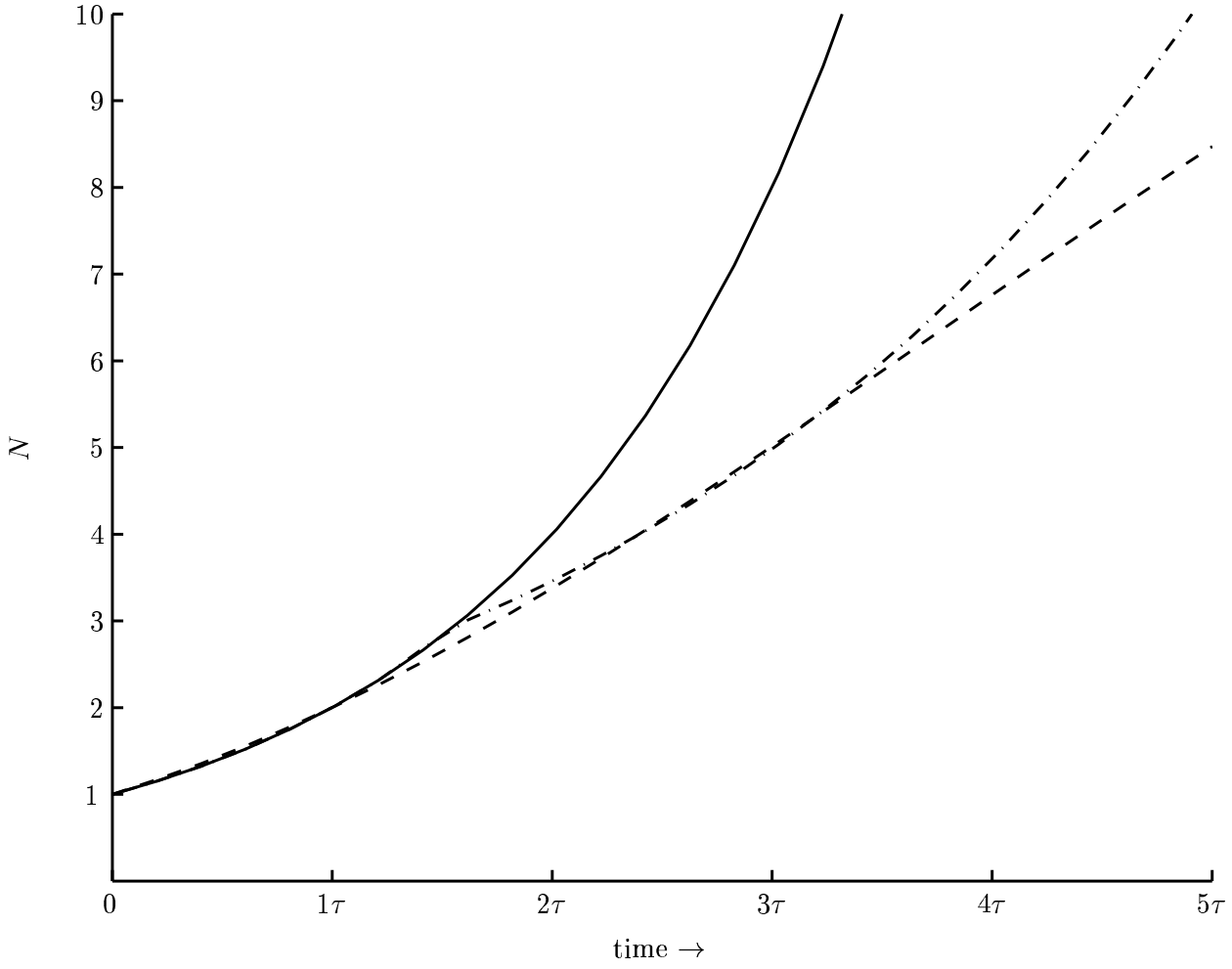

Figure 16: Normalized ($N_0 = 1$) predictions for exponential (—), Gompertzian (−−), and switched exponential (-·-) tumor growth models of untreated cancer growth. Here, τ is τ_e for the exponential model, τ_g for the Gompertzian model, and $\tau_{e,s}$ for the switched exponential model. Parameter values used: $\tau_e = \tau_g = \tau_{e,f} = 2$, $\tau_{e,s} = 3.8$, $\rho_g = 17$, and $N_{th} = 3$

3.2 UNTREATED TUMOR GROWTH MODELING RESULTS

3.2.1 Exponential Growth Model

Untreated tumor growth was modeled for twenty control mice using equation (3.2). The tumor doubling time, τ_e, was estimated for each of the twenty mice, and the average, $\bar{\tau}_e$, was taken to represent the population. The results are shown in Figure 17. These tumor volumes were from separate two studies, and the symbols represent the mean values at each time point normalized to the corresponding initial volumes. The model prediction shown is for the average doubling time, $\bar{\tau}_e \approx 11$ days. One standard deviation in τ_e, approximately 2.3 days, characterizes the observed inter-subject variability in growth rate. The mean model successfully captures the growth dynamics in the experimental data, although slight model underprediction is observed early in the growth trajectory. The doubling time was held constant at $\bar{\tau}_e$ for subsequent modeling of PD drug effect.

3.2.2 Switched Exponential Growth Model

To better characterize untreated tumor growth, the switched exponential model (3.4) was used. Individual parameter estimates were obtained for the same twenty mice. The model prediction is shown with the data from twenty mice in Figure 18. To calculate the lower standard deviation and upper standard deviation used in Figure 18, the largest possible bounds were used ($\bar{N}_{th}$ − std., $\bar{\tau}_{e,f}$ + std., and $\bar{\tau}_{e,s}$ + std.) and ($\bar{N}_{th}$ + std., $\bar{\tau}_{e,f}$ − std., and $\bar{\tau}_{e,s}$ − std.), respectively. The parameter values and their standard deviations are shown in Table 8.

3.2.3 Untreated Growth Model Comparison

To compare the exponential and switched exponential models, the AIC values for the individual animals were calculated and are given in Table 9. The model with two distinct regions of growth consistently outperforms the exponential model. To quantify the effects of using mean parameter estimates, mean AIC values were calculated for each study and for both

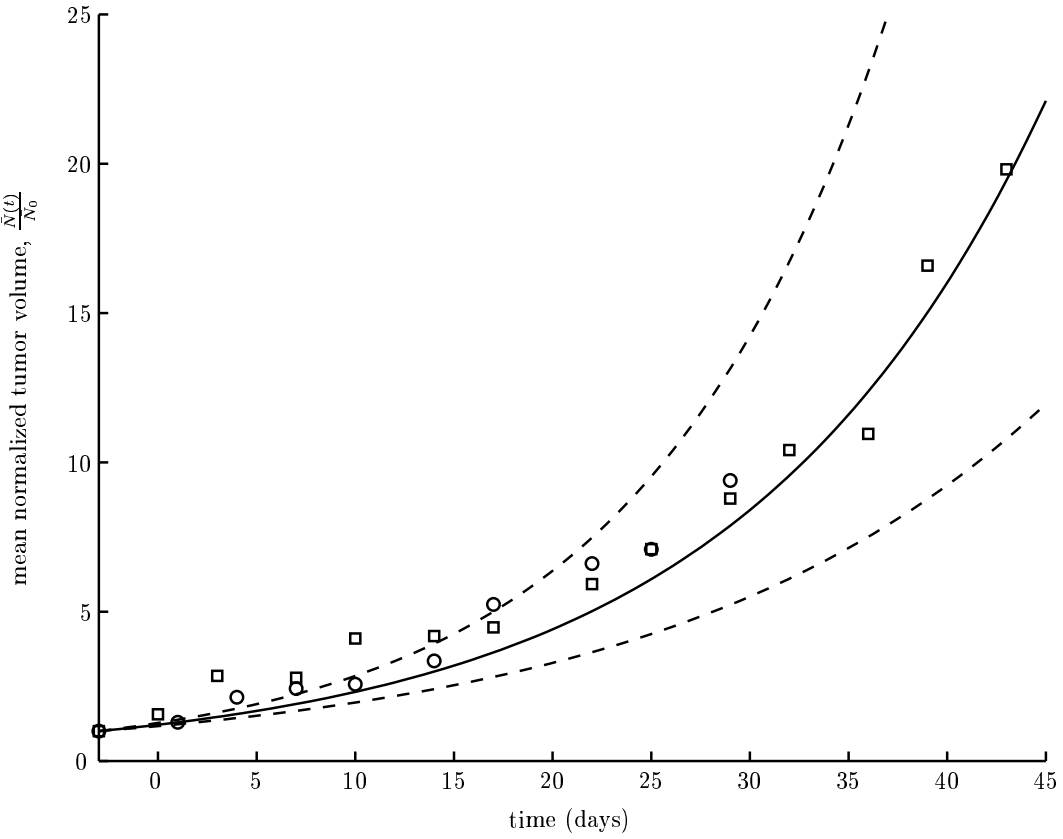

Figure 17: Mean exponential growth model prediction, (—), and one standard deviation in growth rate, (−−), based on individual estimates of τ_e from twenty mice in two studies. The average values of control mice from the first (□) and second (○) studies are also shown normalized to their initial tumor volumes.

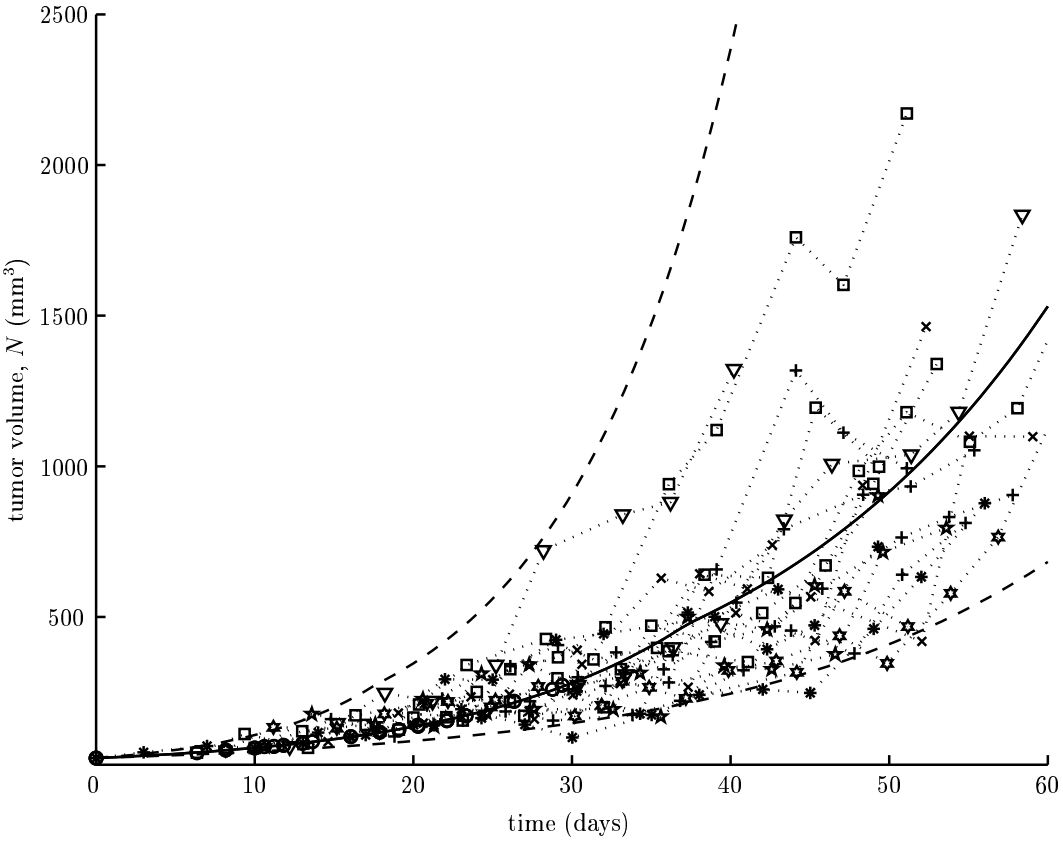

Figure 18: Mean switched exponential growth model prediction, (—), and one standard deviation in growth rate, (−−), based on individual estimates of N_{th}, $\tau_{e,f}$, and $\tau_{e,s}$ from twenty mice in two studies (markers connected by $\cdots$). Initial time points were shifted such that the initial volumes (**o**) would lie on the average model prediction.

Table 8: Mean parameter estimates for switched exponential model of tumor growth calculated from twenty untreated mice.

	Mean	Std. Dev.	
$\bar{N}_{th}$	477.36	183.10	mm^3
$\bar{\tau}_{e,f}$	9.56	3.94	days
$\bar{\tau}_{e,s}$	13.49	7.17	days

studies combined. To calculate the AIC for multiple data sets, sum squared error between all of the data points in each study and the average model prediction were added together and used as the SSE in the AIC calculation (2.5). All of the points used in the SSE calculation were added together as the "number of points". The "number of model parameters" were one and three for the exponential and switched exponential models, respectively. The mean values for each study are also shown in Table 9. For the first study, AIC values favor the switched exponential model based on parameter estimates for both the individuals and the mean. The mean parameters would suggest the exponential model is better at representing the data in study two. These results are not surprising and can be explained by considering Figure 17. The data for study two stop on day 30 because this efficacy trial was halted due to toxicity. No information is available at later time points; hence, $\tau_{e,s}$ and N_{th} cannot be adequately estimated. To better quantify this statement, consider $\bar{N}_{th}$ from Table 8 and Figure 18. The average model predicts $\bar{N}_{th}$ to occur between 35 and 40 days (based on tumor volume predictions), so only a small fraction of the data (10-14%) from study two occurs during the portion of the model where $\tau_{e,s}$ would be active.

3.3 EFFECT MODELING

PD models relate the administration of drugs to observable effects. The effects considered here focus primarily on reductions in both tumor volume (efficacy) and body weight (toxic-

Table 9: AIC for the exponential (3.2) and switched exponential (3.4) models applied to two studies of untreated tumor growth.

Mouse	Exponential		Switched Exponential	
	Study 1	Study 2	Study 1	Study 2
1	92.92	108.65	84.32	77.72
2	80.28	122.97	79.20	120.53
3	78.55	105.30	72.22	100.59
4	70.82	109.85	67.70	106.20
5	102.93	114.83	90.83	111.15
6	87.15	111.76	85.86	106.02
7	81.91	116.23	78.79	93.83
8	84.44	128.80	65.70	123.88
9	90.50	127.63	77.96	125.75
10	100.41	123.25	98.67	103.23
Mean	1036.55	**1343.07**	**1030.06**	1358.95
	2401.07		**2397.14**	

ity). PD effect models can be a simple correlation between an amount of drug administered and decreased mortality rates after a period of time (*e.g.*, 6 months). Alternatively, a more mechanistic approach can be used to relate the drug PK directly to the PD effects. The tumor growth models developed in sections 3.1.3, 3.1.5, and 3.1.6 for the growth of HT29 xenografts in SCID mice establish a nominal description of tumor growth. The presence of the drug, in this case 9NC and 9AC, can be considered a perturbation of this nominal description.

The circulatory system is the primary method for transporting systemically delivered drugs to cancerous tissues is. PK models which relate drug delivery to drug plasma concentration, which can be further coupled to PD effect. Plasma drug concentration predictions can be used to approximate drug concentrations at the site of the tumor based on the rationale that tumors have highly permeable capillaries and are well perfused. The therapeutic effect of the drug on the tumor is then represented mathematically by adding a bilinear kill term to the nominal tumor growth equation. The added nonlinear term is proportional to both the current size of the tumor and the concentration of the drug [12]. The motivation for this functionality is that larger tumors will have more susceptible cells, and higher drug plasma concentrations will more effectively kill tumor cells. Because 9NC inhibits topoisomerase-I, DNA synthesis cannot be completed and tumor cells are stopped in the S phase of the cell–cycle. To incorporate this effect, equation (3.1c) would be modified in the following manner:

$$\dot{S}(t) = k_{G1}G_1(t) - k_S S(t) - k_{eff}C_{eff}(t)S(t) \tag{3.5}$$

Here, $C_{eff}(t)$ is the drug concentration at the site of action. This could be the plasma drug concentration as predicted from a PK model; alternatively, additional functionality, such as delays, nonlinear dynamics, etc., specific to the problem could be included. For example, a drug with effects proportional to the amount of drug above a therapeutic concentration, C_{th}, would define C_{eff} in terms of the plasma concentration of the drug, $C(t)$, as:

$$C_{eff}(t) = (C(t) - C_{th})\mathcal{H}(C(t) - C_{th})$$

The proportionality constant for drug effectiveness is k_{eff}. The exponential and Gompertz models can be augmented with similar PK/PD functionality as follows:

$$\dot{N}_e = \frac{\ln(2)}{\tau_e} N_e(t) - k_{eff} C_{eff}(t) N_e(t) \tag{3.6a}$$

$$\dot{N}_g = \frac{1}{\tau_g} \ln\left[\frac{\ln(\rho_g/N_0)}{\ln(\rho_g/2N_0)}\right] N_g(t) \ln\left[\frac{\rho_g}{N_g(t)}\right] - k_{eff} C_{eff}(t) N_g(t) \tag{3.6b}$$

Since equations (3.6a) and (3.6b) are lumped approximations, they lack the cycle–specificity of the cell–cycle model. Therefore, the effect term is proportional to the total tumor volume.

3.4 PD DRIVEN BY LINEAR PK MODEL

The complexity associated with control algorithm synthesis scales with the complexity of the system models. For the models presented here, a PK/PD model can be derived by combining linear PK with exponential tumor growth. To characterize the anticancer effects of 9NC, the nominal tumor growth model (3.2), developed in section 3.2.1, was combined with the recycle PK model of 9NC lactone and 9AC lactone (2.8) from subsection 2.3.3 in the following manner:

$$\dot{N}(t) = \frac{\ln(2)}{\bar{\tau}_e} N(t) - k_{eff,\mathrm{NCL}} C_{eff,\mathrm{NCL}}(t) N(t) - k_{eff,\mathrm{ACL}} C_{eff,\mathrm{ACL}}(t) N(t) \tag{3.7a}$$

$$C_{eff,\mathrm{NCL}}(t) = \bar{C}_{\mathrm{NCL}}(t - \theta_{eff}) \mathcal{H}(t - \theta_{eff}) \tag{3.7b}$$

$$C_{eff,\mathrm{ACL}}(t) = \bar{C}_{\mathrm{ACL}}(t - \theta_{eff}) \mathcal{H}(t - \theta_{eff}) \tag{3.7c}$$

In the absence of treatment, the tumor proliferates according to the average exponential growth rate, $\bar{\tau}_e$. The average parameter values for the recycle model, found in Table 6, are used to predict $\bar{C}_{\mathrm{NCL}}(t)$ and $\bar{C}_{\mathrm{ACL}}(t)$, the lactone concentrations of 9NC and 9AC, respectively, after 9NC oral administration. The effect terms $k_{eff,\mathrm{NCL}}$ and $k_{eff,\mathrm{NCL}}$ represent the effectiveness of 9NC lactone and 9AC lactone, respectively. To improve the fit to experimental observations, the drug concentrations were delayed by θ_{eff} time units. The effective concentrations of 9NC lactone and 9AC lactone were then defined in terms of $\bar{C}_{\mathrm{NCL}}(t)$, $\bar{C}_{\mathrm{ACL}}(t)$, and θ_{eff} by $\bar{C}_{eff,\mathrm{NCL}}(t)$, and $\bar{C}_{eff,\mathrm{ACL}}(t)$, respectively. This model

Table 10: Mean PD parameters for the effect of the lactone forms of 9NC and 9AC.

	$\bar{k}_{eff,\text{NCL}}\left(\frac{\text{ml}}{\text{day–ng9NC}}\right)$	$\bar{k}_{eff,\text{ACL}}\left(\frac{\text{ml}}{\text{day–ng9AC}}\right)$	$\bar{\theta}_{eff}$ (days)
Mean	2.42×10^{-5}	3.19×10^{-5}	0.7840
Std. Dev.	8.08×10^{-6}	2.54×10^{-5}	0.3778

was fit to the tumor growth data from the ten mice administered 0.67 mg/kg of 9NC on a QD×5×2 schedule. The average values for the PD parameters are given in Table 10. The values of $\bar{k}_{eff,\text{NCL}}$ and $\bar{k}_{eff,\text{ACL}}$ from Table 10 are similar given the observed variability in $\bar{k}_{eff,\text{NCL}}$. One interpretation would be that the two compounds have similar activity. This is consistent with *in vitro* studies [64]. Further analysis is complicated by the drug concentration differences (9NC lactone concentration is an order of magnitude higher than 9AC lactone). Furthermore, parameter variances indicate that a significant statement about the relative efficacy of 9NC and 9AC cannot be made. Finally, from a mathematical perspective, reducing k_{ac} while simultaneously increasing k_{nc} might result in essentially the same PD model prediction; hence a categorical statement of parent/metabolite activity (9NC versus 9AC) based on present data would be premature. Model fit to ten individual mice are shown in Figure 19. While the intersubject variability seen in the data cannot be fully captured by a model of mean behavior, the model was capable of predicting decreases in tumor volume in response to treatment, which is necessary for developing useful treatment algorithms.

By combining a linear PK model (2.8) with a linear growth model (3.2) a PD structure (3.7) has been developed which will be shown to be quite amenable to control algorithm synthesis in Chapter 4. However, this efficacy model was developed using data obtained at a single dose level. To improve the predictive capacity of the PK/PD model over a range of dose levels, a more complex structure was investigated.

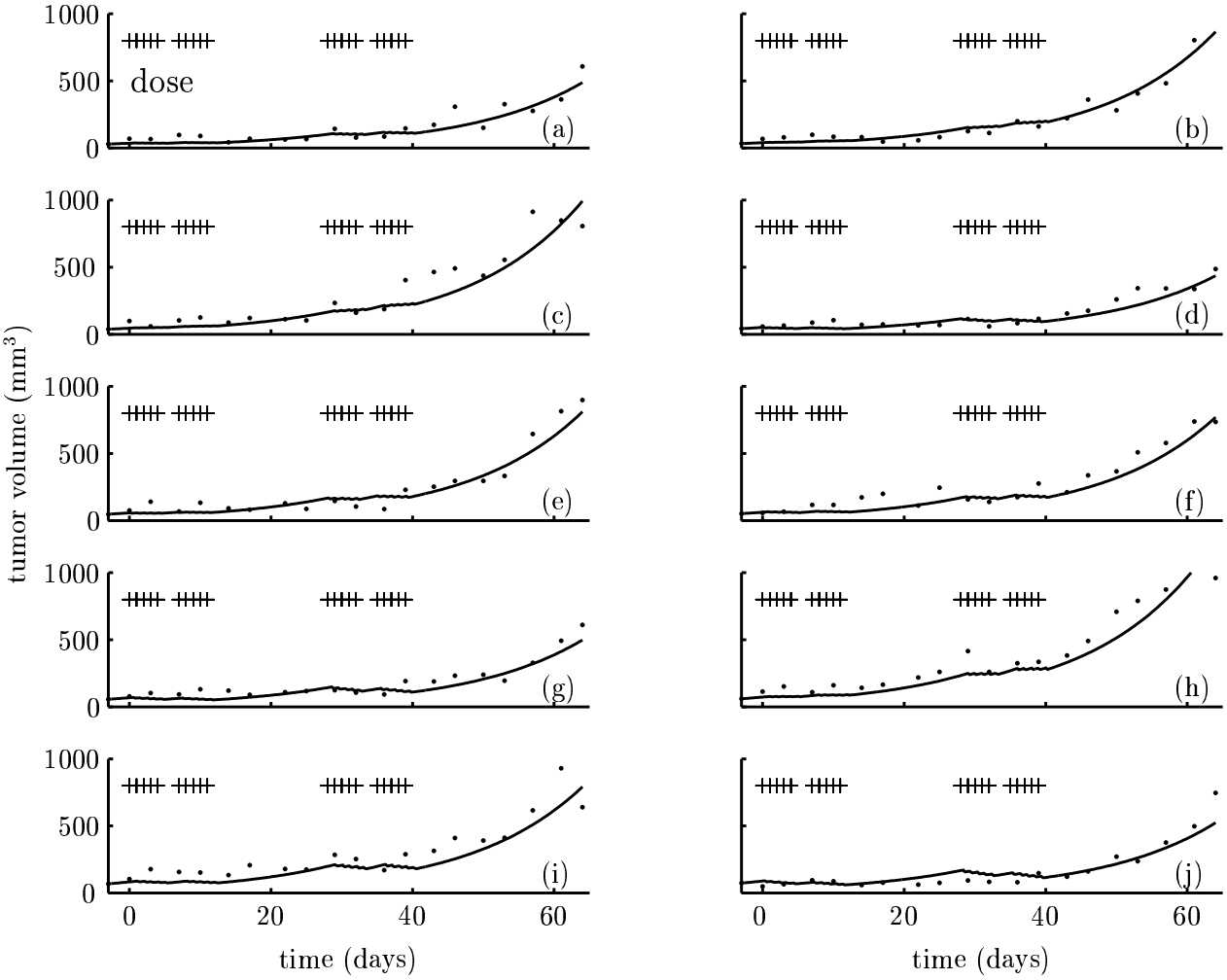

Figure 19: PK/PD model response using average PK predictions from the linear recycle model (2.8) with the PD model shown in equation (3.7). Tumor volume measurements are given by (·) with the drug administered at 0.67 mg/kg on days indicated by (+), and the model prediction is represented by (—).

3.5 PD DRIVEN BY NONLINEAR PK MODEL

To characterize the PD effect over a range of doses, the nonlinear PK model given in equation (2.9) was combined with the switched exponential growth model for untreated cancer (3.4) to provide the following PK/PD model:

$$\dot{N}_s(t) = \frac{\ln(2)}{\bar{\tau}_e(N_s(t))} N_s(t) - k_{eff} C_{eff}(t) N_s(t) \tag{3.8a}$$

$$\bar{\tau}_e(N_s(t)) = \begin{cases} \bar{\tau}_{e,f}, & N_s(t) < \bar{N}_{th} \\ \bar{\tau}_{e,s}, & N_s(t) > \bar{N}_{th} \end{cases} \tag{3.8b}$$

$$C_{eff}(t) = C_{\mathrm{NC}}(t) + C_{\mathrm{AC}}(t) \tag{3.8c}$$

The rate of proliferation is governed by the switched exponential growth model in the absence of drug. When drug is administered, proliferation decreases at a rate proportional to the size of the tumor and $C_{eff}(t)$. The total plasma concentration of 9NC and 9AC was used here based on the rationale that they have similar activities [64]. The concentrations of 9NC and 9AC total, C_{NC} and C_{AC}, respectively, were calculated using the parameters from Table 7. To describe nominal tumor growth, the average values for the switched exponential model parameters given in Table 8 were used. The PK/PD model has a single free parameter, k_{eff}, which was fit individually to thirty mice — three sets of ten mice administered 0.44, 0.67 and 1.0 mg/kg of 9NC QD×5×2. The results for the three different dose levels are shown in Figures 20, 21, and 22, respectively. There are instances where the proposed model structure does not accurately fit the data (*e.g.* Figure 20(i)). In general, however, the model structure (3.8) captures the tumor growth response to 9NC treatment at the three different dose levels. At higher dose levels (Figure 22), the model predicts tumor volume decreases consistent with the experimental data. This ability to predict responses across dose levels is important for the development of treatment algorithms. Figure 23 presents the parameter distribution for k_{eff}. he average value of k_{eff} for the 0.44 mg/kg dose of 9NC was slightly higher than k_{eff} for 9NC doses of 0.67 and 1.0 mg/kg. However, given the parameter distributions at each dose level, the parameter values are not statistically different between dose levels. The time profiles for the product of k_{eff} and the sum of camptothecin concentration and the

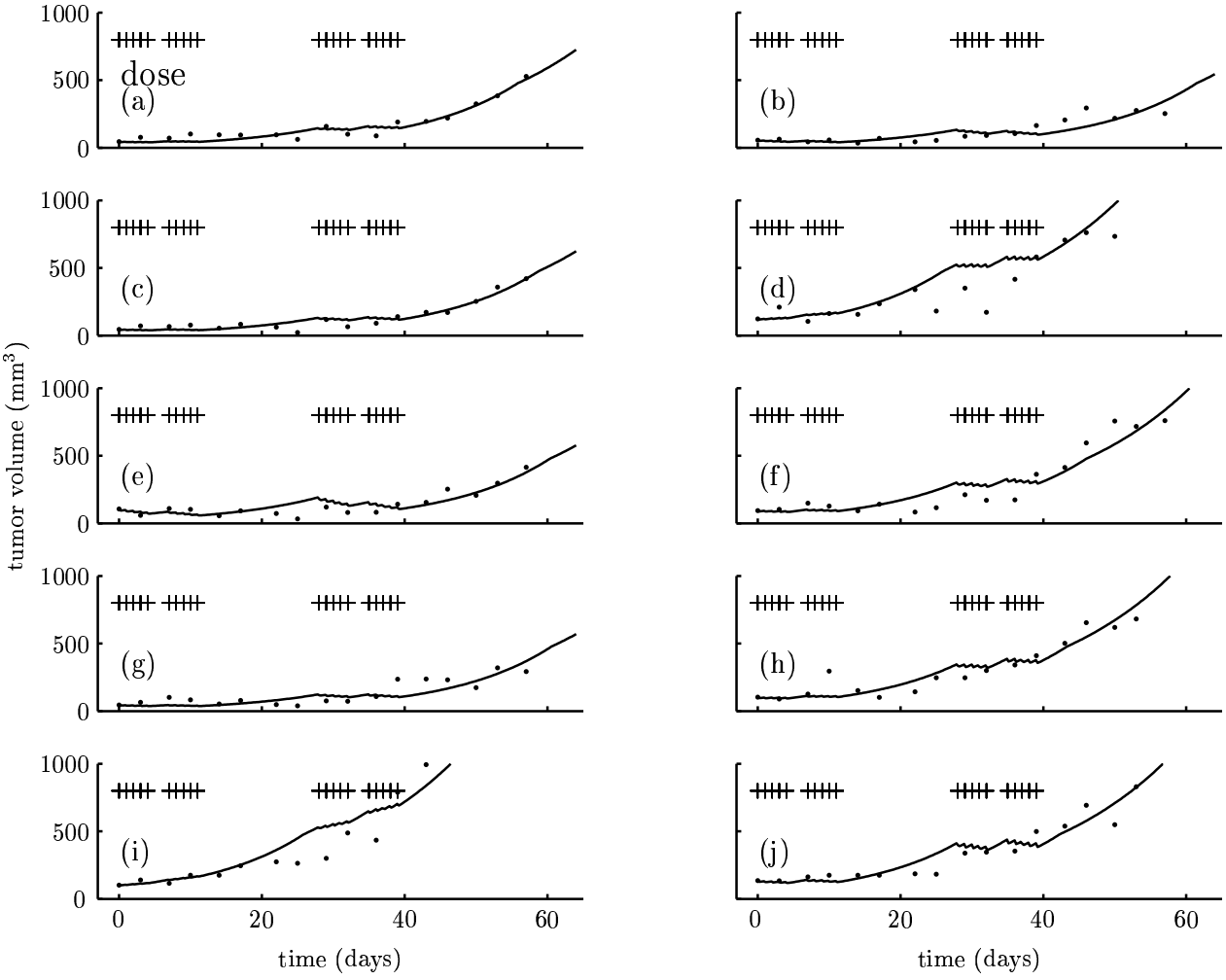

Figure 20: PK/PD model response using predictions from the nonlinear PK model (2.9) with the PD model shown in equation (3.8). Tumor volume measurements are given by (·). Drug was administered at 0.44 mg/kg QD×5×2 on days indicated by (+), and the model prediction is represented by (—). Data for mouse (i) after day 42 lies outside of the plot range.

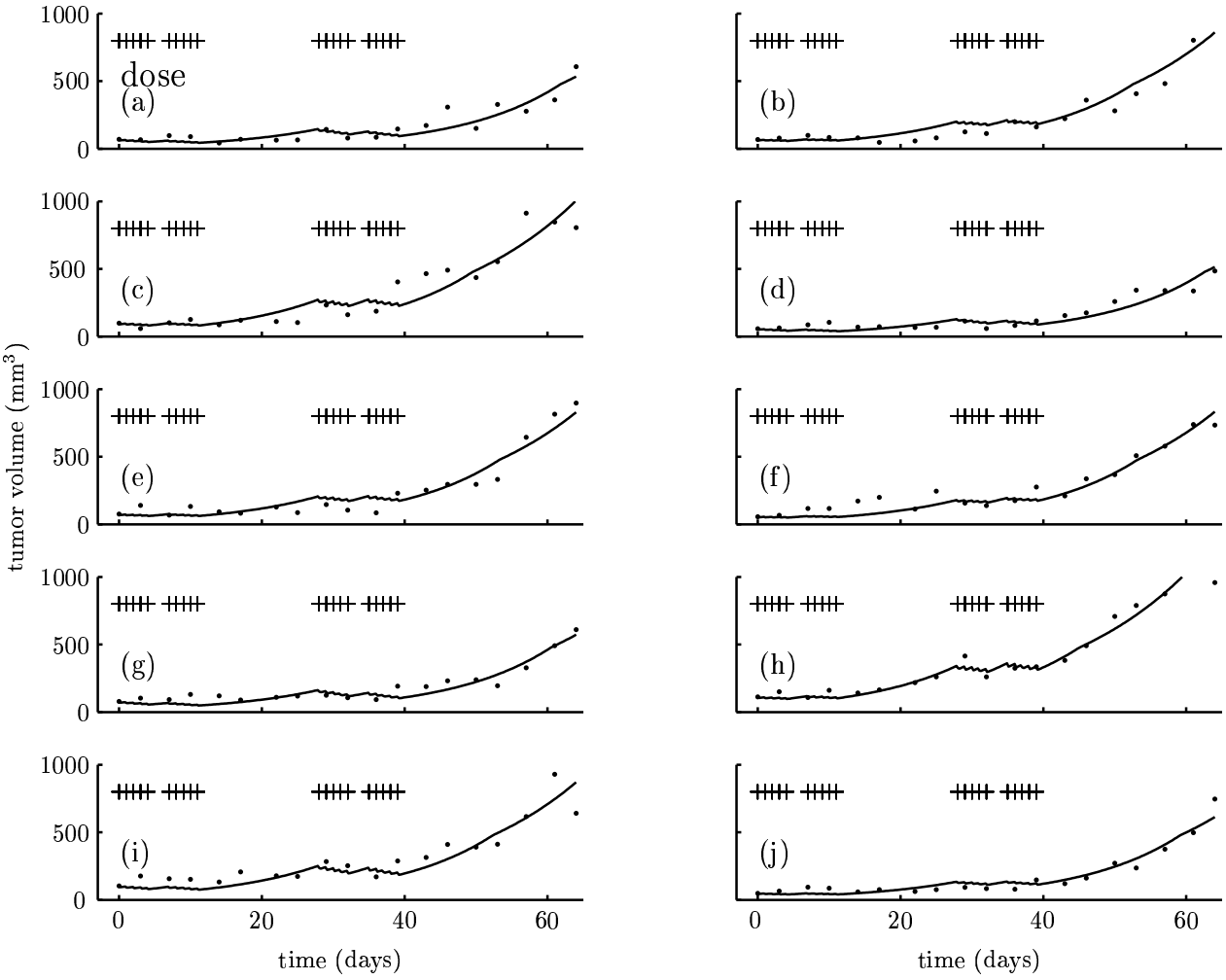

Figure 21: PK/PD model response using predictions from the nonlinear PK model (2.9) with the PD model shown in equation (3.8). Tumor volume measurements are given by (·). Drug was administered at 0.67 mg/kg QD×5×2 on days indicated by (+), and the model prediction is represented by (—).

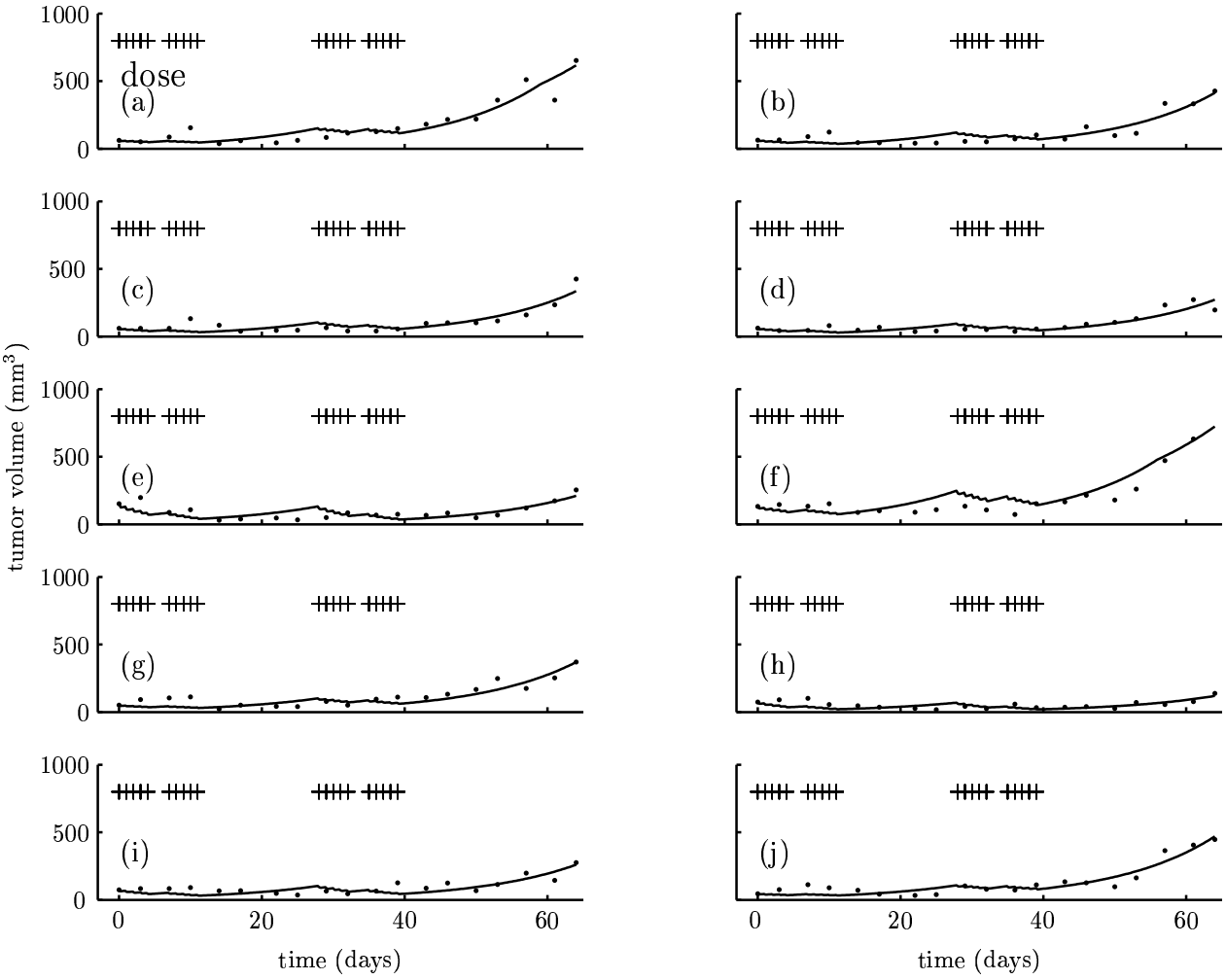

Figure 22: PK/PD model using predictions from the nonlinear PK model (2.9) with the PD model shown in equation (3.8). Tumor volume measurements are given by (·). Drug was administered at 1.0 mg/kg QD×5×2 on days indicated by (+), and the model prediction is represented by (—).

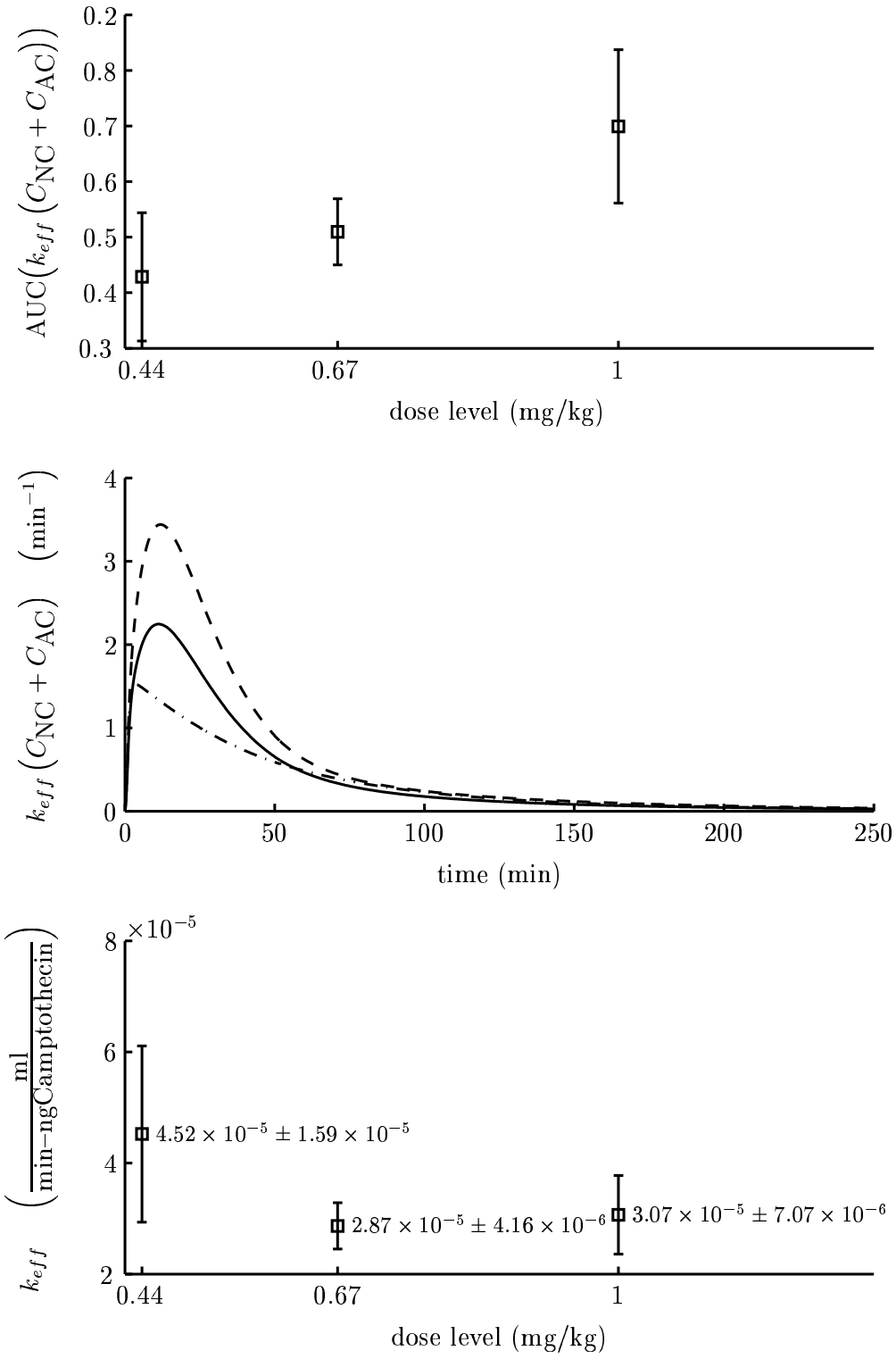

Figure 23: PD parameter analysis — PK/PD parameter distribution (mean ± one standard deviation) for 0.44, 0.67, and 1.0 mg/kg administration of 9NC QD×5×2 (bottom pane); product of k_{eff} and sum of camptothecin concentrations (middle pane), and AUC of $k_d(C_{\mathrm{NC}} + C_{\mathrm{AC}})$ versus time curve (top pane).

area under the concentration versus time curve (AUC) — calculated based on the simulated concentrations using trapezoidal rule — of this product are given in the middle and top panes of Figure 23, respectively. The latter would indicate that the exposure (as measured by AUC) predicted by the nonlinear PK model is approximately linear with dose.

3.5.1 Toxicity Modeling

A common toxicity constraint is an upper bound on drug exposure [12]. Because of inter–patient, or in this case inter–mouse, variability, large variations can occur across a population, and consequently average exposure as a metric for approximating toxicity may provide little utility. As a more quantitative and experimentally accessible metric for assessing toxicity, reductions in body weight were considered. By modeling body weight, a constraint specifying the minimum allowable body weight can be included in the control algorithm formulation. The experimental protocol specifies that animals with body weight below a prescribed value will have treatment withheld until the animal recovers. Therefore, it is advantageous to quantify the effects of 9NC administration on bodyweight. The body weight, B, of a mouse undergoing treatment with 9NC was modeled in the following manner:

$$\dot{B}(t) = k_g B(t) - k_c(C_{\mathrm{NC}}(t) + C_{\mathrm{AC}}(t)) \tag{3.9}$$

Here C_{NC} and C_{AC} are the total plasma plasma concentrations from the nonlinear PK model using the parameters from Table 7 for 9NC and 9AC, respectively. The body mass is assumed to grow at a rate k_g, and the rate of decrease in body mass is first order with respect to the total concentration of camptothecins (C_{NC} and C_{AC}) with a rate constant k_c. The parameters for this model were regressed using PD data for mice which were administered 1.0 mg/kg of 9NC QD×5×2. The mean body weights of ten animals after normalization to their initial conditions are shown in Figure 24 along with the average model prediction. The model is capable of qualitatively capturing body weight reductions in response to drug administration and the subsequent increases at the end of treatment cycles. However, the model does not quantitatively capture the body weight dynamics observed. Furthermore, the bodyweight predicted by the model will continue to increase exponentially when no drug is

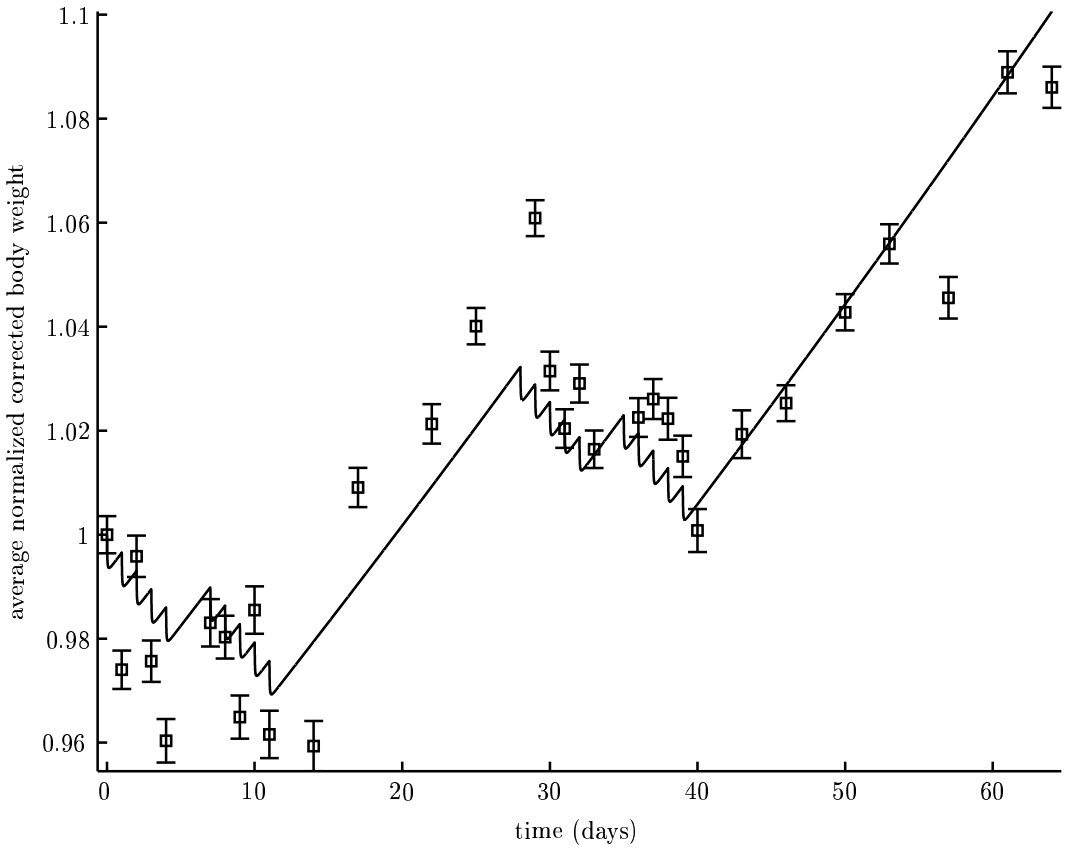

Figure 24: Average normalized body weights of ten animals given 1.0 mg/kg of 9NC *p.o.* QD×5×2 every four weeks.

administered; this is not seen in the control group. This can be accounted for by reinitializing the bodyweight model as measurements become available or at the end of treatment cycles. Another option would be to use standardized growth curves to bound normal body weight changes over the course of the experiment.

The body weight, B, is the total mass of the animal which includes the mass of the tumor. The body weight for toxicity purposes, B_{tox}, is calculated using the following equation:

$$B_{tox}(t) = B(t) - \frac{N(t)}{1000}$$

This corrects (reduces) body weight as the tumor burden changes by removing the mass from that of the animal. The tumor volume, N, is divided by 1000 to convert the volume into a mass — this assumes the density of a tumor is approximately that of water. To provide conservative estimates, a slow body growth rate and a high value of k_c could be used.

3.6 SUMMARY

Two different models were presented to describe untreated growth of HT29 human colon carcinoma xenografts implanted subcutaneously in SCID mice: an exponential model and a switched exponential model. The exponential model was coupled with the linear recycle model of 9NC PK to provide a model of drug efficacy at a dose level of 0.67 mg/kg administered QD×5×2. The PK/PD model driven by linear PK provided the least complex of the two PK/PD representations presented here. The linear PK modeling also indicated which time points (around 30 min) would be important for further development of a dynamic model. To better describe the range of possible doses, a second PK/PD model was constructed. This model combined the nominal growth described by the switched exponential model with the nonlinear model of 9NC PK. By calculating the PK/PD response over a range of doses, it was found that the exposure, as measured by AUC, was linear with respect to dose. A PD model of body weight reductions in response to 9NC administration was also developed using predictions from the nonlinear PK model of 9NC. By constructing a model of body weight changes in response to treatment, a means for determining the recovery time in response to

treatment was developed. The next chapter will focus on (the synthesis of chemotherapy treatment schedules) using the PK/PD models developed in this chapter.

4.0 CLINICALLY–RELEVANT DESIGN OF CANCER CHEMOTHERAPY SCHEDULES

The ultimate objective of chemotherapy is to extend the life of the cancer patient. For clinicians, chemotherapy represents a set of competing objectives: maximize treatment efficacy while maintaining tolerable levels of drug–induced toxicity. Oncologists administer chemotherapeutic drugs following standard regimens; often these are cycles of 21 or 28 days in length. Toxicity is evaluated formally after the first cycle. Based on the toxicity encountered by the patient during the first cycle, the drug dose may be altered or treatment my be withheld until the patient recovers from the effect of the first cycle. Following a second cycle of treatment, the patient is evaluated for efficacy in addition to toxicity. Several cycles of treatment may be given if the patient shows some form of clinical response. When treatment is no longer effecting the tumor burden, or unacceptable toxicity occurs, dosing is terminated.

The drug schedules administered by clinicians are obtained from empirical evidence resulting from preclinical and clinical trials. Engineers have attempted to provide more rigorous methods for determining drug schedules [12, 38, 46, 53]. However, there is a disconnect between recommended engineering approaches and clinical implementation. In order to help bridge this gap, this chapter focuses on the development of solution techniques for clinically applicable problems. These solution methodologies will be shown to solve problems as they are currently posed in the engineering literature. Furthermore, problem extensions that provide dose schedules of greater clinical relevance are formulated and solved. The term clinical relevance refers to the fact that toxicity and efficacy are the primary drivers of treatment, and clinical objectives must be considered. In addition clinicians administer drugs in cycles, so the problem formulation and underlying mathematical models must

incorporate periodic and discrete effects. Finally, the information gained from the periodic evaluation of efficacy and toxicity should be able to be used to update treatment.

4.1 GENERAL PROBLEM FORMULATION

Control of cancer chemotherapy systems with linear PK and macroscopic PD descriptions having bilinear nonlinearities has been considered by several authors [38, 45, 65]. The most common approach has been to consider the fixed final time problem:

$$\min_{\mathcal{D}(t)} \quad J = \mathcal{F}_J(x(t_f, \mathcal{D}(t))) \tag{4.1a}$$

$$\text{s.t.} \quad \dot{x} = \mathcal{F}_t(x(t), \mathcal{D}(t))) \tag{4.1b}$$

$$\mathcal{F}_i(x(t), \mathcal{D}(t)) \leq 0 \tag{4.1c}$$

$$\mathcal{F}_e(x(t), \mathcal{D}(t)) = 0 \tag{4.1d}$$

The functions $\mathcal{F}_J$, $\mathcal{F}_t$, $\mathcal{F}_i$, and $\mathcal{F}_e$, represent arbitrary functions of their respective arguments which may or may not contain nonlinearities. The internal states and dose levels are given by $x(t)$ and $\mathcal{D}(t)$, respectively. The objective is to minimize a function, J, typically the number of cancerous cells or the volume of a tumor, at a final time, $t = t_f$. This is accomplished while satisfying the dynamic constraints (4.1b) defined by the PK and PD of the drug [38, 45]. Also, inequality (4.1c) and equality (4.1d) constraints can be included to limit toxicity and account for logistical concerns. Due to the dynamic constraints, optimal control theory provides a convenient solution structure, and it has been applied previously by several groups [12, 13, 16, 18, 38, 38, 44, 45, 46, 47, 48].

When considering the objectives and constraints clinicians face, the above formulation (4.1) and its solution may not provide practically applicable results — mathematically optimal may not be the same as clinically optimal (or even clinically relevant). It is possible to formulate mathematical problems which can provide clinically relevant results [66]. Model–based controllers for the continuous infusion of insulin have been developed which provide implementable results. The ability to implement cancer chemotherapy schedules predicted

by dosing algorithms is dependent on the formulation used. The remainder of this chapter will focus on the analysis of case studies which are representative of the class of scheduled chemotherapy problems. The objective is to determine optimal, but clinically relevant, drug administration schedules for anticancer drugs described by macroscopic PK and PD models. Before addressing the specific case studies, the complexity of the problem will be reduced with a variable transformation, and the types of constraints considered will be motivated and formulated based on clinical and mathematical grounds.

4.1.1 Continuous–Time Constraint Formulation

The constraints from the general problem statement (4.1) come from a variety of sources. The dynamic constraints (4.1b) represent the PK/PD models of drug distribution and host response. The inequality and equality constraints, (4.1c) and (4.1d), respectively, are derived primarily from three areas of concern: financial limitations, logistical restrictions, and toxicity constraints. Foregoing such restrictions, an algorithm to determine the optimal dosing regimen would deliver as much drug as possible as frequently as possible, thereby leading to tumor eradication. Toxicity and logistics will be considered explicitly below; financial considerations are not addressed in the course of this dissertation.

Logistical constraints can be thought of as restrictions associated with managing treatment. For example, inconsistent drug administration times may lead to a patients who forget to take their medication [67]; likewise, varying dose levels in a non periodic manner may lead to patients taking the wrong dose. Treatment requiring the direct attention of hospital staff, *e.g.* intravenous infusions, are fundamentally limited by the working schedules of the medical professionals. Similarly, drugs delivered in pill form are administered in discrete amounts — *e.g.*, three pills every other day. Problem formulation and solution methodologies should be able to account for the discrete nature and limitations imposed by logistical constraints (*e.g.*, bounding administration times based on work schedules, selecting from discrete treatment options, etc.). Let a set of l drug levels, $1 \leq l \leq m_l$, represent the treatment options at a given time t (*e.g.*, one pill, two pills, etc.). This constraint would be formulated as a discrete

variable:

$$D(t) = Q_{dose}(1), \quad \text{or} \quad Q_{dose}(2), \quad \cdots, \qquad Q_{dose}(m_l) \tag{4.2}$$

Here, $Q_{dose}(l)$ is the vector of possible dosing values.

Toxicity constraints vary widely by drug class and are physically manifested as reductions in the patient's immune system function, fatigue, nausea, loss of body weight, and pain experienced by the patient, among other factors. It is common to characterize toxicity constraints in terms of both the drug PK and measurable PD effects [12]. Some PK–derived constraints are illustrated in Figure 25. Placing a limit on exposure is a common toxicity constraint. Total exposure, AUC_{exp}, is commonly calculated by integrating drug plasma concentration over the treatment interval:

$$\text{AUC}_{exp} = \int_0^{t_f} C(t)dt \leq C_{cum} \tag{4.3}$$

Equation (4.3) limits the cumulative toxicity of the drug, as measured by the total area under the solid line in Figure 25, which cannot exceed C_{cum}. Alternatively, drugs may not become effective until a therapeutic plasma concentration is reached (C_{th}). Once C_{th} has been reached, the effective drug concentration (C_{eff}) is that concentration above C_{th}. For such drugs, the effective exposure, AUC_{eff}, is represented by the shaded region of the PK profile in Figure 25. An effective drug concentration (C_{eff}) can then be defined in terms of the therapeutic drug concentration (C_{th}) in a piecewise fashion:

$$C_{eff}(t) = \begin{cases} 0 & C(t) \leq C_{th} \\ C(t) - C_{th} & C(t) > C_{th} \end{cases} \tag{4.4}$$

Therefore, drug administration which does not increase the plasma concentration to at least C_{th} is ineffective and undesirable. The dose applied at time t_3 shown in Figure 25 contributes to the total exposure but not the effective exposure; this may add to toxicity via (4.3), but will not contribute to treatment effect. Acute toxicity is reached when the drug plasma concentration exceeds some maximum, C_{max}. This is a state constraint given by:

$$C(t) \leq C_{max} \qquad \forall t \in [0, t_f] \tag{4.5}$$

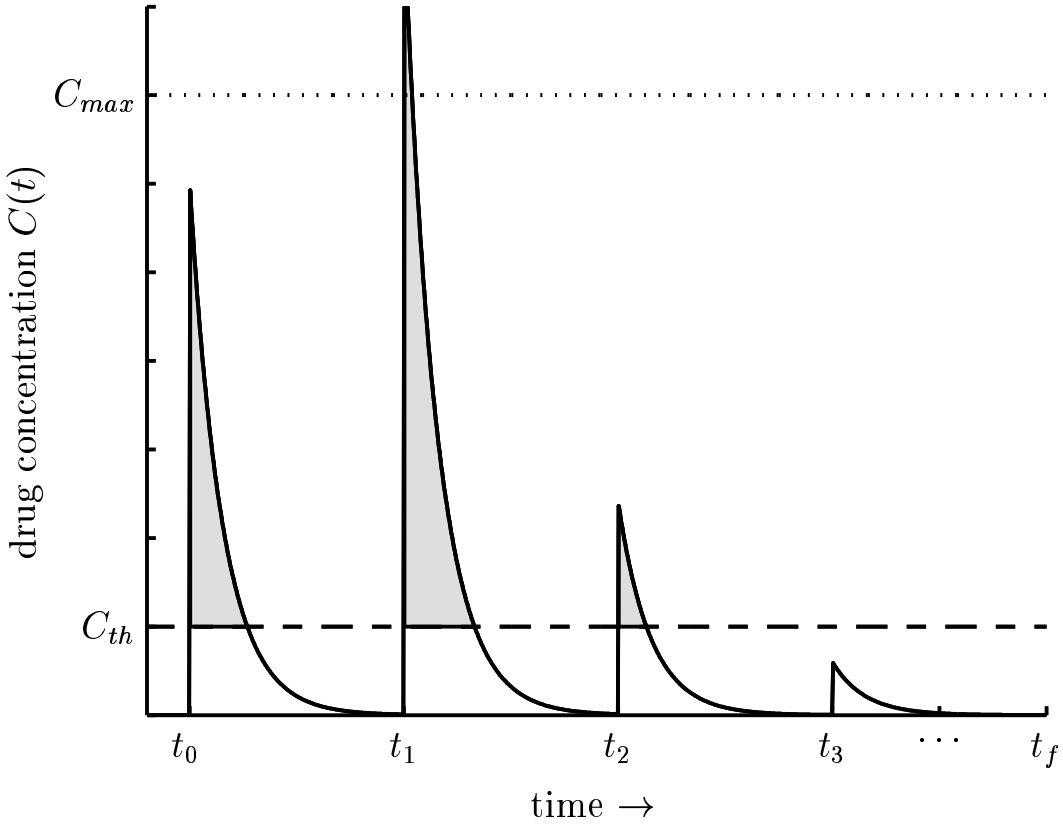

Figure 25: Plasma PK profile for a drug delivered intravenously as a bolus having first order elimination illustrating the minimum therapeutic drug concentration, C_{th} $(--)$, the maximum tolerable drug concentration, C_{max} $(\cdots)$, and the exposure (total exposure: area under the concentration versus time curve, AUC_{exp}; effective exposure: shaded area, AUC_{eff}) over the dosing interval, $(t_0 \leq t_i \leq t_f,\ \forall i \in \mathbb{I}^+ \leq f)$.

Since this is an intravenously administered drug, C_{max} can be defined in terms of D_{max}. In Figure 25, this constraint is violated by the dose at t_1. Depending on the drug, this could result in death or some form of irreversible harm. Non-intravenously administered drugs, those delivered orally for example, will have peak values described by their PK. In this case, relationships between C_{max} and D_{max} can be constructed using the PK model.

It is also possible to restrict the amount of drug which can be administered at any given point in time. This can be a result of discrete dosing quantities (*e.g.*, pills) or because the drug was found to be effective only over a particular range of doses. In the latter case, considered here, a semicontinuous variable is encountered at each dosing opportunity, as follows:

$$\begin{aligned} D_{lb} \leq \quad & D(t_i) \quad \leq D_{max} \\ \text{or} \quad & D(t_i) \quad = 0 \qquad \forall i \in [1, \cdots, m_q] \end{aligned} \tag{4.6}$$

Here D_{lb} and D_{max} are the lower and upper bounds of the continuous portion of the therapeutic dosing range, respectively, and m_q is the final dosing point. The upper bound is typically based on the MTD, or the amount of drug which will produce chronic side effects. The lowest amount of drug which can be administered and have an observable effect defines the lower bound. Also, q is the set of all possible times in which drugs may be administered during treatment, thereby making t_i the i^{th} dosing time for the set of values in m_q. For an intravenously administered drug, C_{max} may relate directly to D_{max}.

4.1.2 Discrete–Time Constraint Formulation

In order to cast the problem in the mixed–integer programming framework, the constraints must be discretized. For the discrete formulations, k will denote the current time step with a system step size of h. Hence k exists on the range $[1, m_k]$, and the final time point, m_k, is defined as $m_k = \frac{t_f}{h}$. The subscript $_d$ will be used to indicate the discrete variants of continuous variables. For example, continuous states, $x(t)$, and outputs such as plasma drug concentration, $C(t)$, or logarithmically transformed tumor size, $P(t)$, would have the discrete variable counterparts $x_d(k)$, $C_d(k)$ and $P_d(k)$, respectively.

Given systems with PK described by linear ODEs, the state equations relating to drug PK can be written in matrix form:

$$\dot{\underline{x}}(t) = \underline{\underline{A}}\,\underline{x}(t) + \underline{\underline{B}}\,\underline{u}(t) \tag{4.7}$$

Where $\underline{\underline{A}}$ is the state transition matrix and $\underline{\underline{B}}$ is the input coefficient matrix. The PK equations can then be discretized exactly for any step size h yielding [68]:

$$\underline{x}_d(k+1) = \underline{\underline{A}}_d\,\underline{x}_d(k) + \underline{\underline{B}}_d\,\underline{u}_d(k) \tag{4.8}$$

The coefficients $\underline{\underline{A}}_d$ and $\underline{\underline{B}}_d$ are the discrete–time forms of the state transition and input coefficient matrices, respectively, and can be written in terms of their continuous counterparts [68]:

$$\underline{\underline{A}}_d = e^{\underline{\underline{A}}h}, \qquad \underline{\underline{B}}_d = \underline{\underline{A}}^{-1}(\underline{\underline{A}}_d - \underline{\underline{I}})\underline{\underline{B}} \tag{4.9}$$

To force a system to choose from a discrete set of possibilities, such as the magnitude of a dose from a set of possible doses, $Q_{dose}(l)$, as shown in (4.2), the binary variable $b_{d,dose}(q,l)$ is introduced. The constraint (4.2) is replaced in discrete–time with:

$$D_d(q) = \sum_{i=1}^{m_l} b_{d,dose}(q,i)Q_{dose}(i) \qquad \forall q \in [1, m_q] \tag{4.10a}$$

$$1 = \sum_{i=1}^{m_l} b_{d,dose}(q,i) \qquad \forall q \in [1, m_q] \tag{4.10b}$$

At each dosing opportunity, q, equation (4.10b) ensures that only one dosing value is selected.

The cumulative toxicity constraint (4.3) contains an integral term which can be approximated using the trapezoidal rule [69]:

$$AUC_{d,exp} = \frac{h}{2}C_d(1) + h\sum_{j=2}^{m_k-1} C_d(j) + \frac{h}{2}C_d(m_k) \leq C_{cum} \tag{4.11}$$

This yields the discretized total exposure $AUC_{d,exp}$.

Discrete counterparts of linear state inequality constraints, such as the acute toxicity constraint found in (4.5), are formulated by replacing the continuous variables with their discrete counterparts. Therefore, (4.5) can be replaced with:

$$C_d(k) \leq C_{max} \qquad \forall k \in [1, m_k] \tag{4.12}$$

One issue which can arise from discretization is that the plasma concentration might be greater than C_{max} between discretization points. This is not a problem for intravenously administered drugs described by first order kinetics when administered as either a bolus or a rectangular wave in which the initial and final dosing times lie on time steps. In this situation the peak associated with any given drug administration occurs during the time of administration, and on a discretization point. In general, however, the maximum of a continuous system in response to an input may occur between discretization points. This can be overcome by choosing suitably small values for h, knowing the time of a peak, or by mapping a dose level to a peak drug concentration (*e.g.*, through an existing PK model).

The requirement that the effective drug concentration is nonzero only when the plasma concentration is greater than the therapeutic concentration creates a semicontinuous variable. This is written in a piecewise fashion in equation (4.4). In discrete time this can be written as linear inequalities by introducing the binary variable $b_{d,th}(k)$ at each time step, and requiring that the following inequalities be satisfied [70]:

$$C_d(k) - C_{th} \leq (C_{max} - C_{th})(1 - b_{d,th}(k)) \tag{4.13a}$$

$$0 \leq C_{d,eff}(k) \tag{4.13b}$$

$$(C_{max} - C_{th})(1 - b_{d,th}(k)) \geq C_{d,eff}(k) \tag{4.13c}$$

$$C_{th} - C_d(k) \leq C_{th} b_{d,th}(k) \tag{4.13d}$$

$$0 \leq C_{d,eff}(k) - (C_d(k) - C_{th}) \tag{4.13e}$$

$$C_{th} b_{d,th}(k) \geq C_{d,eff}(k) - (C_d(k) - C_{th}) \tag{4.13f}$$

Consider the situation when the drug plasma concentration is below the therapeutic value ($C_d(k) \leq C_{th}$). In this case, the left hand side of (4.13d) will be greater than zero which requires $b_{d,th}(k)$ to be one. This forces the left hand side of (4.13c) to be zero, resulting in

$C_{d,eff}(k)$ being zero also. The left hand side of (4.13a) will be negative, so this constraint will be satisfied. The right hand side of constraints (4.13e) and (4.13f) will be positive on the range $[0, C_{th}]$, so these constraints will also be satisfied.

Alternatively, consider the case where the drug is having an effect ($C_d(k) > C_{th}$). This forces $b_{d,th}(k)$ to be zero for the constraint (4.13a) to be satisfied. Thus, $C_{d,eff}(k)$ will be forced to take on the value $C_d(k) - C_{th}$ because the left hand side of constraints (4.13e) and (4.13f) will be zero. Furthermore $C_{d,eff}(k)$ will exist on the range $[0, (C_{max} - C_{th})]$ satisfying the constraints (4.13b) and (4.13c). Finally the the constraint (4.13d) will always be satisfied because the left hand side will have a maximum value of zero.

Similarly, the constraint requires that drugs only be administered in the therapeutic range (4.6) can also be transformed into a set of linear inequalities by the introduction of a binary variable.

$$D_{lb} b_{d,u}(k) \leq D(k) \leq D_{max} b_{d,u}(k) \qquad \forall k \in [1, m_k] \tag{4.14}$$

When $b_{d,u}(k)$ is zero, $D(k)$ must be zero. When the drug is to be administered, $b_{d,u}(k)$ must be one, and $D(k)$ must lie between D_{lb} and D_{max}.

4.2 CASE STUDY I: INTRAVENOUSLY ADMINISTERED DRUG WITH GOMPERTZIAN PROLIFERATION

The first case study considered was taken from the engineering literature. This system, originally studied by Martin and Teo, consists of a tumor proliferating in a Gompertzian

fashion (3.3) and an intravenously administered drug [12]. The following system was analyzed using optimal control and control vector parameterization techniques [12]:

$$\dot{C}(t) = D(t) - \gamma C(t) \tag{4.15a}$$

$$\dot{N}_g(t) = \frac{1}{\tau_g} \ln\left[\frac{\ln(\rho_g/N_0)}{\ln(\rho_g/2N_0)}\right] N_g(t) \ln\left[\frac{\rho_g}{N_g(t)}\right] - k_{eff} C_{eff}(t) N_g(t) \tag{4.15b}$$

$$C_{eff}(t) = (C(t) - C_{th})\mathcal{H}(C(t) - C_{th}) \tag{4.15c}$$

$$C(0) = C_0 \tag{4.15d}$$

$$N_g(0) = N_0 \tag{4.15e}$$

The PK of the drug is described by equation (4.15a) where the plasma drug concentration, $C(t)$, increases with intravenous infusions of the drug, $D(t)$, and decreases according to first–order elimination kinetics at a rate γ. The change in the number of cancer cells is described by equation (4.15b). The cancerous cells proliferate in a Gompertzian fashion described by τ_g, ρ_g, and N_0, as discussed in section 3.1. The drug effect is proportional, with constant of proportionality k_{eff}, to the number of cancer cells, $N_g(t)$, and the effective drug plasma concentration, C_{eff}; $C_{eff}(t)$ is the drug concentration above the minimum therapeutic concentration, C_{th}. The initial drug concentration and number of cancer cells are given by C_0 and N_0, respectively.

The parameters considered for this case study [12] are provided in Table 11, and a time step of $h = 1$ day was used. The rate of elimination for the drug, D, is slow enough that a timestep of one day will not lead to a significant loss of information. Three values of k_{eff} were considered representing different levels of drug efficacy [12]. Highly effective, marginally effective, and ineffective drugs were represented by $k_{eff,1}$, $k_{eff,2}$ and $k_{eff,3}$, respectively.

4.2.1 Constraint Formulation

It was assumed that the drug could be administered weekly with a final time, t_f, of 52 weeks [12]. The maximum allowable plasma concentration was C_{max}; this bounded the amount of drug that could be administered at any point in time leading to the constraint [12]:

$$C(t) \leq C_{max} \qquad \forall t \leq t_f \tag{4.16}$$

A cumulative toxicity constraint (4.17) was placed on the system for the treatment period [12], as follows:

$$\int_0^{t_f} C(t)dt \;\; \leq \;\; C_{cum} \tag{4.17}$$

The final constraint placed on the system dealt with efficacy. Since it was undesirable for the status of a patient to decrease (*e.g.*, tumor burden to increase), the number of cancer cells was not allowed to increase to a number larger than the initial condition.

$$N_g(t) \leq N_0 \qquad \forall\, t \tag{4.18}$$

4.2.2 Optimal Control Problem

The optimal control problem considered by Martin and Teo [12] was given as:

$$\begin{aligned} \min\nolimits_{D(t)} \quad & N_g(t_f) \\ \text{s.t.} \quad & (4.15),\ (4.17),\ (4.16),\ (4.18) \end{aligned} \tag{4.19}$$

The objective here is to minimize the tumor volume at a final time while satisfying the dynamic constraints (4.15), the cumulative toxicity constraints (4.17), the maximum plasma drug concentration (4.16) and the efficacy constraint (4.18) This equation had nonlinear growth and death terms as well as the discontinuity associated with the therapeutic drug concentration (C_{th}).

4.3 MILP PROBLEM REFORMULATION

4.3.1 PD Variable Transform

Because of the bilinear term from the drug PD (either (3.6a) or (3.6b)), the optimization from (4.1) is a nonlinear programming (NLP) problem. Nonlinear optimizations can possess local minima, and efforts to eliminate nonlinearities can improve the likelihood of achieving the global optimum. The effect of the bilinear kill term can be included, and the explicit nonlinearity removed, by performing the following logarithmic transformation [47]:

$$P(t) = \ln(N(t)) \Leftrightarrow N(t) = e^{P(t)} \Leftrightarrow \dot{N}(t) = \dot{P}(t)e^{P(t)} \tag{4.20}$$

Notice that $\ln(N(t))$ increases monotonically with $N(t)$ such that the value of drug administration which minimizes $N(t_f)$ will also minimize $P(t_f)$. The transform in (4.20) can be applied to cancerous masses under both exponential and Gompertzian growth resulting in:

$$\dot{P}(t) = \frac{\ln(2)}{\tau_e} - k_{eff}C_{eff}(t) \tag{4.21a}$$

$$\dot{P}(t) = \frac{1}{\tau_g}\ln\left[\frac{\ln(\rho_g/N_0)}{\ln(\rho_g/2N_0)}\right](\ln\rho_g - P(t)) - k_{eff}C_{eff}(t) \tag{4.21b}$$

By logarithmically transforming the PD equations (3.6a) and (3.6b), cancer proliferating exponentially can be described by an ODE (4.21a) which is linear in effective drug concentration ($C_{eff}(t)$). Also, PD models with bilinear kill terms in which cancer proliferates in a Gompertzian fashion can be reduced to an ODE (4.21b) which is linear in both effective drug concentration ($C_{eff}(t)$) and transformed tumor size ($P(t)$). Each transformed model has a positive constant term which accounts for proliferation and a negative term accounting for the presence of the drug.

The first step in the reformulation involved the logarithmic transformation from equation (4.20). By performing this transformation on the PD equation (4.15b) the nonlinear growth and bilinear kill nonlinearities were eliminated yielding:

$$\dot{P}(t) = \frac{1}{\tau_g}\ln\left[\frac{\ln(\rho_g/N_0)}{\ln(\rho_g/2N_0)}\right](\ln\rho_g - P(t)) - k_{eff}(C(t) - C_{th})\mathcal{H}(C(t) - C_{th}) \tag{4.22}$$

The discontinuous drug effect was accounted for during discretization. In discretizing the system, the dynamic constraints were converted into algebraic constraints. The plasma drug concentration was discretized at a time step h [68] and resulted in a piecewise continuous function (4.23):

$$C_d(k+1) = \begin{cases} -\frac{1}{\gamma}\left(e^{-\gamma h}-1\right)\frac{u(q)}{h} + e^{-\gamma h}C_d(k) & \text{when } k = hq \\ e^{-\gamma h}C_d(k) & \text{otherwise} \end{cases} \tag{4.23}$$

The input is present along with a decay term at time steps which coincide with drug administration times. When no drug can be administered, the plasma concentration simply decays at the rate γ. The discontinuous effective drug concentration, $C_{eff}(t)$, from equation (4.15c) was accounted for using the methodology discussed in section 4.1.2. By applying the binary variable $b_{d,th}(k)$, and enforcing the constraints found in equation (4.13) at each timestep, k, the discontinuous effective drug concentration was reduced to linear inequalities.

The logarithmically transformed PD (4.22) was discretized using Euler's method [69]:

$$P_d(k+1) = P_d(k) + hF_d(P_d(k), C_{d,eff}(k)) \tag{4.24}$$

$$F_d(k) = \frac{1}{\tau_g}\ln\left[\frac{\ln(\rho_g/N_0)}{\ln(\rho_g/2N_0)}\right](\ln\rho_g - P(t)) - k_{eff}(C(t)-C_{th})\mathcal{H}(C(t)-C_{th}) \tag{4.25}$$

Note that F_d is the discretized right hand side of equation (4.22). The discrete–time form of the acute toxicity constraint (4.16) was represented with the following state constraint:

$$C_d(k) \leq C_{max} \qquad \forall k \in [1, m_k] \tag{4.26}$$

Cumulative toxicity for this system (4.17) was replaced with equation (4.11), the trapezoidal rule approximation of the integration (4.17). The efficacy constraint (4.18) was incorporated in the following manner:

$$P_d(k) \leq \ln(N_0); \quad \forall k \in [3, m_k] \tag{4.27}$$

It is important to notice that the efficacy constraint was not enforced for the first two time steps. The nature of discrete–time systems without direct feedthrough dictates that the effects of an input change on states not manifest until subsequent time steps. In this case,

manipulated variable changes at time step one induce plasma drug concentration changes at time step two. These manipulated variable changes then indirectly affect the number of cancer cells at time step three. Since the cells are continuously proliferating, the continuous–time efficacy constraint cannot be satisfied until the third time step.

Based on the discretization results above, the continuous problem (4.19) was recast as the following MILP:

$$\begin{aligned} \min_{D_d(q)} \quad & P_d(m_k) \\ \text{s.t.} \quad & (4.11),\ (4.13),\ (4.23),\ (4.24),\ (4.26),\ (4.27) \end{aligned} \tag{4.28}$$

4.3.2 MILP Results

Solutions for each value of k_{eff} case were found using the optimization software CPLEX in the General Algebraic Modeling System (GAMS) and are shown in Figure 26. The objective function values ($N(t_f)$) for both the MILP and optimal control solutions are shown for each value of k_{eff} in Table 12. Problem formulations contained approximately 4106 equations, 1873 continuous variables and 364 discrete variables, and solution required less than a second to solve on a dual AMD Athlon 1.8 GHz machine with one GB of RAM.

The solutions shown in Figure 26 are qualitatively similar to those presented by Martin and Teo [12]. An initial dose was administered at the first time step in all instances. This was done to accommodate the efficacy constraint (4.27) and drives the number of cancer cells down initially. As the cancer population approached the initial number of cells, more drug was administered to satisfy the efficacy constraint. This was most evident for drug efficacies $k_{eff,3}$ and $k_{eff,2}$. At the end of the treatment cycle, the drug was administered in large amounts to reduce the final time tumor volume (the objective) such that the cumulative toxicity constraint (4.11) was met and the acute toxicity constraint (4.26) was not violated.

When considering the highly effective drug, ($k_{eff,1}$), the optimal control solution found by Martin [12] and MILP solution achieved essentially the same result. For the moderately effective drug ($k_{eff,2}$) the MILP solution was clinically indistinguishable (within measurement error) from the optimal control solution. However, there were quantifiable differences between the two methodologies when considering the ineffective drug ($k_{eff,3}$). This can be

Table 11: PK/PD parameters taken from the Martin and Teo case study [12]. Here $[D]$ are the units of drug concentration/mass of drug delivered.

parameter	value	units
τ_g	150	days
ρ_g	10^{12}	cells
N_0	10^{10}	cells
$k_{eff,1}$	2.7×10^{-2}	$\frac{1}{\text{days}\cdot[D]}$
$k_{eff,2}$	8.4×10^{-3}	$\frac{1}{\text{days}\cdot[D]}$
$k_{eff,3}$	1.5×10^{-3}	$\frac{1}{\text{days}\cdot[D]}$
γ	.27	$\frac{1}{\text{days}}$
C_{th}	10	$[D]$
C_{max}	50	$[D]$
C_{cum}	4.1×10^{3}	$[D]\cdot$days
t_f	364	days

Table 12: Objective function values, $N(t_f)$, for the MILP and optimal control (OC) solutions [12].

	$k_{eff,1}$	$k_{eff,2}$	$k_{eff,3}$
MILP	< 1	333	1.9×10^9
OC	< 1	1.2×10^3	1.8×10^9

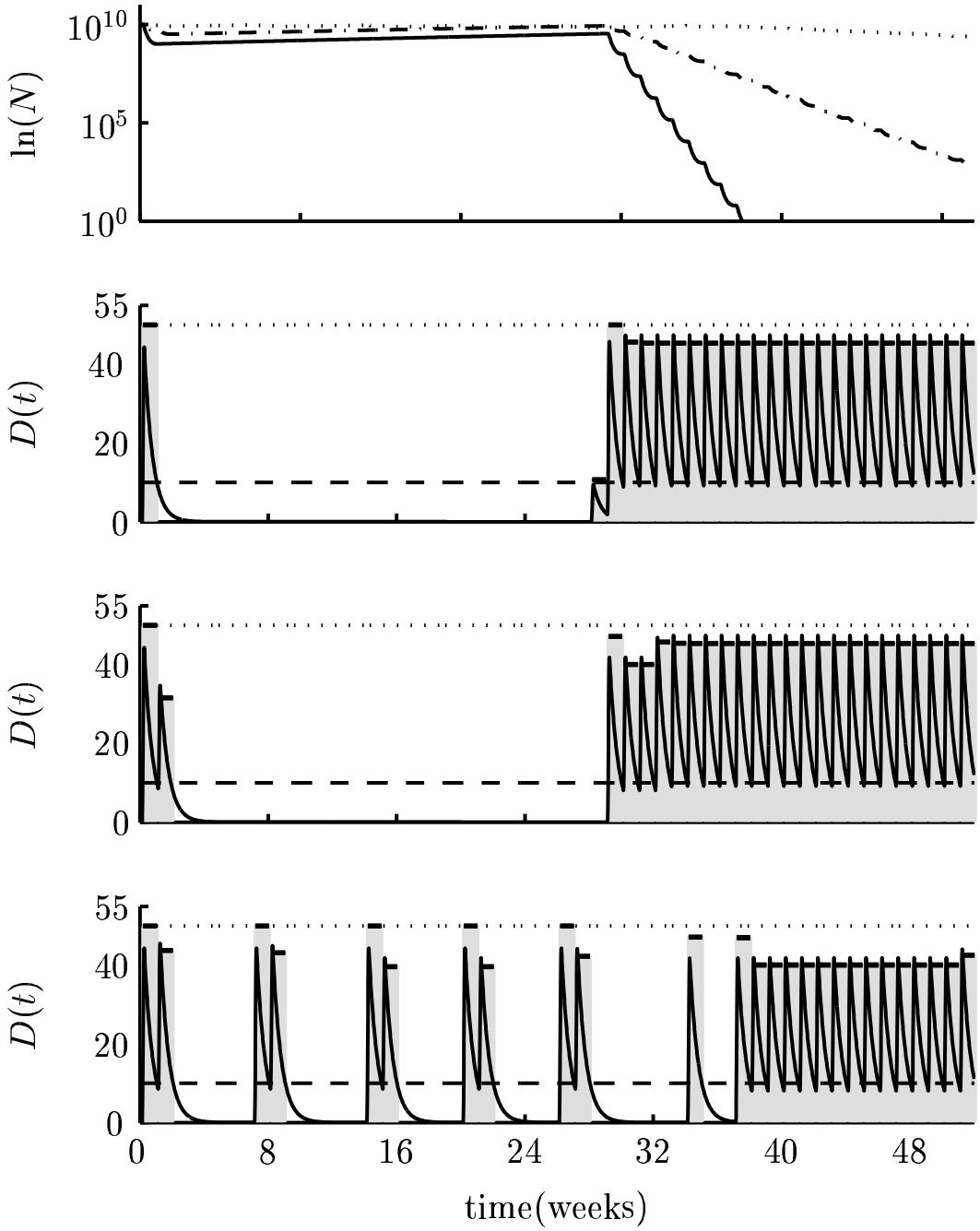

Figure 26: Case study I response to treatment. Top pane: tumor volume predictions for the three drug types: $k_{eff,1}$ (—), $k_{eff,2}$ (-·-) and $k_{eff,3}$ ($\cdots$). Remaining panes: dose schedule (bar/shaded region) and concentration (—) for drugs $k_{eff,1}$ (2^{nd} pane), $k_{eff,2}$ (3^{rd} pane) and $k_{eff,3}$ (bottom pane); C_{th} ($--$) and C_{max} ($\cdots$) in panes 2-4.

resolved by decreasing the stepsize, h. However, there is a compromise. Extremely small values for h leads to more mathematical operations. Consequently, roundoff errors associated with floating point mathematics begin to dominate. On the other end of the continuum, extremely large values for h lead to discretization error. Hence, the value for h must be selected to balance these effects. A more accurate discretization scheme, such as Runga–Kutta, could be employed, but this leads to a significant increase in the number of algebraic constraints associated with the PK/PD model.

4.3.3 Clinical Relevance

Clinicians make use of periodic feedback to evaluate the efficacy of treatment and to adjust treatment as necessary to mitigate side effects. To approach the cancer chemotherapy dosing problem from a more practical perspective, the problem from equation (4.28) was reformulated as a receding horizon problem:

$$\begin{aligned} \min_{D_d(q)} \quad & \sum_{i=1}^{m_p} (P_d(i) - T_d(i))^2 + \Gamma_u \sum_{i=1}^{m_q} D_d(i) \\ \text{s.t.} \quad & (4.11),\ (4.13),\ (4.23),\ (4.24),\ (4.26),\ (4.27) \end{aligned} \tag{4.29}$$

This mixed–integer quadratic programming problem (MIQP) minimizes the deviations between the transformed tumor volume, $P_d(i)$, and a specified target, $T_d(i)$, over a horizon of w_p points (two weeks per point). The input penalty term, weighted by Γ_u, was added to penalize small drug doses. This formulation assumes the patient returns every eight weeks for evaluation and the prediction horizon (w_p) for optimization purposes is initially 26 (one trajectory point every two weeks), and decreases by 4 times the number of treatment periods preceding the current period (a receding horizon formulation [71, 72]).

The problem in (4.29) was modeled in GAMS and solved using CPLEX. This resulted in a series of 6 optimizations. Each optimization contained approximately 1894 equations, 865 continuous variables, 168 discrete variables and the solution was found in less than a second. The calculations were performed on a dual AMD Athlon 1.8 GHz machine with one GB of memory.

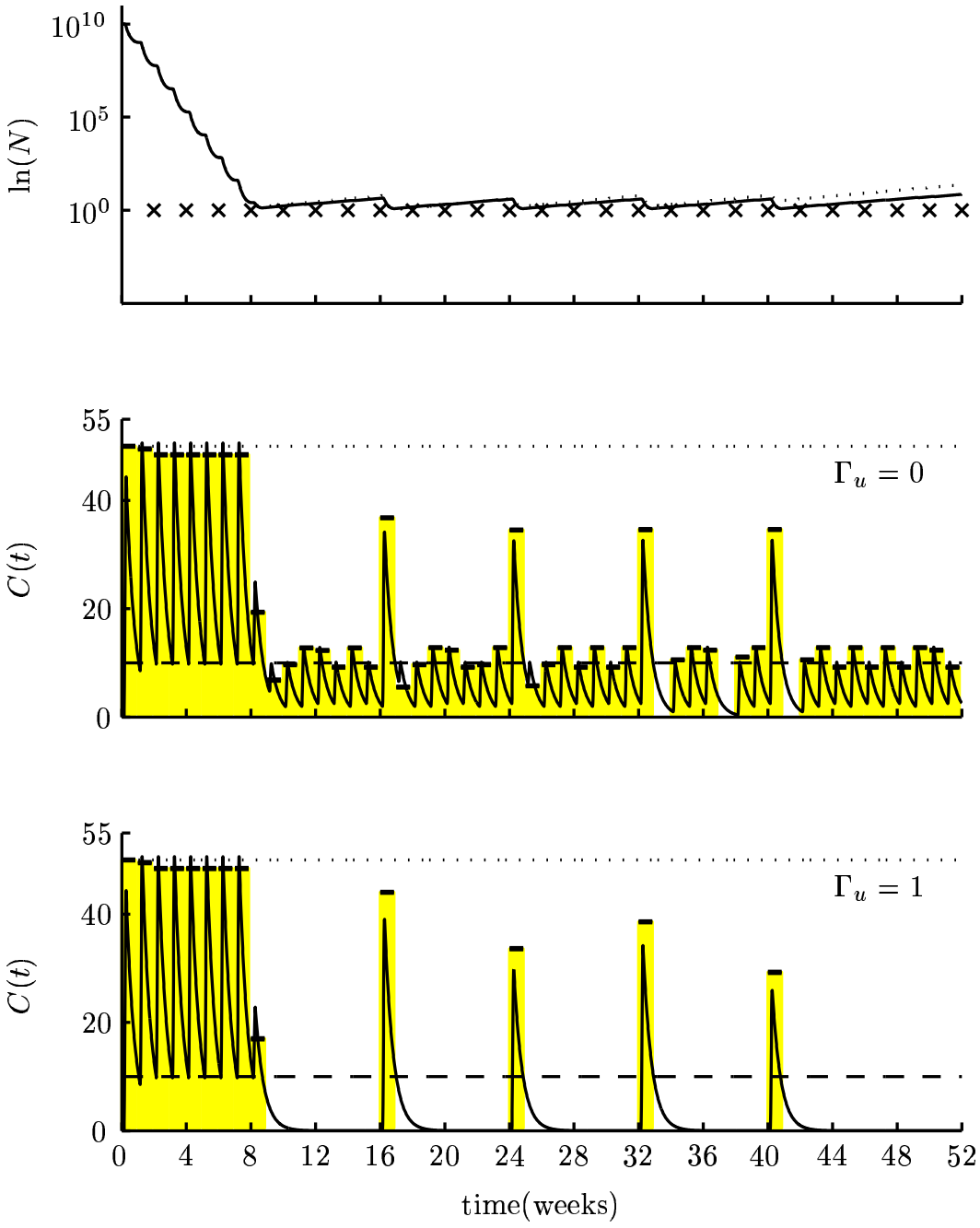

Figure 27: Case study I receding horizon solution for $k_{eff,1}$. Top pane: predicted tumor response profile, P_d, and desired response, T_d, ($\times$) for $\Gamma_u = 0$ (—) and $\Gamma_u = 1$ ($\cdots$). Other panes: drug administration levels (bar/shaded region) and plasma concentrations (—) for $\Gamma_u = 0$ (middle pane) and $\Gamma_u = 1$ (bottom pane); C_{th} ($--$) and C_{max} ($\cdots$) in the middle and bottom panes.

Table 13: Total exposure, AUC_{exp}, and effective exposure, AUC_{eff}, for solutions to (4.29) and the given input weights, Γ_u.

	$\Gamma_u = 0$	$\Gamma_u = 1$	units
AUC_{exp}	3438	2069	$[d]\cdot$days
AUC_{eff}	1110	1061	$[d]\cdot$days
$\frac{\text{AUC}_{eff}}{\text{AUC}_{exp}}$	0.32	0.54	—

The results for the most efficacious drug, $k_{eff,1}$, are shown in Figure 27. The trajectory specified in Figure 27 represents the desire to decrease the tumor burden as quickly as possible. For the two cases presented here, a large amount of drug is administered during the first cycle. This rapidly eliminates a large number of the cancerous cells. With $\Gamma_u = 0$, the focus was on adhering to the trajectory and resulted in many small doses being administered. While dose levels were predicted which led to immediate plasma levels at or below the therapeutic level, C_{th}, these administrations did combine with subsequent administrations to increase the effective exposure.

While this result is mathematically optimal, it is suboptimal from a clinical perspective. A significant amount of drug was being administered at variable small doses that contributed to the cumulative exposure, without contributing significantly to the efficacy of the treatment. Furthermore, the use of variable small doses is a dose preparation concern in the clinic. By increasing the penalty for drug administration to $\Gamma_u = 1$, the administration profile in the bottom pane of Figure 27 was obtained. This tracked the trajectory well, as indicated by the dotted line in the top pane of Figure 27, with a greater fraction of the drug exposure above C_{th}. Table 13 contains the total exposure, AUC_{exp}, the effective exposure, $\text{AUC}C_{eff}$, and the ratio of the effective to total exposure. By changing Γ_u from zero to one the fraction of the effective drug exposure increases from a third to over one half. This is desirable because all drug administered contributes to toxicity but not necessarily efficacy.

4.4 CASE STUDY II: LINEAR PK/BILINEAR PD EFFECT

The second case study considers the effects of the lactone forms of 9NC and 9AC modeled in equation (3.7). The tumor volume increases exponentially, and bilinear kill terms employ PK concentration predictions after oral administration. The state and output equations are as follows:

$$\dot{x}_0(t) = -\frac{x_0(t)}{\tau_0} + \frac{D(t)}{\tau_0} \tag{4.30a}$$

$$\dot{x}_1(t) = \frac{x_0(t)}{\tau_1} - \frac{x_1(t)}{\tau_1} + \frac{x_3(t)}{\tau_1} \tag{4.30b}$$

$$\dot{x}_2(t) = \frac{\beta_1\alpha_2}{\tau_2}x_1(t) - \frac{x_2(t)}{\tau_2} + \frac{x_4(t)}{\tau_2} \tag{4.30c}$$

$$\dot{x}_3(t) = \mathcal{H}(t-\theta)x_1(t-\theta)\frac{\alpha_1}{\tau_r} - \frac{x_3(t)}{\tau_r} \tag{4.30d}$$

$$\dot{x}_4(t) = \mathcal{H}(t-\theta)x_2(t-\theta)\frac{\alpha_1}{\tau_r} - \frac{x_4(t)}{\tau_r} \tag{4.30e}$$

$$\dot{x}_5(t) = \frac{\ln(2)}{\tau_e}x_5(t) - k_{eff,\mathrm{NCL}}C_{eff,\mathrm{NCL}}(t)x_5(t) - k_{eff,\mathrm{ACL}}C_{eff,\mathrm{ACL}}(t)x_5(t) \tag{4.30f}$$

$$C_{\mathrm{NCL}}(t) = \beta_1 k_p x_1(t) \tag{4.30g}$$

$$C_{eff,\mathrm{NCL}}(t) = C_{\mathrm{NCL}}(t-\theta_{eff})\mathcal{H}(t-\theta_{eff}) \tag{4.30h}$$

$$C_{\mathrm{ACL}}(t) = \beta_1 k_p x_2(t) \tag{4.30i}$$

$$C_{eff,\mathrm{ACL}}(t) = C_{\mathrm{ACL}}(t-\theta_{eff})\mathcal{H}(t-\theta_{eff}) \tag{4.30j}$$

$$N_e(t) = x_5(t) \tag{4.30k}$$

The details of this model, including parametric descriptions, were discussed in Chapters 2 and 3. Briefly, equations (4.30a)-(4.30e) represent the PK of the lactone forms of 9NC and 9AC. The concentrations of 9NC and 9AC in the plasma are given by the outputs $C_{\mathrm{NCL}}(t)$ and $C_{\mathrm{ACL}}(t)$, respectively. Equation (4.30f) accounts for the drug PD, and the tumor volume is given by $N_e(t)$. The effective concentrations of the drug and metabolite are the plasma concentrations delayed by θ_{eff}. The initial state of the system is $\underline{x}(0) = [0,\ 0,\ 0,\ 0,\ 0,\ N_0]^\top$, where no drug is present and the tumor volume is initially N_0.

4.4.1 Continuous Constraint Formulation

Based on the mathematical representation in equation (4.30), the optimal dosing regimen was determined for a treatment interval of four weeks ($t_f = 33600$ minutes). For this system, logistical constraints associated with drug dosing were considered as well. Based on work schedules, drugs could be administered no more often than once every weekday (*i.e.*, no weekends). For a cycle of treatment, four weeks in this case, there were twenty possible dosing times q.

To bound the amount of drug that can be administered, a cumulative exposure constraint was placed on the system for each treatment period. Currently, 9NC is administered once daily, Monday–Friday, at 0.67 mg/kg, for two weeks, followed by two weeks with no drug being administered (QD×5×2) [55]. This schedule is then repeated at four week intervals. It was assumed that the cumulative toxicity should not exceed that encountered when administering 9NC using the current standard of practice (0.67 mg/kg QD×5×2 = 6.7 mg/kg, per four weeks). Typically this would be a bound on the integrated drug plasma concentration versus time curve; however, the result of this integral for systems modeled by linear PK is proportional to the amount of drug administered. As such, a limit was placed on the total mass of drug delivered:

$$\int_0^{t_f} D(t) \leq 6.7 \frac{\text{mg}}{\text{kg}} \tag{4.31}$$

After administration of 9NC, the plasma levels are below the detectable limit by the end of a day. Since the period between administrations is at least a day, there are no combinatorial effects between doses. The amount of drug delivered on any given day was bounded above by the MTD of 1 mg/kg and bounded below by the minimum effective dose of 0.44 mg/kg:

$$0.44 \frac{\text{mg}}{\text{kg}} \leq D(t_i) \leq 1.0 \frac{\text{mg}}{\text{kg}} \qquad \text{or} \qquad D(t_i) = 0 \qquad \forall i \in [1, \cdots, m_q] \tag{4.32}$$

4.4.2 Continuous Problem Formulation

With an understanding of the constraints imposed on the system, the continuous problem was formulated as:

$$\begin{aligned} \min_{D(q)} \quad & N_e(t_f) \\ \text{s.t.} \quad & (4.30),\ (4.31),\ (4.32) \end{aligned} \tag{4.33}$$

The discontinuities in the manipulated variable $D(t)$ and the bilinear kill term from equation (4.30f) indicate that this is a nonlinear programming problem (NLP) with dynamic constraints. Solutions to this optimization would include local minima. Martin has shown that control vector parameterization can be used to guarantee a global optimum for this problem is found [12]. However, including alternate constraints or altering the current constraints could supplant the ability of optimal control theory to determine the global optimum (*i.e.* the introduction of path or state constraints). To guarantee optimality, options were explored to eliminate nonlinearities and restate the problem such that a global optimum could be guaranteed in the current form and the problem could be easily extended as well.

4.4.3 MILP Problem Reformulation

By substituting the values from equation (4.20) into equation (4.30f), the tumor growth equation becomes:

$$\dot{P}(t) = \frac{\ln(2)}{\tau_e} - k_{eff,\mathrm{NCL}} C_{eff,\mathrm{NCL}}(t) - k_{eff,\mathrm{ACL}} C_{eff,\mathrm{ACL}}(t) \tag{4.34}$$

The discontinuity in the range of drug administration was reformulated as in (4.14), thereby introducing the binary decision variable $b_{d,u}(q)$. The constraints in equation (4.32) were replaced with:

$$0.44 b_{d,u}(q) \frac{\mathrm{mg}}{\mathrm{kg}} \leq D_d(q) \leq 1.0 b_{d,u}(q) \frac{\mathrm{mg}}{\mathrm{kg}} \qquad b_{d,u}(q) \in \{0,1\} \forall d \tag{4.35}$$

When $b_{d,u}(q)$ is zero, then $D_d(q)$ must be zero, and when $b_{d,u}(q)$ is one then $D_d(q)$ must lie within the therapeutic range. The cumulative toxicity limit (4.31) was replaced with the following summation:

$$\sum_{q=1}^{20} D_d(q) \leq 6.7 \tag{4.36}$$

Finally, the PK equations (4.30a) through (4.30e) were written in the matrix form:

$$\underbrace{\begin{bmatrix} \dot{x}_0 \\ \dot{x}_1 \\ \dot{x}_2 \\ \dot{x}_3 \\ \dot{x}_4 \end{bmatrix}}_{\dot{\underline{x}}(t)} = \underbrace{\begin{bmatrix} -\frac{1}{\tau_0} & & & & \\ \frac{1}{\tau_1} & -\frac{1}{\tau_1} & & -\frac{1}{\tau_1} & \\ & -\frac{\alpha_2\beta_1}{\tau_1} & -\frac{1}{\tau_2} & & \frac{1}{\tau_2} \\ & & & -\frac{1}{\tau_r} & \\ & & & & -\frac{1}{\tau_r} \end{bmatrix}}_{\underline{\underline{A}}} \underbrace{\begin{bmatrix} x_0 \\ x_1 \\ x_2 \\ x_3 \\ x_4 \end{bmatrix}}_{\underline{x}(t)} + \underbrace{\begin{bmatrix} 1 & 0 & 0 \\ 0 & 0 & 0 \\ 0 & 0 & 0 \\ 0 & \frac{\alpha_1}{\tau_r} & 0 \\ 0 & 0 & \frac{\alpha_1}{\tau_r} \end{bmatrix}}_{\underline{\underline{B}}} \underbrace{\begin{bmatrix} D(t) \\ x_1(t-\theta)\mathcal{H}(t-\theta) \\ x_2(t-\theta)\mathcal{H}(t-\theta) \end{bmatrix}}_{\underline{u}(t)} \tag{4.37}$$

The delayed states in equations (4.30d) and (4.30e) have been transformed into inputs $u_1(t)$ and $u_2(t)$, respectively, to facilitate simulation. The state equations from (4.37) can be discretized for any step size h in terms of $\underline{\underline{A}}$ and $\underline{\underline{B}}$ as shown in equations (4.8) and (4.9). The logarithmically transformed PD from equation (4.34) was also discretized using Euler's method [69]. The continuous dynamic constraints from equations (4.30) and (4.34) were recast in discrete–time form as follows:

$$\underline{x}_d(k+1) = \underline{\underline{A}}_d \underline{x}_d(k) + \underline{\underline{B}}_d \underline{u}_d(k) \tag{4.38a}$$

$$P_d(k+1) = P_d(k) + h\Big(\frac{\ln 2}{\tau_e} - k_{eff,\mathrm{NCL}} C_{d,eff,\mathrm{NCL}}(k) - k_{eff,\mathrm{ACL}} C_{d,eff,\mathrm{ACL}}(k)\Big) \tag{4.38b}$$

$$C_{d,\mathrm{NCL}}(k) = \beta_1 k_p x_{1,d}(k) \tag{4.38c}$$

$$C_{d,eff,\text{NCL}} = C_{d,\text{NCL}}(k - \theta_{d,eff})\mathcal{H}(k - \theta_{d,eff}) \tag{4.38d}$$

$$C_{d,\text{ACL}}(k) = \beta_1 k_p x_{2,d}(k) \tag{4.38e}$$

$$C_{d,eff,\text{ACL}} = C_{d,\text{ACL}}(k - \theta_{d,eff})\mathcal{H}(k - \theta_{d,eff}) \tag{4.38f}$$

$$\underline{x}_d(1) = [0,\ 0,\ 0,\ 0,\ 0,\ \ln(N_0)]^\top \tag{4.38g}$$

Where $\theta_{d,eff} = \lfloor \theta_{eff}/h \rfloor$, or θ_{eff}/h rounded down to the nearest integer. By utilizing the binary variables introduced in equation (4.35), the nonlinear transform from (4.20), and the discretization (4.38), the dose regimen determination problem can be restated as follows:

$$\begin{aligned} \min_{D_d(q)} \quad & P_d(m_k) \\ \text{s.t.} \quad & (4.35),\ (4.36),\ (4.38) \end{aligned} \tag{4.39}$$

The resulting optimization is a MILP which can be solved to optimality given a reasonable step size h, which is selected such that the fastest dynamics are adequately captured.

defined by the fastest dynamic equation.

4.4.4 MILP Results

The parameters used in this case study were given in Table 6. The initial tumor volume was assumed to be $N_0 = 40$ mm^3 and a discretization step size of $h = 20$ min was used. The system was modeled in the General Algebraic Modeling System (GAMS) using the bdmlp solver. For a four week treatment window, the resulting problem had $m = 2016$ steps, 20202 equations, 20201 continuous variables and 20 discrete variables. The optimal solution was found in 109 seconds and is shown in Figure 28 along with the current standard of preclinical practice. In this case study, the final tumor volumes using both dosing regimens are not experimentally differentiable. While the MILP–derived regimen is mathematically optimal (the final tumor volume from the QD×5×2 was -3.2×10^{-9} mm^3 larger than that found using the optimal dosing regimen), the results suggest that an exponentially growing tumor affected in a bilinear fashion by a drug with linear PK has a final tumor volume determined solely by the amount of drug administered and is independent of the dosing schedule.

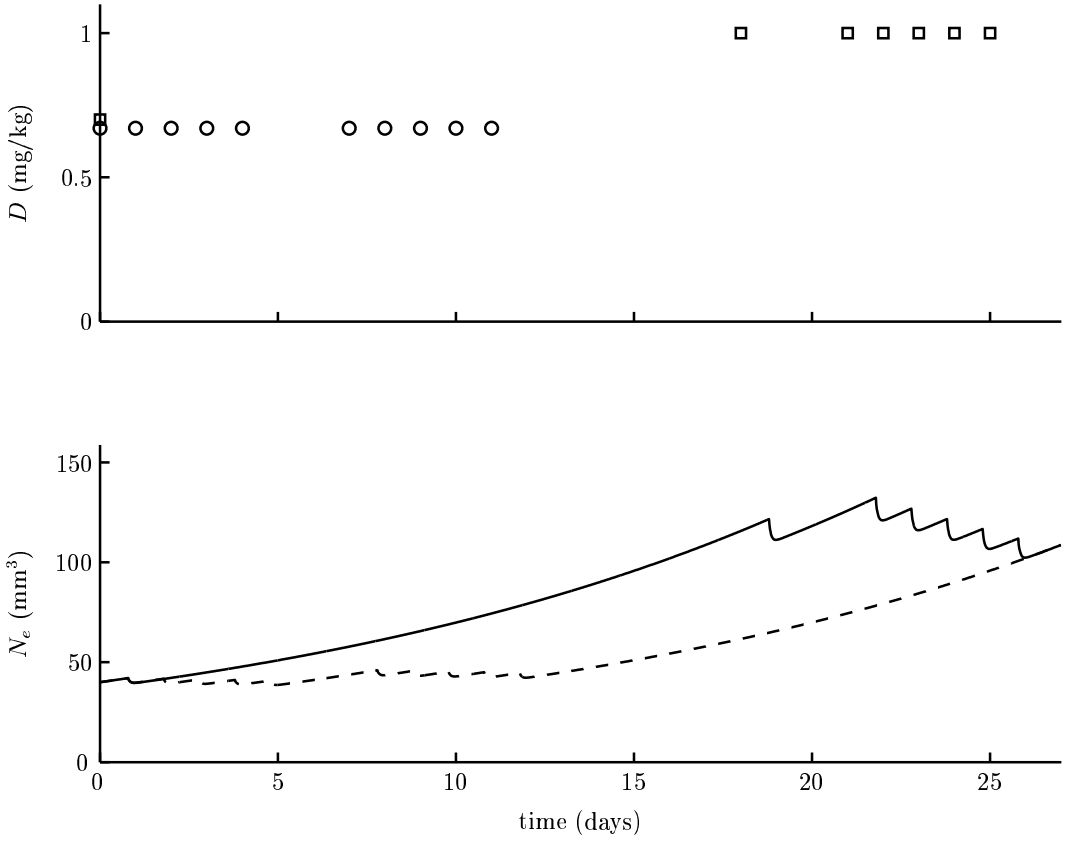

Figure 28: Case study II response to treatment. Top pane: optimal dosing profile (□), as suggested by the MILP (4.39), and current standard of practice (○). Bottom pane: tumor volume in response to the optimal dosing profile (—) and the current standard of practice (−−).

The independence of outcome to dose schedule can be shown using a simple example. Consider the following simple model of exponential growth in response to an intravenously administered drug:

$$\begin{array}{rrcl} \text{PK:} & \dot{x}_0(t) & = & -\frac{x_0(t)}{\tau_0} + \frac{u(t)}{\tau_0} \\ \text{PD:} & \dot{x}_1(t) & = & -\frac{\ln(2)}{\tau_e} x_1(t) - k_{eff} x_1(t) x_0(t) \\ & N(t) & = & x_1(t) \end{array} \tag{4.40}$$

Let the input be a bolus, $u(t) = M\delta(t)$, occurring at some time ($t = t_i$). The objective is to evaluate the effect of this input on tumor size, $x_1(t)$, at some final time ($t = t_f$). The transformation in equation (4.20) was carried out and applied to (4.40) to provide the following dynamic *linear* system:

$$\begin{array}{rcl@{\qquad}rcl} \dot{x}_0(t) & = & -\frac{x_0(t)}{\tau_0} + \frac{u(t)}{\tau_0} & x_0(0) & = & 0 \\ \dot{x}_t(t) & = & \frac{\ln(2)}{\tau_e} - k_{eff} x_0(t) & x_t(0) & = & \ln(x_1(0)) = K \\ N_t(t) & = & x_t(t) & & & \end{array} \tag{4.41}$$

Now consider the input profile $u(t) = M\delta(t-\theta)\mathcal{H}(t-\theta)$ — a bolus of magnitude M applied at an arbitrary time θ. Based on this input, equation (4.41) can be transformed into the Laplace domain and solved analytically to provide the following time domain representation for $N_t(t)$:

$$N_t(t) = \underbrace{\frac{\ln(2)}{\tau_e}\frac{1}{K}\left(e^{Kt} - 1\right)}_{\text{growth}} \underbrace{- k_{eff} M \left(\frac{1}{\tau_0 K + 1} e^{K(t-\theta)} - \frac{1}{\tau_0}\frac{1}{\frac{1}{\tau_0} + K} e^{-\frac{(t-\theta)}{\tau_0}} \right) \mathcal{H}(t-\theta)}_{\text{death}} \tag{4.42}$$

The time domain result (4.42) can be segregated into growth and death terms as shown. In the absence of drug administration, the tumor will continue to increase exponentially. The presence of an input will decrease the tumor volume according to the death term. By increasing or decreasing θ the dynamic response will change. However, the point of interest for final time problems is the state of the system after the influence of drug administration has passed. For a first order linear system this occurs approximately at the time $t_f > \theta + 5\tau_0$ [26]. At t_f, the overall decrease in tumor size (*i.e.*, $N_t(t_f)$) will be the same regardless of when the drug is administered provided it is not given within $5\tau_0$ of t_f. This is a straightforward application of the superposition principle [68].

4.5 CASE STUDY III: NONLINEAR PK/SWITCHED EXPONENTIAL GROWTH

The final case study considered utilizes the nonlinear PK/PD model of 9NC and 9AC efficacy, (2.9), and the linear model of toxicity (3.9). The state and output equations are given by:

$$\dot{x}_1(t) = \frac{x_2(t)}{\tau_u} - \frac{x_1(t)}{\tau_u} \tag{4.43a}$$

$$\dot{x}_2(t) = \frac{D_u(t)}{\tau_u} - \frac{x_2(t)}{\tau_u} \tag{4.43b}$$

$$\dot{x}_3(t) = \frac{x_4(t)}{\tau_l} - \frac{x_3(t)}{\tau_l} \tag{4.43c}$$

$$\dot{x}_4(t) = \frac{D_l(t) + x_5(t)}{\tau_l} - \frac{x_4(t)}{\tau_l} \tag{4.43d}$$

$$\dot{x}_5(t) = \beta_1 \frac{x_3(t)}{\tau_r} - \frac{x_5(t)}{\tau_r} \tag{4.43e}$$

$$\dot{x}_6(t) = \alpha_2(x_1(t-\theta_2) + \alpha_1 x_3(t-\theta_2))\mathcal{H}(t-\theta_2)\frac{D_{last}}{\tau_{nl}} - x_6(t)\frac{D_{last}}{\tau_{nl}} \tag{4.43f}$$

$$\dot{x}_7(t) = \frac{\ln(2)}{\bar{\tau}_e(x_7(t))} x_7(t) - k_{eff} C_{eff}(t) x_7(t) \tag{4.43g}$$

$$\dot{x}_8(t) = k_g x_9(t) - k_c C_{eff}(t) \tag{4.43h}$$

$$C_{eff}(t) = C_{\mathrm{NC}}(t) + C_{\mathrm{AC}}(t) \tag{4.43i}$$

$$C_{\mathrm{NC}}(t) = x_1(t)\frac{K_u}{D_{last}} + K_l \alpha_1 x_3(t) \tag{4.43j}$$

$$C_{\mathrm{AC}}(t) = (x_1(t) + x_3(t)\alpha_1)\beta_2 K_a + x_6(t) K_a \tag{4.43k}$$

$$N_s(t) = x_7(t) \tag{4.43l}$$

$$B(t) = x_8(t) \tag{4.43m}$$

$$B_{tox}(t) = x_8(t) - \frac{x_7(t)}{1000} \tag{4.43n}$$

$$\bar{\tau}_e(x_7(t)) = \begin{cases} \bar{\tau}_{e,f}, & x_7(t) < \bar{N}_{th} \\ \bar{\tau}_{e,s}, & x_7(t) > \bar{N}_{th} \end{cases} \tag{4.43o}$$

The methodology behind the construction of this model was covered in Chapters 2 and 3. Equations (4.43a) through (4.43f) represent the PK of 9NC and 9AC after oral administration of 9NC. Tumor proliferation and PD response (efficacy) to 9NC administration is characterized by equation (4.43g). Toxicity, in terms of body weight reduction, is described

by equation (4.43h). The outputs $C_{\mathrm{NC}}(t)$ and $C_{\mathrm{AC}}(t)$ represent the plasma concentrations of 9NC and 9AC total, respectively. Tumor volume, mouse body weight and the corrected body weight are given by the outputs N_s, B, and B_{tox}, respectively. The initial state of the system is $\underline{x}(0) = [0,\ 0,\ 0,\ 0,\ 0,\ 0,\ N_0,\ B_0]^\top$, where no drug is present, the tumor volume is initially N_0, and the initial body weight is B_0.

4.5.1 Continuous Constraint Formulation

Based on the mathematical representation in equation (4.30), the optimal dosing regimen was determined for a treatment interval of N_{weeks} ($t_f = N_{weeks} \times 7(\text{days/week}) \times 1440(\text{minutes/day})$). The same logistical constraints apply as those from section 4.4. Work schedules dictate that drugs could only be delivered once each weekday. For N_{weeks} of treatment, there are $q = N_{weeks} \times 5$ possible dosing times.

The semicontinuous dosing constraint from section 4.4, equation (4.32), is still valid. The amount of drug administered at any dosing opportunity is either zero or must lie somewhere between an upper and lower bound, 1.0 and 0.44 mg/kg, respectively. In section 4.4, a toxicity bound was placed on total exposure. In this case study, a lower bound on B_{tox} is considered:

$$B_{tox}(t) \geq B_{min} \tag{4.44}$$

4.5.2 Continuous Problem Formulation

The continuous problem can be formulated as

$$\begin{aligned} \min_{D(q)} \quad & N_s(t_f) \\ \text{s.t.} \quad & (4.32),\ (4.43),\ (4.44) \end{aligned} \tag{4.45}$$

The optimization in (4.32) is a NLP because of the nonlinear PK, discontinuities in $D(t)$, and the bilinear kill term. This problem can be reformulated as a MILP which can be solved to global optimality.

4.5.3 MILP Problem Reformulation

4.5.3.1 Parameterized PK Nonlinearities such as those found in the nonlinear 9NC PK model (4.43a)–(4.43f) can make optimizations quite complicated. To eliminate these nonlinearities, we make use of the fact that both 9NC and 9AC are cleared at a rate such that any drug from a dose on a given day is below the level of detection by the following day. While the range of doses is continuous (0.44 – 1.0 mg/kg), realistically there are a set of doses, $l = [1, m_l]$, which can be distinguished from each other. For each of these doses, a PK profile can be calculated *a priori* such that 9NC and 9AC concentrations at all the times after a given dose are parameterized by dose magnitude. The set of steps per day is given by $z = [1, m_z]$. The algorithm then selects from the set of profiles each dosing opportunity. This is achieved by introducing the binary variable $b_{d,dose}(q, l)$ at each dosing opportunity for each possible dose level. The dynamic PK equations can then be replaced with the following constraints:

$$C_{d,\mathrm{NC}}(k) = \begin{cases} \sum_{i=1}^{m_l} b_{d,dose}(q,i) Q_{\mathrm{NC}}(j,i), & k = Q_{map}(q) - 1 + j, \ \forall j \in [1, \cdots, m_z] \\ 0, & \text{otherwise} \end{cases} \tag{4.46a}$$

$$C_{d,\mathrm{AC}}(k) = \begin{cases} \sum_{i=1}^{m_l} b_{d,dose}(q,i) Q_{\mathrm{AC}}(j,i), & k = Q_{map}(q) - 1 + j, \ \forall j \in [1, \cdots, m_z] \\ 0, & \text{otherwise} \end{cases} \tag{4.46b}$$

$$1 = \sum_{i=m_1}^{l} b_{d,dose}(j,i) \ \forall j \in [1, \cdots, m_q] \tag{4.46c}$$

$$C_{d,eff}(k) = C_{d,\mathrm{AC}}(k) + C_{d,\mathrm{NC}}(k) \tag{4.46d}$$

Where $Q_{\mathrm{NC}}(z, l)$ and $Q_{\mathrm{AC}}(z, l)$ are matrices of precalculated concentrations of 9NC and 9AC, respectively. The parameter $Q_{map}(q)$ is a map between the dosing opportunity (q) and the timestep (k) in which it occurs. For example, the second dosing opportunity, $q = 2$, with a time step of one minute occurs at $k = 2881$, so $Q_{map}(2) = 2881$. The constraint (4.46c) ensures that only one dose level is selected at any given dosing opportunity.

4.5.3.2 PD Variable Transform The tumor growth equation (4.43g) is transformed using the method found in (4.20) such that the tumor growth model becomes:

$$\dot{P}(t) = \mathcal{F}_s(P(t)) - k_{eff}C_{eff}(t) \tag{4.47a}$$

$$\mathcal{F}_s(P(t)) = \begin{cases} \frac{\ln(2)}{\bar{\tau}_{e,f}}, & P(t) < \ln\left(\bar{N}_{th}\right) \\ \frac{\ln(2)}{\bar{\tau}_{e,s}}, & P(t) > \ln\left(\bar{N}_{th}\right) \end{cases} \tag{4.47b}$$

The discontinuity in the rate of proliferation is a piecewise continuous function of $P(t)$. As shown in equation (4.13), this behavior can be accounted for by adding a binary variable $b_{d,P}(k)$ and replacing (4.47) with the following constraints [70]:

$$P_d(k) - \ln \bar{N}_{th} \leq (\ln(N_{max}) - \ln(\bar{N}_{th}))(1 - b_{d,P}(k)) \tag{4.48a}$$

$$(1 - b_{d,P}(k))\left(\frac{\ln(2)}{\bar{\tau}_{e,s}} - \frac{\ln(2)}{\bar{\tau}_{e,f}}\right) \leq \mathcal{F}_{d,s}(k) - \frac{\ln(2)}{\bar{\tau}_{e,f}} \tag{4.48b}$$

$$(1 - b_{d,P}(k))\left(\frac{\ln(2)}{\bar{\tau}_{e,s}} - \frac{\ln(2)}{\bar{\tau}_{e,f}}\right) \geq \mathcal{F}_{d,s}(k) - \frac{\ln(2)}{\bar{\tau}_{e,f}} \tag{4.48c}$$

$$\ln \bar{N}_{th} - P_d(k) \leq \ln(\bar{N}_{th}) b_{d,P}(k) \tag{4.48d}$$

$$b_{d,P}(k)\left(\frac{\ln(2)}{\bar{\tau}_{e,f}} - \frac{\ln(2)}{\bar{\tau}_{e,s}}\right) \leq \mathcal{F}_{d,s}(k) - \frac{\ln(2)}{\bar{\tau}_{e,s}} \tag{4.48e}$$

$$b_{d,P}(k)\left(\frac{\ln(2)}{\bar{\tau}_{e,f}} - \frac{\ln(2)}{\bar{\tau}_{e,s}}\right) \geq \mathcal{F}_{d,s}(k) - \frac{\ln(2)}{\bar{\tau}_{e,s}} \tag{4.48f}$$

Where $\mathcal{F}_{d,s}(k)$ is the discrete–time form of $\mathcal{F}_s(P(t))$. The values N_{min} and N_{max} are smallest and largest possible tumor volume, respectively. The lower bound is represented by zero, and the upper bound is represented at each timestep by the predicted size of the tumor at that timestep in the absence of treatment.

4.5.3.3 Effect of Transform on Body Weight Calculations

By performing the PD transform (4.20) as employed in (4.47), the body weight calculation becomes:

$$B_{d,tox}(k) = B_d(k) - \frac{e^{P_d(k)}}{1000}$$

To avoid the nonlinearity associated with the exponential term, a conservative estimate was made. The transformed tumor volume, $P_d(k)$, was replaced with the value it would take if no drug were administered, $Q_{Pnom}(k)$:

$$B_{d,tox}(k) = B_d(k) - \frac{e^{Q_{Pnom}(k)}}{1000} \tag{4.49}$$

And the bound on body weight is given by:

$$B_{tox}(t) \geq B_{min} \tag{4.50}$$

It is possible for the tumor size to increase at the nominal rate which would yield large values of Q_{Pnom} at the end of treatment cycles. This could lead to conservative dose schedules being returned by the controller for the cycle. Two options that address this problem are: (i) a less conservative value for B_{min} could be used, or (ii) the duration of treatment cycles could be reduced to allow the clinician more frequent feedback and model correction. Shorter cycles would be preferred from the perspective of patient safety.

4.5.3.4 Dynamic Equations

The remaining dynamic equations (4.43h) and (4.47b) can now be discretized for a stepsize h using the Euler's method [69]:

$$P_d(k+1) = P_d(k) + h\left(\mathcal{F}_{d,s}(k) - k_{eff}C_{d,eff}(k)\right) \tag{4.51a}$$

$$B_d(k+1) = B_d(k) + h\left(k_g B_d(k) - k_c C_{d,eff}(k)\right) \tag{4.51b}$$

Table 14: Parameters used in Case Study III.

parameter	value	units
B_0	20	g
B_{min}	$0.98B_0$	g
N_0	40	mm^3
h	5	min
t_f	8	weeks

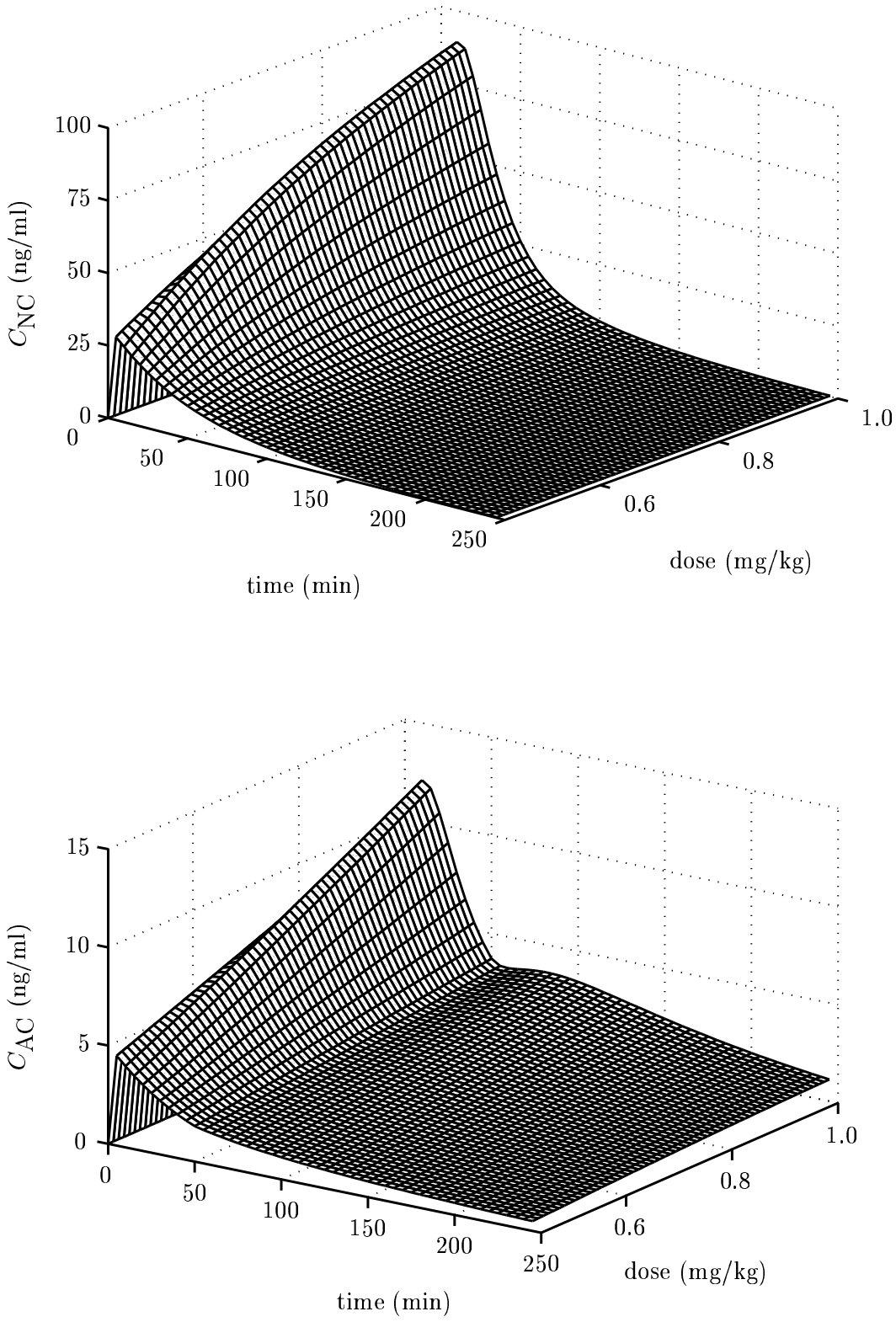

Figure 29: Mesh plot of concentration profiles of 9NC (top pane) and 9AC (bottom pane) total for dose levels ranging from 0.44 to 1.0 mg/kg 9NC in 0.01 mg/kg increments.

until the latter portion of treatment when a maximum amount of drug was administered such that the toxicity constraint (4.50) was not violated.

4.5.5 MILP Results: Shrinking Horizon Problem

As before, a more clinically relevant reference trajectory for the tumor volumes to follow was specified. This was done by minimizing the tumor volumes at the end of each week. This can be stated mathematically as:

$$\begin{aligned} \min_{b_{d,dose}(q,l)} \quad & \sum_{i}^{m_p} P_d(i) \quad \forall i \in [2016, 4032, 6048, \cdots, 16128] \\ \text{s.t.} \quad & (4.46),\ (4.48),\ (4.49),\ (4.50),\ (4.51), \end{aligned} \tag{4.53}$$

Here i is the index corresponding to 1 week (1 week = 100080 min/h min). The same set of parameters and possible dose levels used in the final time problem, Table 14 (section **??**), were used here. The problem (4.53) was modeled in GAMS and solved using CPLEX. The same number of equations and variables were generated, and the optimal solution was found in approximately 11 hours. The dosing profile and corresponding body weights and tumor volumes are shown in Figure 31. By modifying the objective function, a more clinically relevant treatment regimen was developed. The body weight satisfied the constraint while the tumor volume was gradually reduced over the treatment window.

Next the amount of drug administered was constrained to be either the maximum possible value (1.0 mg/kg) or none at all. This is similar to the clinical case where a pill will either be administered or not at each dosing opportunity. All of the parameters from (4.53) were the same with the exception of the possible dose levels, which were 0 and 1.0 mg/kg. Once formulated, this problem had $m_k = 16,128$ time steps, 193,575 equations, 112,977 continuous variables, 16,208 discrete variables, and a solution time of 22 minutes. The solution is shown in Figure 32. When considering the solutions provided in Figures 31 or 32, the first four weeks of drug administration would be implemented. At the end of four weeks, measurements of body weight and tumor volume would be made. New dosing profiles would then be calculated for the next eight weeks and the first four weeks implemented. This process would then be

repeated until tumor progression occurred, unacceptable toxicity resulted, or clinical response was obtained.

To place the controller results into perspective, they will be compared to the current standard of practice, QD×5×2 every four weeks, shown in Figure 33. Table 15 summarizes the results presented in this section. Minimizing tumor volumes at a final time has already been established to be of little clinical relevance. The results presented in Figure 31 delivered a total of 25.76 mg/kg of 9NC and have minimum and maximum tumor volumes of 7.9 and 42.1 mm^3 respectively. The solution to the more constrained problem shown in Figure 32 delivered slightly more drug, 27 mg/kg of 9NC. The binary dosing option also had a wider range of tumor volumes 6.7 and 44.2 mm^3 for the minimum and maximum values, respectively. Both of the solutions had body weight values above the 98% level specified. The finely graded dosing option had a minimum normalized corrected body weight of 0.982, while the the binary dosing option had a minimum normalized corrected body weight of 0.98, both satisfying the toxicity constraint. The standard of practice delivers 20 mg/kg over the eight week window with a minimum normalized corrected body weight of 0.972. The maximum tumor volume is lower than the two solutions previously discussed at 40 mm^3 while the minimum tumor volume is higher at 10.5 mm^3.

Each of the dosing profiles have their positives aspects. Considering the clinically relevant aspects of the problem, the solution to the trajectory tracking problem which constrained the dosing to be either 0 or 1.0 mg/kg, shown in Figure 32, would be considered optimal. While allowing the controller to select from more possible doses yields a more mathematically optimal solution, clinicians would find little difference between the two trajectory tracking solutions in terms of efficacy. However, the binary dosing option is preferred for two reasons. The first is that it eventually becomes periodic. Regular, or periodic, administration is preferred over the more erratic schedule shown in Figure 31. The chance for error is significantly reduced by constraining the dose levels to fixed discrete values. This is highly relevant when considering oral drugs prescribed in pill form.

Table 15: Summary of relevant statistic for different dosing profiles: (i) minimizing tumor volume at a final time, (ii) trajectory tracking using a near continuous dosing profile, (iii) trajectory tracking allowing dose levels of 0 or 1.0 mg/kg of 9NC, and (iv) the current standard of practice (QD×5×2 every four weeks).

	Dosing Profile:	$\max(N(t))$ (mm^3)	$\min(N(t))$ (mm^3)	$\min\left(\frac{B_{tox}(t)}{B_0}\right)$ (–)	$\sum_{i=1}^{m_q} D(q)$ (mg/kg)
(i)	Minimize $N(t_f)$, Figure 30	86.5	5.2	0.980	28.48
(ii)	Trajectory, Figure 31	42.1	7.9	0.982	25.76
(iii)	Trajectory, Figure 32	44.3	6.7	0.981	27.0
(iv)	QD×5×2, Figure 33	40.0	10.5	0.972	20.0

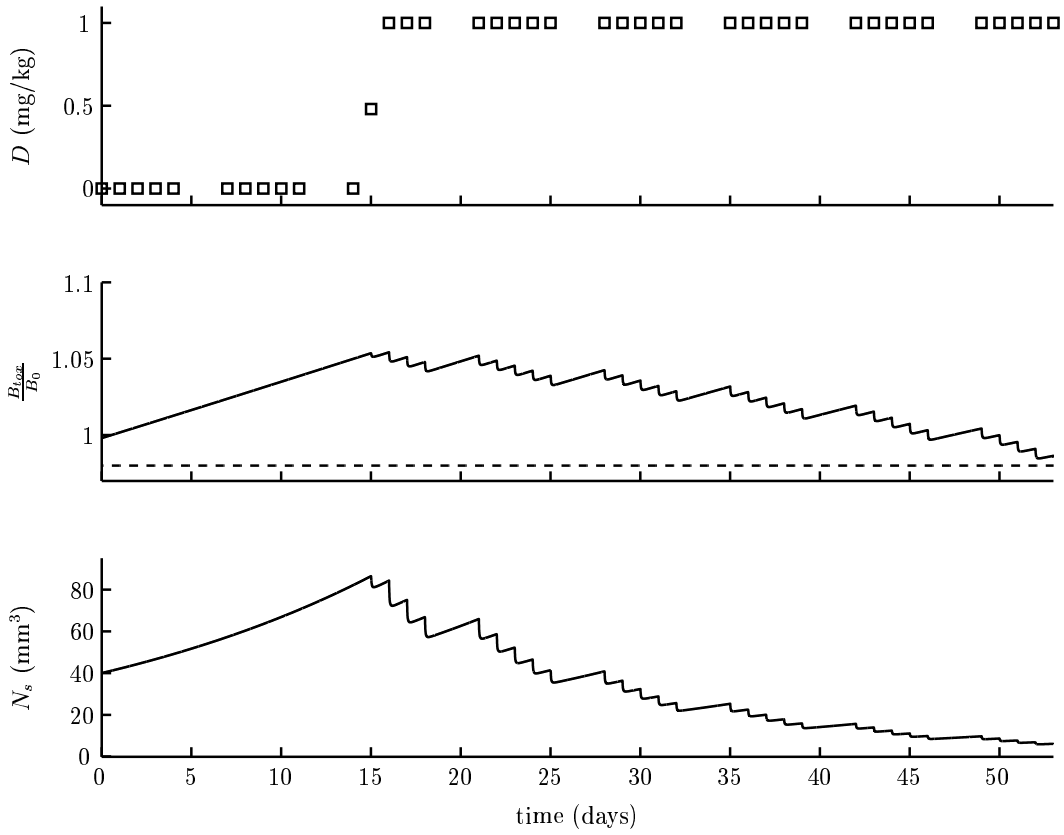

Figure 30: Case study III response to treatment — Minimizing tumor burden at a final time (eight weeks). Top pane: optimal dosing profile (□), as suggested by the MILP (**??**). Middle pane: corrected body weight (—) and lower bound on corrected body weight (−−). Bottom pane: tumor volume in response to the optimal dosing profile (—).

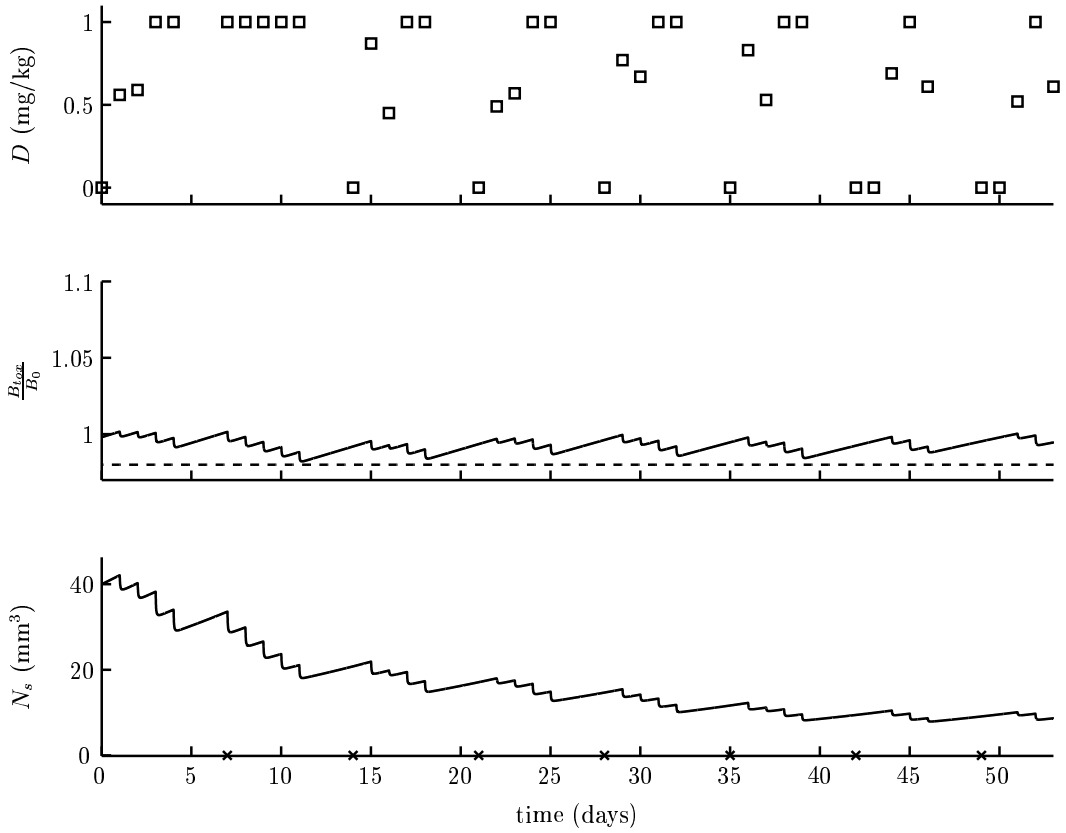

Figure 31: Case study III response to treatment — Trajectory tracking of zero tumor volume every week. Top pane: optimal dosing profile (□), as suggested by the MILP (4.53). Middle pane: corrected body weight (—) and lower bound on corrected body weight (−−). Bottom pane: tumor volume in response to the optimal dosing profile (—) and desired trajectory (×). Possible dose levels 0 to 1.0 mg/kg in 0.01 mg/kg increments

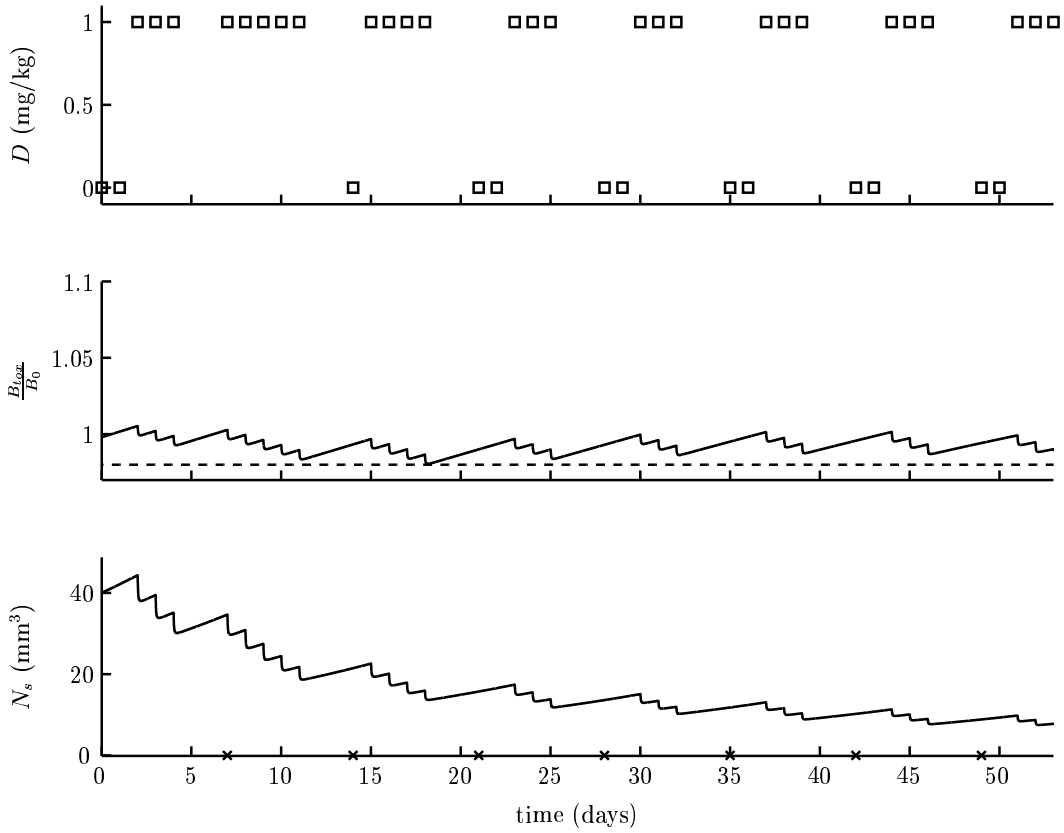

Figure 32: Case study III response to treatment — Trajectory tracking of zero tumor volume every week. Top pane: optimal dosing profile (□), as suggested by the MILP (4.53). Middle pane: corrected body weight (—) and lower bound on corrected body weight (−−). Bottom pane: tumor volume in response to the optimal dosing profile (—) and desired trajectory (×). Possible dose values: 0 and 1.0 mg/kg

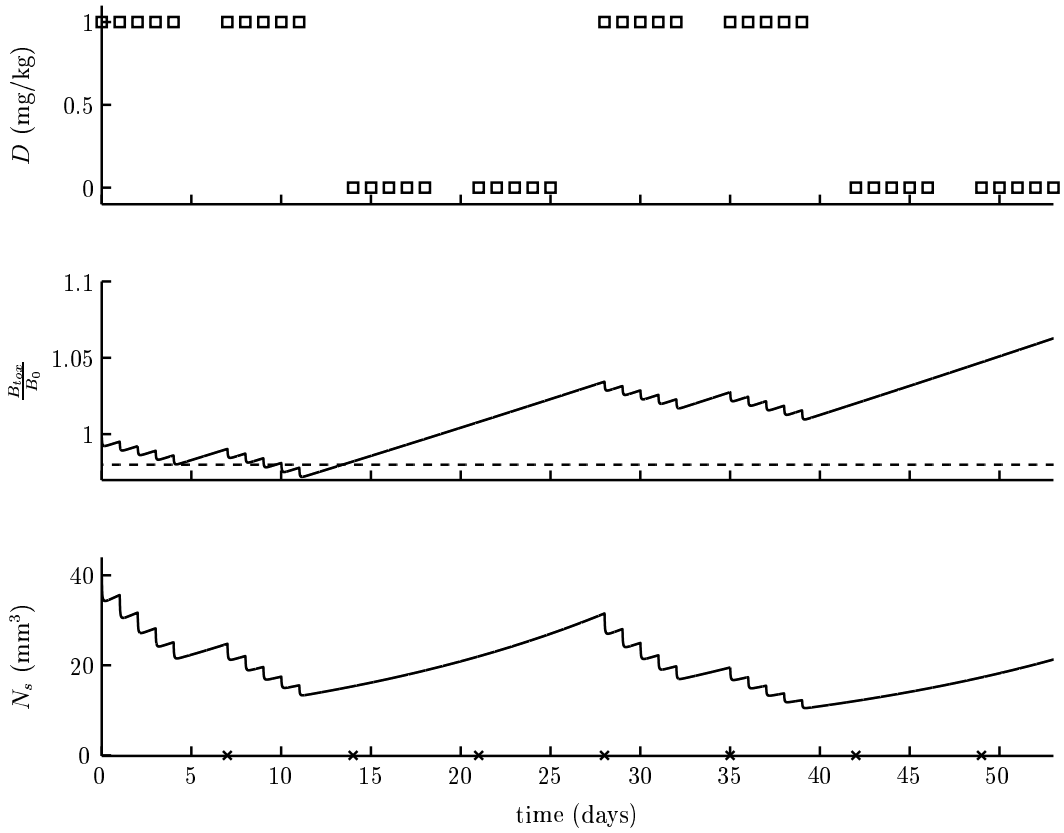

Figure 33: Case study III response to treatment — standard of practice dosing. Top pane: QD×5×2 every four weeks (□), representing the current standard of practice (4.53). Middle pane: corrected body weight (—) and lower bound on corrected body weight (-·-). Bottom pane: tumor volume in response to the dosing profile (—) and desired trajectory (×). Possible dose values: 0 and 1.0 mg/kg

4.6 SUMMARY

In this chapter three case studies in chemotherapy control were presented. The first, studied previously by Martin and Teo [12], was reformulated as a MILP and a solution similar to that of the original authors was calculated. This resulted in treatment being withheld for a significant period of time and large amounts of drug being administered over the last half of the treatment cycle. This mathematically optimal solution would be ethically questionable for a clinician to implement due to the long window in which no treatment would be delivered. It is neither intuitive nor desirable from a clinical perspective to withhold treatment for long periods of time when no complications due to toxicity or other extenuating circumstances have been encountered. In an effort to develop a more pragmatic solution, a shrinking tumor objective was considered. A trajectory specifying a rapid reduction in tumor volumes over time was used as the objective, and the result was a more clinically acceptable treatment regimen.

The remaining two case studies focused on the 9NC treatment of SCID mice bearing HT29 human colon carcinoma xenografts as modeled in chapters 2 and 3. The second case study considered exponentially growing tumors with PD driven by linear PK and cumulative toxicity constraints. Cumulative toxicity constraints were shown to be inadequate because tumors under exponential growth with bilinear PD driven by linear PK gain no benefit by altering the dosing schedule due to the principle of superposition. The third case study consisted of a switched exponential tumor model coupled with a nonlinear PK model and a model of body weight reductions in response to treatment. When attempting to minimize the final tumor volume, a solution which applied as much drug as possible at the end of the treatment cycle was obtained. As in case study I, the objective function was modified to yield a more clinically amenable treatment strategy. The receding horizon framework makes use of periodic feedback and addresses the fact that endpoints are not clearly defined. In the event that measurements vary significantly from the predictions, new parameter estimates could be obtained and the dosing schedule recalculated (although the parameter update step was not address in the present work). In theory, treatment would continue along this path until

the subject no longer responded to treatment or the tumor volume fell below measurable levels.

5.0 CONCLUSIONS AND RECOMMENDATIONS

5.1 CONTRIBUTIONS

The work discussed here has focused on modeling and control of cancer chemotherapy with a primary focus on developing control methodologies that could be clinically applicable. The methodologies used are based on those used to optimize and control industrial processes. Novel modeling and control approaches to cancer therapy problems were developed which provide a basis for the design of clinically relevant drug schedules.

5.1.1 PK/PD Modeling

The models developed here are empirical data–driven models of drug PK and PD. Two novel models were introduced to describe the PK of 9NC. A linear model of the plasma disposition of 9NC lactone and 9AC lactone in response to oral administration of 9NC at 0.67 mg/kg to SCID mice was developed. Based on experimental data for total concentrations of 9NC and 9AC at 9NC dosing levels of 0.44, 0.67, and 1.0 mg/kg, a nonlinear PK model was developed to capture the observed nonlinear dynamics.

Untreated tumor growth was characterized for twenty mice using two different macroscopic models. A simple model characterized the exponential growth of the implanted tumors. A more complicated model structure was investigated which segregated tumor growth into two regimes. Initially the tumor grew quickly, and after reaching a threshold size, the rate of proliferation decreased. This was referred to as a switched exponential model and was capable of accurately predicting tumor volumes over a wider range of times and eliminated the underpredictions found in the exponential model at early time points.

Based on the PK and untreated tumor growth models, two PK–driven PD models were developed. The first PK/PD model coupled the linear PK of 9NC lactone and 9AC lactone with the exponential growth model. This resulted in a description of drug distribution and efficacy having a single nonlinear (bilinear) term. An alternative structure combined the nonlinear PK model with the switched exponential growth model to develop a more complex PK/PD model that captured treatment response across a range of dose levels. The nonlinear PK model was also used to drive a toxicity model which predicted body weight changes in response to drug administration.

The models developed here were designed to balance predictive accuracy with model complexity. Predictive accuracy is important because model accuracy limits the theoretically achievable performance of a controller [8]. The importance of model complexity can be seen when trying to develop control algorithms. As the number of states and nonlinearities increase and the nonlinear character becomes more complicated [73, 74, 75, 76, 77], control algorithm synthesis may become markedly harder. More information could be used to improve the accuracy of the model. Since 9NC and 9AC are cycle–specific compounds, a model capable of predicting the population of cells in the cell–cycle would lead to a better predictions of exposure. More complicated models, such as PBPK models, will provide more information about specific tissues. Model reduction techniques may be necessary when implementing these models in control algorithms.

5.1.2 Cancer Control

Engineering approaches to chemotherapy dose scheduling have typically focused on elegant mathematical solutions using optimal control theory. While these solutions are appealing in theory, they are not generally relevant in the clinic. A different approach was developed in this work, where tools common to plant scheduling and operations research were utilized. Any chemotherapy scheduling algorithms should embrace the concept that toxicity and efficacy are the primary drives of treatment. In mathematical terms, a dose scheduling algorithm should meet clinically relevant objectives in terms of efficacy, without violating toxicity constraints.

A mixed–integer programming methodology was employed because it is flexible when considering constraints, especially those encountered in the clinic. Constraints such as semi-continuous or discrete dosing ranges, therapeutic thresholds, and categorical classification of toxicities lend themselves well to (mixed–)integer programming representations. Different variants of the final time problem — minimizing tumor volume at some final time — have been considered by engineers [12, 44, 53, 46]. However, final times in a clinical setting are not well defined *a priori*. The goal of a clinician is to eliminate the tumor burden while maintaining patient quality of life; speed of elimination is a secondary objective. This can be stated mathematically as a trajectory tracking problem. While trajectory tracking can be encumbering from an optimal control perspective, it is easily implemented by posing the problem as a MIQP.

To demonstrate the utility of this methodology, a theoretical drug/tumor system previously studied by Martin and Teo was considered [12]. By reformulating the problem and eliminating certain nonlinearities by variable transformation, a MILP solution strategy was developed that solved the problem as originally posed. The solution to minimizing the tumor burden at a final time yielded results which postponed treatment until the end of the treatment interval. From a treatment perspective, it would be unethical to withhold treatment for such an extended period of time. The theoretical system was then considered in a more clinically relevant framework. By altering the objective function in the reformulation, it was specified that the tumor burden be eliminated rapidly by establishing a trajectory of small tumor volumes for treatment to follow. While this resulted in a numerically larger tumor population at the end of the treatment horizon, the final tumor populations were less than one for both the optimal control and the MINLP solutions. The rapid elimination led to a more clinically acceptable method of treatment. The suggested dosing schedule delivered a large amount of drug initially which drove the tumor volume down, and the remainder of treatment consisted of a maintenance doses which tracked the trajectory well.

Next a preclinical system was considered. The effects of 9NC on HT29 tumor–bearing SCID mice was studied. Two different case studies were developed around this system. The first consisted of an exponential tumor growth PD model driven by a linear PK model of 9NC lactone and 9AC lactone. This was the least complicated model constructed from this

system. To constrain the toxicity of this system, cumulative drug exposure was used. The maximum allowable exposure was set to that experienced under the current standard of practice (0.67 mg/kg QD×5×2). Because linear PK results in a direct link between drug administration and exposure (AUC), an upper bound was placed on the total amount of drug which could be administered. A mathematical analysis found that the overall effect of drug administration on a tumor burden — described with linear PK, exponential tumor growth, and a bilinear kill term — was the same provided the effect of all doses was observed by the end of treatment.

The same preclinical system was reconsidered except this time it was described by nonlinear PK, a switched exponential tumor growth model, and toxicity quantified in terms of body weight. This problem was treated similarly to the Martin and Teo problem. To account for the nonlinear PK, concentrations of 9NC and 9AC total were precalculated for a range of dose levels. The algorithm was then allowed to select from this range of precalculated dose levels. This eliminated the nonlinearity associated with the 9NC PK. A lower bound was placed on the corrected body weight to bound the toxic effects of treatment. The objective was specified to reduce tumor volumes over an eight week period. Solutions were found to lie on toxicity boundaries and a cyclical treatment methodology eventually evolved. This resulted in a treatment schedule with consistent reductions in tumor volumes along a trajectory which was better, in terms of efficacy, than the standard QD×5×2 every four weeks.

5.2 FUTURE WORK

Clinical oncologists and pharmacologists design experiments to answer specific questions. It is possible for engineers and mathematicians to pick through the literature and find data to drive their modeling and control efforts. However, to truly make an impact on the field of oncology, strong interdisciplinary collaboration is required. All of the modeling work discussed above will require additional experimental data to validate, and model and control studies will drive new experiments. This will be a cyclical process where experiments drive

models and modeling results drive experiments may bring new treatment methodologies to the clinic that would otherwise be unavailable due to the data on theoretical shortcomings.

5.2.1 Detailed Modeling

Under the premise that model accuracy limits achievable controller performance [8], a better understanding of tumor progression, drug distribution, and PD effects would enhance the ability of control algorithms to aid clinicians in their dosing decisions. While detailed models can lead to difficulties in controller synthesis, they can provide insight into the underlying mechanisms of cancer progression and treatment. This insight could then be used to inform more control–relevant models in an iterative fashion.

5.2.1.1 Cancer Progression Models There are several different areas in which modeling of cancer progression could be improved. Many chemotherapeutics are cycle specific, and they have their greatest effect on cells in certain phases of the cell–cycle. The models presented in this work treated cancer as a lumped mass, and no distinction was made between cancer cells. Population models are one method which can account for the heterogeneity found between the states of cancer cells. Cell–cycle dynamics have been addressed by considering purely theoretical systems [15, 16]. More recently, cell–cycle representations have been applied actual experimental systems to characterize to characterize the transition rates between the different phases of the cell–cycle [78, 79, 80]. These can lead to improvements in chemotherapy scheduling by determining the population of cells susceptible to treatment and how chemotherapy effects these phase transition rates (*i.e.* when cells will defensively enter the quiescent phase to avoid treatment effects).

Proliferation can also be considered on a more detailed level. Cells communicate and regulate their own intracellular process through complicated chemical signals. In the last decade much effort has been devoted to mapping out and isolating these pathways [81, 82, 83, 84]. Often, research focuses on correlating the presence or absence of chemical signals with specific cellular events [85, 86, 87]. Cellular dynamics are robust and result in redundant pathways [88]. Isolated identification of signal pathways ignores these redundancies. A

systemic approach is required to identify the interactions between the different signaling mechanisms.

5.2.1.2 Detailed PK Models The PK models presented in this work attempted only to account for plasma drug concentrations. Chemotherapy is a systemic form of treatment, and drugs distribute throughout an organism after administration. Understanding where the drug distributes may provide more accurate information for PD modeling. By obtaining local tissue concentrations, a more direct relationship between drug administration and the amount of exposure experienced by diseased tissues can be found. Drug disposition also provides a metric for bounding exposure to both diseased and healthy tissues. This can be accomplished with the development of PB/PK models [21] and using such models to drive PD models.

5.2.1.3 Constraint Formulation Most constrained optimization routines result in solutions which lie on the boundary of constraints. With the understanding that efficacy and toxicity drive treatment, the predominate toxicities associated with any given chemotherapeutic drug needs to be quantified and modeled. Two primary complications arise here: available measurements and mechanisms of action. A drug known to have neurotoxicity can be difficult or impossible to measure at the site of toxicity, the brain. The specific mechanism of action (*e.g.* duration of exposure, cumulative exposure, etc.) which results in toxicity will guide treatment. In the absence of direct measurements and a clear understanding of toxicity mechanics, indirect measurements may need to be developed to inform models which can predict toxicity within a reasonable range.

5.2.2 Multi-drug Chemotherapy

The focus of this work has been to study the effects of a single compound on a solid tumor in an animal model. Methods for assessing the effects of combining drugs to better treat cancer are currently under development [89, 90, 91, 92, 93]. Considering efficacy, there are three different outcomes which can result from combining drugs. The combination can

create a synergistic effect and enhance the overall effectiveness of treatment. It could be that combining drugs decreases the effectiveness of treatment and creates an antagonistic effect. Finally, the effects of the individual compounds may simply combine in an additive manner.

The efficacy of combined chemotherapy may be affected by the order in which drugs are administered **??**. Consider two drugs, A and B, which attack the S and M phases of the cell–cycle, respectively. These drugs should be administered such that A is administered when cells are most likely to be in the synthesis phase. Similarly, when most cells are in the mitosis phase, drug B should be administered. Administering large amounts of B could eliminate the population of cells in M. One response might be that more nutrients are now available and cells in the quiescent G_0 phase may enter the proliferating portion of the cell–cycle. Drug A could then be administered as more cells enter the S phase. An alternative response to large amounts of B being administered might be that many cells enter the quiescent phase in response to the toxicity of their micro–environment. In this case, most treatment would be ineffective because quiescent cells are not affected by most chemotherapeutics. An accurate model of cell–cycle dynamics would provide more insight into the problem and aid in scheduling combination chemotherapy.

5.2.3 Patient Variability

It is common for patients to respond quite differently to anticancer drugs [94]. Response variations could be attributed to different rates of drug elimination, reduced liver function, variations in body weight, the presence or absence of specific genes, etc [94]. Because of the toxic nature of chemotherapy, it is important to account for such variability. From a model–based control perspective, this can be characterized by estimating patient–specific parameters.

Models can be developed initially in animals, and then adapted to humans based on data from clinical trials. Clinical trials can provide a population mean behavior. Population averages provide a starting point for treatment. For well–tolerated compounds, population means can be used to design the first cycle of treatment. For particularly toxic substances, conservative estimates for model parameters could be used to schedule the first cycle of

treatment. After the first cycle of treatment has been delivered and responses collected, deviations from the expected response can be used to reestimate patient specific parameters. This update is not limited to the first cycle; at any point where a patient response deviates significantly from the expected, a parameter update could be performed. Reestimation of parameters would start with the current set of parameters as the initial guess and least squares estimate would then be performed to obtain the new set of parameters. If data suggests the PK parameters are incorrect (*e.g.* blood samples suggest reduced liver function which may be reducing the rate of drug metabolism), then it may be necessary to obtain another set of PK data to reestimate the PK parameters.

This seems very straightforward, however there are complicating factors. Detailed animal models can be developed because different tissue measurements are more readily available. This may not be the case in humans. Consider obtaining patient–specific parameters for drug disposition in the kidney. Direct measurement of drug concentration in the kidney may not be clinically feasible. In this regard, it may be necessary to develop indirect measurements based in part on the concentration of the drug in the urine. Also, heuristics may be used when indirect measures are not available. These methodologies would be most useful for drugs which are know to have toxic effects on specific organs.

5.3 IMPLEMENTATION

The focus of this work was the development of treatment schedules in mice. However, the ultimate goal is to apply these methodologies in a clinical setting. To implement these concepts clinically, PK/PD models are necessary. Ideally, an individual specializing in modeling would work in tandem with clinicians and animal pharmacologists during the drug discovery process. Models for specific drug/tumor combinations could then be developed and modified as more information becomes available. This process is ideal because the modeler can help inform experiments. As new compounds enter clinical trials, model parameters representing the most conservative estimates can be used initially in humans. Parameters can be reestimated as human data becomes available. The data from clinical trials can be

used to create population estimates for model parameters. Eventually, drugs approved for clinical use could then have patient specific schedules developed. A patient would enter the clinic and be given a drug. Blood would be draw at specified times based on the PK model structure and the dynamics of the drug. This would provide patient specific PK parameters. Conservative estimates of population PD parameters would then be used to predict schedules for the first two cycles of treatment. This would then provide data for patient specific PD parameters. These parameters could then be updated at the end of each treatment cycle.

APPENDIX A

NOMENCLATURE

Abbreviations	
AIC	Akaike's information criterion
AUC	area under the curve
9NC	9-nitrocamptothecin
9AC	9-aminocamptothecin
DLT	dose limiting toxicity
GAMS	general algebraic modeling system
LD	lethal dose
PK	pharmacokinetic (s)
PB/PK	physiologically–based pharmacokinetic(s)
PD	pharmacodynamic (s)
MAP	murine antibody profile
MILP	mixed–integer linear programming problem
MINLP	mixed–integer nonlinear programming problem
MIQP	mixed–integer quadratic programming problem
MTD	maximum tolerated dose
NLP	nonlinear programming problem
NONMEM	nonlinear mixed–effects modeling

OC	optimal control
ODE	ordinary differential equation(s)
QD×5×2	five days/week for two weeks every four weeks
SCID	severe combined immunodeficient
SSE	sum squared error
Std. Dev.	standard deviation

Notation	
$\underline{\underline{A}}$	state transition matrix
b	binary decision variable
$b_{th}(k)$	binary variable used to switch the therapeutic drug level on and off
b_u	binary variable used to enable semicontinuous dose ranges
b_{dose}	binary variable used to switch between acceptable dose levels
B	body weight
$\underline{\underline{B}}$	input coefficient matrix
B_0	initial body weight
B_{min}	lower bound on B_{tox}
B_{tox}	body weight corrected for tumor volume ($B - N/1000$)
C, $C(t)$	drug concentration
C_{max}	maximum allowable plasma drug concentration
C_{th}	minimum plasma drug concentration for therapeutic effect
D	amount of drug administered (total mass)
D_{last}	the most recent amount of drug delivered (concentration in mg/kg)
D_l	the amount of drug given which falls below Threshold
D_{lb}	minimum effective dose
D_u	the amount of drug given which falls above Threshold

D_{max}	maximum tolerable dose
$F(\cdot)$	generic function of $(\cdot)$
G_i	number of cells in i^{th} phase of the cell cycle
G, $G(s)$	Laplace domain transfer function
h	stepsize for discrete systems
i	index variable
j	index variable
$_d$	subscript indicating the current variable is in the discrete time
J	objective function
K	process gain
k	discrete timestep
k_i & k_{ij}	rate constants
k_{eff}	efficacy proportionality constant
l	set of possible dosing levels
ℓ	length of a tumor during measurement
M	number of cells in the mitosis phase of the cell cycle
m	final element in a set
m_k	final time step
m_l	final dosing level
m_p	final trajectory point
m_q	final dosing opportunity
m_z	final timestep in a day
N_0	initial tumor volume
N	tumor size (number of cells or volume)
N_e	tumor size described by exponential growth
N_g	tumor size described by Gompertzian growth
N_s	tumor size described by switched exponential growth

N_{th}	threshold tumor size for switching between fast ($\tau_{e,f}$) and slow ($\tau_{e,s}$) growth rates in the switched exponential model
N_{weeks}	treatment window in weeks/treatment horizon
p	set of points in the trajectory tracking problems
Q	parameters (vector or matrix) which are constants for optimization purposes
$Q_{dose}(l)$	matrix of drug concentrations at different dose levels, l
$Q_{\mathrm{AC}}(z,l)$	matrix of 9NC concentrations at different timesteps of the day, z,for different dose levels, l
$Q_{\mathrm{NC}}(z,l)$	matrix of 9NC concentrations at different timesteps of the day, z,for different dose levels, l
$Q_{map}(q)$	mapping dosing opportunities q to their corresponding timesteps k
$Q_{Pnom}(k)$	vector of nominal tumor growth in the absence of treatment
S	number of cells in the DNA synthesis of the cell cycle
p	prediction horizon used in the receding horizon problem
P	log transformed tumor growth
q	discrete dosing opportunities
s	Laplace domain variable
S	number of cells in the DNA synthesis phase of the cell–cycle
t	time
t_f	final time of treatment window
u	input to a system
v	compartmental volume
w	width of a tumor during measurement or week in which a measurement is taken
x	internal state variable
X	internal state variable in the Laplace domain

y	outputs
z	set of timesteps in a day
Threshold	switch used in nonlinear PK model of 9NC representing the maximum amount of 9NC which will take a particular pathway

Greek Letters	
α	fraction of a state
β	complementary fraction of a state ($\beta = 1 - \alpha$)
Γ	weight of the importance of a term in the objective function
γ	rate of elimination of drug in Martin and Teo case study [12]
ρ_g	plateau population in Gompertzian growth
τ	system time constant, unless specified otherwise
τ_e	doubling time for tumor volumes in exponential growth
$\tau_{e,s}$	doubling time active during larger tumor volumes in the switched exponential model
$\tau_{e,f}$	doubling time active during smaller tumor volumes in the switched exponential model
τ_g	doubling time for tumor volumes in exponential growth phase of Gompertzian growth
θ	time delays
θ_{eff}	delay between plasma concentration and drug effect on tumor

Calligraphic Letters	
$\mathcal{F}(\cdot)$	used to describe generic functions of $(\cdot)$
$\mathcal{D}(t)$	generic drug dose
$\mathcal{H}(\cdot)$	Heaviside/step function
$\mathcal{L}\{\cdot\}$	Laplace transform operator
$\mathcal{P}$	generic model parameters

$\mathcal{Y}(t)$	generic system outputs
$\hat{\mathcal{Y}}(t)$	generic model predictions of system outputs

APPENDIX B

EXPERIMENTAL METHODS

B.1 PK EXPERIMENTAL METHODS

All experimental data presented here (PK and PD) were obtained from studies carried out by our collaborators at the University of Pittsburgh Cancer Institute. The analytical methods used in the present work are based on the experiments conducted by Zamboni and coworkers [95]. In order to eliminate redundancies, only differences between the present methods and those presented in [95] will be highlighted.

B.1.1 Reagents

All chemicals for HPLC analysis were HPLC grade and purchased from Fisher Scientific (Pittsburgh, PA). N,N-Dimethylacetamide (DMA) was purchased from Sigma-Aldrich (Milwaukee, WI); polyethylene glycol 400, liquid (PEG 400) was purchased from Baker (Phillipsburg, NJ). Camptothecin, N,N-dimethylformamide and carbonyl iron (pentacarbonyl iron) were purchased from Sigma-Aldrich, (St. Louis, MO). 9NC and 9AC were provided by SuperGen (Dublin, CA). 5-fluorouracil was purchased as the clinical formulation, Adrucil (Pharmacia & Upjohn, Kalamazoo, MI)

B.1.2 Drug Formulations

9NC was prepared at concentrations of 0.1, 0.067 or 0.044 mg/ml in vehicle (2% DMA in 1 mM phosphoric acid:PEG 400(49:51, v/v)). 9NC doses and vehicle were administered orally (*p.o.*) at a volume of 0.01 ml/g body weight using a 20-gauge oral gavage needle and 1 ml syringe. Two different PK studies were conducted. In the first, a single dose of 0.67 mg/kg 9NC was administered, and doses of either 0.44, 0.67, or 1.0 mg/kg were administered in the second study.

B.1.3 Mice

Female C.B-17 SCID mice (4-6 weeks of age, specific-pathogen-free) were obtained from the National Cancer Institute (NCI) Animal Production Program (Frederick, MD) and were allowed to acclimate to the University of Pittsburgh Central Animal Facility for 1 week prior to initiation of study. Mice were housed in autoclaved microisolator caging and were given Prolab ISOPRO RMH 3000 Irradiated Lab Diet (PMI Nutrition International, Brentwood, MO) and autoclaved water *ad libitum*. Animal rooms were maintained on a 12-hour light/dark cycle with at least 12 air changes/hour, and temperature was maintained at 72 $\pm$ 2 °F. All animals were handled in accordance with the Guide to the Care and Use of Laboratory Animals [96] and on a protocol approved by the Institutional Animal Care and Use Committee of the University of Pittsburgh. Analysis of sentinel mice housed in 1/5 dirty bedding every three months confirmed that the study mice remained MAP (murine antibody profile) test-negative throughout the study.

B.2 TUMOR LINE, IMPLANTATION, MEASUREMENTS, AND CALCULATIONS

HT29 human colon xenografts were obtained from the NCI Tumor Repository (Frederick, MD) and were MAP test-negative. HT29 tumors were passaged in C.B-17 SCID female mice as approximately 25 mg fragments implanted subcutaneously on the right flank by

aseptic techniques. Fragments of tumor (approximately 25 mg) harvested from passage mice were subsequently implanted subcutaneously into study mice. Mice were observed twice daily. Both tumor volumes and body weights were recorded twice weekly. Tumor volumes were measured using a digital caliper. Tumor volumes, V, were calculated from the formula: $V = \frac{\ell \times w^2}{2}$ where ℓ was the longest tumor diameter, and w was the shortest diameter perpendicular to the direction of ℓ.

B.3 PHARMACOKINETIC STUDIES

Pharmacokinetic studies were performed in non-tumor-bearing female C.B-17 SCID mice and in female C.B-17 SCID mice bearing HT29 tumors at 27 days post tumor implantation. Mice were stratified into groups of three such that the mean and median body weight and tumor volumes in the tumor-bearing cohorts were similar across groups. Animals were fasted overnight prior to dosing, and a dose of 0.44, 0.67 or 1.0 mg/kg 9NC was administered by oral gavage to the mice as a single bolus based on fasted body weight. After 9NC administration, groups of three mice were euthanized by CO_2 inhalation, and blood was collected by cardiac puncture, using heparinized syringes and needles, at each of the following times: 5, 15, 30, 60, 90, 120, 240, 360, 420, 960, 1440 and 2880 min. Three additional mice were euthanized at five minutes after dosing with vehicle. Blood was transferred to microcentrifuge tubes and stored on ice for less than three minutes before plasma was obtained by centrifugation of whole blood at 13,000×g for 4 minutes.

B.4 DETERMINATION OF 9NC AND 9AC LACTONE CONCENTRATIONS

B.4.1 Plasma Sample Preparation for HPLC Analysis

The sample preparation methods were modified from those developed for human trials [95]. Deionized, distilled water was used for conditioning the solid phase extraction (SPE) cartridges. Mouse plasma sample volumes of 200 μl were used instead of the 1 ml volumes used in the human studies.

The plasma for the determination of both 9NC and 9AC lactone forms was processed as soon as it was obtained. Plasma samples (200 μl) were mixed with 2.5 μl of internal standard (2 μg/ml camptothecin in acetone) and loaded onto preconditioned solid phase extraction (SPE) cartridges (Waters OASIS^{TM} HLB 1 ml, 30 mg, Waters Associates, Millford, MA) conditioned with 1 ml of methanol and equilibrated with 1 ml of distilled deionized water. After application of the plasma, the cartridges were washed with 1 ml of 5% methanol in water, which eluted the carboxylate forms of the camptothecins from the column. The lactone forms of 9NC, 9AC, and camptothecin were eluted from the columns with 0.5 ml of methanol and these aliquots were stored frozen at -70 °C until analysis. Thus these SPE eluates contained only the lactone forms of the compounds of interest. This method was evaluated in the laboratory of our collaborators for 9NC to demonstrate that only the lactone form is retained on the SPE column and the carboxylate form is not retained. This method has previously been published for 9AC lactone by Takimoto and coworkers [39].

B.4.2 HPLC Analysis

The HPLC analysis used in the present study was also used in the human studies presented in [95], with adjustments as follows. For the reduction, 12 μl of the reducing reagent (25 mg reduced pentacarbonyl iron/ml H_2O) and 6 μl of 12 N HCl were added to 120 μl of each eluate or methanolic plasma supernatant. These samples were vortexed for 1 min and sonicated for 30 min at 70 °C. The samples were then centrifuged (10,000×g for 4 min). Reduction of 9NC to 9AC by reduced pentacarbonyl iron is 54% efficient. Prior to

placing these supernatants in siliconized (3% surfasil in toluene) HPLC autosampler vials, the reduced methanolic supernatants (150 μl) were mixed with 75 μl of 0.5 M ammonium acetate in water, pH 5.5, while the supernatants from the reduced eluates (150 μl) were diluted with 100 μl of 0.5 M ammonium acetate in water, pH 5.5. The mobile phase used here was isocratic (9% methanol, 23% acetonitrile and 68% 0.1M ammonium acetate, pH 5.5), at a flowrate of 1.0 ml/min.

B.5 DETERMINATION OF 9NC AND 9AC TOTAL CONCENTRATIONS

In order to more directly quantify the concentration of 9NC and 9AC in plasma, a more direct analytical method was used. While the method above provided lactone concentrations of 9NC and 9AC, this method only provides the total concentrations of each substance because all 9AC and 9NC in plasma were converted to lactone forms. A liquid chromatography-quadrupole mass spectrometer (LC-MS/MS) was first used to obtain the total concentration of 9AC in the plasma samples (C_{AC}). The plasma samples were then reduced to convert all of the 9NC to 9AC. After reduction, the plasma samples were analyzed again with the LC-MS/MS to determine the total concentration of 9AC ($C_{\mathrm{AC+NC}}$). The original total concentration of 9NC was then calculated by subtracting C_{AC} from $C_{\mathrm{AC+NC}}$.

B.6 PD EXPERIMENTAL METHODS

Tumor implantation was described in section B.2. Mice bearing HT29 tumors were stratified to treatment groups of 10 mice on day 19 post implantation (three days prior to treatment) such that mean and median body weight and tumor volumes for the groups of mice were not statistically different. Tumor volumes on day 19 were between 26 and 71 mm^3. Treatment groups were as follows: control; vehicle-treated control; positive control (5-fluorouracil, 20 mg/kg); 9NC 1.0 mg/kg/day; 9NC 0.67 mg/kg/day; and 9NC 0.44 mg/kg/day. Treatment began on day 21, and this was defined as study day zero. Mice on the efficacy study received

daily doses by oral gavage for 5 days/week for two weeks followed by a two week period of no treatment before the treatment regimen was repeated (QD×5×2) every four weeks. The positive control group received doses intraperitoneally (i.p.) on the same schedule. At the completion of the efficacy study, mice were euthanized, and complete necropsies were performed.

APPENDIX C

GENERATING DOSING PROFILES

Several files are utilized when generating the optimal dosing profile. As an example, the trajectory tracking problem with only two dosing options (0 and 1.0 mg/kg) will be discussed. The file gen_minlp_results.m is called and sets the optimization specific parameters and calls the file run_gams_nonlinear.m. The file, run_gams_nonlinear.m, then generates the following input files:

- input-dose_to_acconc.inc
- input-dose_to_ncconc.inc
- input-objective_function.inc
- input-parameters.inc
- input-sets.inc

These correspond to the parameterized concentrations of 9AC, the parameterized concentrations of 9NC, the objective function, model parameters, and the sets used in tams. After dumping these input files, run_gams_nonlinear.m executes the gams optimal_dose_profile.gms. When executing optimal_dose_profile.gms, the input files a previously listed and the following files are generated:

- output-dose_levels-min_max.txt
- output-state_values-min_max.txt

The first file contains three columns. The first column corresponds to the index of the dosing opportunity, the second column corresponds to the time step, and the third column

corresponds to the the dosing level in mg/kg. The second output file contains relevant states of the system. The first column corresponds to the time in minutes, the second and third columns correspond to the concentrations of 9NC and 9AC, respectively. The tumor volume, body weight, and corrected body weight are given by the fourth, fifth, and sixth columns, respectively. The second output file (state values) contains several thousand rows, and was truncated to accommodate inclusion into this document.

C.1 SOURCECODE FILES

Begin file: `gen_minlp_results.m`

```
function [] = gen_minlp_results()

cfg.analysis.timestep       = 5; % minutes
cfg.analysis.finalweek      = 8; % prediction horizon
cfg.analysis.stepsperday    = floor(1440/cfg.analysis.timestep);
cfg.analysis.dose2mass      = 10^6/1000*20.75;
cfg.analysis.finaltimestep = ...
     cfg.analysis.stepsperday*7*cfg.analysis.finalweek;
cfg.analysis.simstepsize    = 0.1;
cfg.analysis.effectiveinf   = 80*1440;   % in minutes
cfg.analysis.N0             = 40;        % initial tumor vol mm3
cfg.analysis.B0             = 20; % initial body weight g
                                  %— beginning of treatment
cfg.analysis.B0CYCLE        = 20; % initial body weight g
                                  %— beginning of cycle
cfg.analysis.BMIN           = .98;% bound body weight
                                  %(fraction of body weight
                                  % which must remain after
                                  % treatment
cfg.analysis.DLB            = 0.44;
cfg.analysis.DUB            = 1.0;
cfg.analysis.DMIN           = 0.00;
cfg.analysis.DMAX           = 1.0;
cfg.analysis.plotrange      = [0 1440];
cfg.analysis.dose_range     = .44:.01:1.0;
cfg.analysis.simonly        = 0;
cfg.analysis.rungams        = 1;% 1  --- execute the
                                %        optimization
                                % 0  --- read old results

cfg.analysis.gams_file      = 'optimal_dose_profile.gms';
cfg.generic.gams_binary     = '/misc/opt/bin/gams';
cfg.generic.gams_directory = sprintf('%s/GAMS/MINLP', pwd);
```

```
% days to minimize tumor volume
cfg.analysis.Ntimes        = (1:1:8)*7;
% vector of possible doses
cfg.analysis.dose_range    = [1.0];
% prefix used for writing parameters
cfg.analysis.prefix        = 'min_max';

results.min_max = run_gams_nonlinear(cfg);
```

End file: `gen_minlp_results.m`

Begin file: `run_gams_nonlinear.m`

```
function [results]=run_gams_nonlinear(cfg)
% function []=run_gams_nonlinear(cfg)
%
% cfg -- configuration variable, a structure really.
%
% the analysis field is used to specify different
% parameters of the analysis
%
%
%cfg.analysis.timestep      = 5; % minutes
%cfg.analysis.finalweek     = 12; % prediction horizon
%cfg.analysis.stepsperday   = ...
% floor(1440/cfg.analysis.timestep);
%cfg.analysis.dose2mass     = 10^6/1000*20.75;
% ng of drug;
%cfg.analysis.finaltimestep = ...
% cfg.analysis.stepsperday*7*cfg.analysis.finalweek;
%cfg.analysis.simstepsize   = 0.1;
%cfg.analysis.effectiveinf  = 80*1440;   % in minutes
% initial tumor volume in cubic mm
%cfg.analysis.N0            = 40;
% initial uncorrected body weight in grams
% -- beginning of treatment
% initial uncorrected body weight in grams
% -- beginning of cycle
%cfg.analysis.B0            = 20;
%cfg.analysis.B0CYCLE       = 20;
% bound body weight (fraction of body weight which
% must remain after treatment)
%cfg.analysis.BMIN          = .97;
% days to minimize tumor volume
%cfg.analysis.Ntimes        = (1:1:8)*7;
% days to minimize tumor volume
%cfg.analysis.Ntimes        = 7*cfg.analysis.finalweek;
%cfg.analysis.DLB           = 0.44;
```

```
%cfg.analysis.DUB           = 1.0;
%cfg.analysis.DMIN          = 0.00;
%cfg.analysis.DMAX          = 1.0;
%cfg.analysis.plotrange     = [0 1440];
%cfg.analysis.dose_range    = [0.44 0.67 1.0];
%cfg.analysis.dose_range    = .44:.01:1.0;
% 1 --- execute the optimization
% 0 --- read old results
%cfg.analysis.rungams       = 1;
%
% prefix used for writing parameters
%cfg.analysis.prefix        = 'final_time';
%cfg.analysis.gams_file     = 'optimal_dose_profile.gms';
%cfg.generic.gams_binary    = '/misc/opt/bin/gams';
%cfg.generic.gams_directory = sprintf('%s/GAMS/MINLP_002', pwd);
% 1 - only run simulation for dose levels;
%cfg.analysis.simonly       = 0;


%
% initializing the return variable
%
results = [];


%
% creating dose times vector
%
cfg.analysis.dose_times = [];
cntr = 1;
for week=0:(cfg.analysis.finalweek - 1)
  for day=0:6
    % only dosin monday--friday
    if day <5
      cfg.analysis.dose_times  = ...
             [cfg.analysis.dose_times
             cntr week*7+day ];
      cntr = cntr+1;
    end
  end
end
cfg.analysis.dose_times(:,2)= ...
  cfg.analysis.dose_times(:,2)*cfg.analysis.stepsperday + 1;

%
% initialing cfg variable
%

%cfg.generic = init_config;



%
% loading various parameters (PK, tumor growth, PD)
```

```
%

% tumor growth parameters
cfg.params.tumor_growth = fetch_parameters_tumor_growth;

% converting tumor growth parameters from days to minutes:
cfg.params.tumor_growth.average.tauef = ...
cfg.params.tumor_growth.average.taues*1440;
cfg.params.tumor_growth.average.taues = ...
cfg.params.tumor_growth.average.taues*1440;


% loading nonlinear pk parameters
cfg.params.nonlinear_pk = fetch_parameters_nonlinear_pk;

% loading nonlinear pd parameters
cfg.params.nonlinear_pd = fetch_parameters_pd_nonlinear;

% loading nonlinear toxicity parameters
cfg.params.body_weight  = fetch_parameters_body_weight;

%
% generating pk profiles for possible dosing levels
%
%if cfg.analysis.rungams
 disp('calculating pk profiles');
  cfg.analysis.profiles.time_range = ...
  0:cfg.analysis.timestep:1440;
  for i=1:max(size(cfg.analysis.dose_range))
    dlevels = [0, cfg.analysis.dose_range(i)];
    [t,x,y] = runsim(cfg, dlevels);
    % resampling at time steps
   cfg.analysis.profiles.nc(:,i) =...
   resample_data(cfg.analysis.profiles.time_range,t,y(:,9));
   cfg.analysis.profiles.ac(:,i) = ...
   resample_data(cfg.analysis.profiles.time_range,t,y(:,10));
  end


 disp('calculating variable bounds');
 cfg.bounds = fetch_bounds(cfg);

%end


%
% dumping the information for gams
%
if cfg.analysis.rungams
  dump_gams(cfg)
end


%
```

```
% executing gams
%

if cfg.analysis.rungams
  exec_gams(cfg);
end


%
% reading results
%

  [results] = read_gams_results(cfg);



function [bounds]=fetch_bounds(cfg);
% calculating the bounds on PK states

 bounds                  = [];
 dlevels                 = [0, cfg.analysis.DUB];
 cfg.analysis.plotrange  = [0 2*1440];

 % running simulation in response to maximum
 % allowable dose
 [t,x,y] = runsim(cfg, dlevels);

 % upper bound here
 y = max(y,[],1);
                          % lower bounds are all zero
 bounds.x1.ub  = y(1);    bounds.x1.lb  = 0;
 bounds.x2.ub  = y(2);    bounds.x2.lb  = 0;
 bounds.x3.ub  = y(3);    bounds.x3.lb  = 0;
 bounds.x4.ub  = y(4);    bounds.x4.lb  = 0;
 bounds.x5.ub  = y(5);    bounds.x5.lb  = 0;
 bounds.x6.ub  = y(6);    bounds.x6.lb  = 0;
 bounds.CNC.ub = y(9);    bounds.CNC.lb = 0;
 bounds.CAC.ub = y(10);   bounds.CAC.lb = 0;



function [t,x,y]=runsim(cfg,dlevels);
%
% the first 7 outputs are the states
% the next two are the concentration
% of 9nc and 9ac respectively
%

% initializing variables
t = 0; x = 0; y = 0;

delta         =  cfg.analysis.simstepsize*5;
drug          = [0 0];
lastdose      = [0 0];
```

```
[ndoses, tmp] = size(dlevels);

for i=1:ndoses
drug = [drug
        dlevels(i,1)          0
        dlevels(i,1)+delta    dlevels(i,2)/(2*delta)
        dlevels(i,1)+2*delta  dlevels(i,2)/(2*delta)
        dlevels(i,1)+3*delta  0                      ];

lastdose = [lastdose
            dlevels(i,1)               dlevels(i,2)
            dlevels(i,1)+1440-delta    dlevels(i,2)];

end


drug = [drug
        cfg.analysis.effectiveinf 0];


     inlcond = [0 0 0 0 0 0 0 cfg.analysis.N0 cfg.analysis.B0];
     options = simset(                                  ...
        'InitialState',                inlcond,         ...
        'solver',                       'ode4',         ...
        'FixedStep',       cfg.analysis.simstepsize,   ...
        'SrcWorkspace',                 'current'       ...
        );
warning off;
  [t,x,y] = sim('pkpd_nonlinear_full', ...
                cfg.analysis.plotrange, ...
                options);
warning on;

%
% dumping the information for gams
%

function []=dump_gams(cfg)

%
% dumping sets
%
[numdoses, tmp]=size(cfg.analysis.dose_times);
[doseopts.ntimesteps, doseopts.ndoses] = ...
 size(cfg.analysis.profiles.nc);

FID = fopen(sprintf('%s/input-sets.inc', ...
            cfg.generic.gams_directory), 'W');
  fprintf(FID, 'k         discrete time  /1*%d/ \n', ...
          cfg.analysis.finaltimestep);
  fprintf(FID, 'q         dosing time    /1*%d/ \n', ...
          numdoses);
  fprintf(FID, 'spd       steps per day  /1*%d/\n', ...
         doseopts.ntimesteps);
```

```
  fprintf(FID, ...
  'dlvls     number of possible dose levels  /1*%d/\n', ...
  doseopts.ndoses + 1);
fclose(FID);

%
% dumping scalars
%
FID = fopen(sprintf('%s/input-parameters.inc', ...
cfg.generic.gams_directory), 'W');
discrete_theta = ...
floor(cfg.params.nonlinear_pk.theta/cfg.analysis.timestep);
fprintf(FID, '*                              \n');
fprintf(FID, '* analysis specific            \n');
fprintf(FID, '*                              \n');
fprintf(FID, 'timestep  discretizatoin step size  /%.8e/\n', ...
cfg.analysis.timestep);
fprintf(FID, 'numsteps  number of time steps  /%d/  \n', ...
cfg.analysis.finaltimestep);
fprintf(FID, '*                                    \n');
fprintf(FID, '* tumor growth parameters            \n');
fprintf(FID, '*                                    \n');
fprintf(FID, 'tauef     fast growth rate    /%.8e/\n', ...
cfg.params.tumor_growth.average.tauef    );
fprintf(FID, 'taues     slow growth rate    /%.8e/\n', ...
cfg.params.tumor_growth.average.taues    );
fprintf(FID, 'nth       switching size      /%.8e/\n', ...
cfg.params.tumor_growth.average.nth      );
fprintf(FID, '*                              \n');
fprintf(FID, '* nonlinear pd parameters      \n');
fprintf(FID, '*                              \n');
fprintf(FID, 'keff    rate of cell kill      /%.8e/\n', ...
cfg.params.nonlinear_pd.summary.average);
fprintf(FID, '*                                  \n');
fprintf(FID, '* body weight model parameters     \n');
fprintf(FID, '*                                  \n');
fprintf(FID, 'tauw  rate of mouse doubling       /%.8e/\n', ..
cfg.params.body_weight.d10.nave.tauw);
fprintf(FID, 'kd    effect of drug on bodyweight   /%.8e/\n', ...
cfg.params.body_weight.d10.nave.kd);
fprintf(FID, '*                                                  \n');
fprintf(FID, '* miscalleneous parameters                         \n');
fprintf(FID, '*                                                  \n');
fprintf(FID, 'N0      initial condition   /%.8e/\n', ...
cfg.analysis.N0);
fprintf(FID, 'B0      initial body weight (treatment) /%.8e/\n', ...
cfg.analysis.B0);
fprintf(FID, 'B0CYCLE initial body weight (cycle)     /%.8e/\n',...
cfg.analysis.B0CYCLE);
fprintf(FID, 'BMIN    minimum body weight (fraction)  /%.8e/\n', ...
cfg.analysis.BMIN);

fprintf(FID, 'dose_times(q) possible dose times  /\n');
for i=1:numdoses
```

```
  fprintf(FID, '   %2d   %5d        \n', ...
   cfg.analysis.dose_times(i,1),...
   cfg.analysis.dose_times(i,2) );
end
fprintf(FID, ' /                \n');

fprintf(FID, 'dose_levels(dlvls) possible dose levels              /\n');
for i=1:max(size(cfg.analysis.dose_range))
  fprintf(FID, '   %2d   %5e        \n', i, ...
  cfg.analysis.dose_range(i) );
end
fprintf(FID, ' /                \n');
fclose(FID);

%
% dumping objective function
%

FID = fopen(sprintf('%s/input-objective_function.inc', ...
 cfg.generic.gams_directory), 'W');
  fprintf(FID,'obj .. z =e= ');
  for i=1:max(size(cfg.analysis.Ntimes))
    % ignoring anything after the final week
    if cfg.analysis.Ntimes(i) >= cfg.analysis.finalweek
      if i > 1
        fprintf(FID,' + ');
      end
      fprintf(FID,' TUMOR(''%d'') ', ...
      cfg.analysis.Ntimes(i)*cfg.analysis.stepsperday);
    end
  end
  fprintf(FID,'; \n', cfg.analysis.finaltimestep);
fclose(FID);

%
% dumping pk profiles
%
FIDNC = fopen(sprintf('%s/input-dose_to_ncconc.inc',...
cfg.generic.gams_directory), 'W');
FIDAC = fopen(sprintf('%s/input-dose_to_acconc.inc',...
cfg.generic.gams_directory), 'W');

%
% printing headers
%
fprintf(FIDNC, ...
' TABLE ALLNCCONC(spd,dlvls) "Concentrations of
  9NC at different dose levels"\n');
fprintf(FIDAC, ...
' TABLE ALLACCONC(spd,dlvls) "Concentrations
  of 9AC at different dose levels"\n');

%
% printing the column headings
```

```
%
fprintf(FIDNC, '          ');
fprintf(FIDAC, '          ');
for j=1:doseopts.ndoses + 1 % gotta get the zero column
    fprintf(FIDNC, '%15d',j);
    fprintf(FIDAC, '%15d',j);
end
fprintf(FIDNC, '\n');
fprintf(FIDAC, '\n');
for i=1:doseopts.ntimesteps
  fprintf(FIDNC, ' %7d',i);
  fprintf(FIDNC, '%15.4e',0);

  fprintf(FIDAC, ' %7d',i);
  fprintf(FIDAC, '%15.4e',0);

  for j=1:doseopts.ndoses
  fprintf(FIDNC, '%15.4e',cfg.analysis.profiles.nc(i,j));
  fprintf(FIDAC, '%15.4e',cfg.analysis.profiles.ac(i,j));
  end

  if i==doseopts.ntimesteps
  fprintf(FIDNC, ';\n');
  fprintf(FIDAC, ';\n');
  end
  fprintf(FIDNC, '\n');
  fprintf(FIDAC, '\n');
end

fclose(FIDNC);
fclose(FIDAC);

%
%
%  dumping user defined solution
%
%
if cfg.analysis.simonly
  if (max(size(cfg.analysis.specified_dose_levels)) ...
      == numdoses)

  FID = fopen(sprintf('%s/input-specified_dose_levels.inc',...
  cfg.generic.gams_directory), 'W');
  fprintf(FID, ...
  'specified_dose_levels(q) user specified dose levels /\n');
  for i=1:numdoses
    fprintf(FID, '   %2d   %d    \n', i, ...
    cfg.analysis.specified_dose_levels(i) );
  end
  fprintf(FID, ' /               \n');
  fclose(FID);
  else
  end
end
```

```
function [generic]=init_config;
generic.gams_binary     = '/misc/opt/bin/gams';
generic.gams_directory = sprintf('%s/GAMS/MINLP_002', pwd);
%-----------------------------------------------------------------------



%-----------------------------------------------------------------------
function []=exec_gams(cfg);


% assigning directories
wd.matlab = pwd;
wd.gams   = cfg.generic.gams_directory;

% executing gams
exec_string = sprintf('%s %s', ...
  cfg.generic.gams_binary, ...
  cfg.analysis.gams_file);
cd(wd.gams);

disp(sprintf('GAMS working directory: %s',pwd))
%save /tmp/goat.mat;

system(exec_string);


% backing up the solutions
exec_string = ...
 sprintf( ...
 'cp output-dose_levels.txt output-dose_levels-%s.txt', ...
                      cfg.analysis.prefix);
system(exec_string);

exec_string = sprintf(...
'cp output-state_values.txt output-state_values-%s.txt', ...
                      cfg.analysis.prefix);
system(exec_string);

% returing to the matlab directory
cd(wd.matlab);
%-----------------------------------------------------------------------

%-----------------------------------------------------------------------
function [results]=read_gams_results(cfg);
results = [];


load_str = sprintf('load %s/output-dose_levels-%s.txt', ...
                   cfg.generic.gams_directory,          ...
                   cfg.analysis.prefix);
eval(load_str);
```

```
load_str = sprintf('load %s/output-state_values-%s.txt', ...
                   cfg.generic.gams_directory,           ...
                   cfg.analysis.prefix);
eval(load_str);

tmp_str = sprintf('dl = output_dose_levels_%s ;', ...
cfg.analysis.prefix);
eval(tmp_str);
tmp_str = sprintf('sv = output_state_values_%s ;', ...
cfg.analysis.prefix);
eval(tmp_str);

results.doses.dose_time  = dl(:,2);
results.doses.dose_level = dl(:,3);


results.states.sim_time   = sv(:,1);
results.states.CNC        = sv(:,2);
results.states.CAC        = sv(:,3);
results.states.TUMOR      = sv(:,4);
results.states.BW         = sv(:,5);
results.states.BWc        = sv(:,6);

results.profiles          = cfg.analysis.profiles;
```

%——

End file: `run_gams_nonlinear.m`

Begin file: `input-dose_to_acconc.inc`

```
TABLE ALLACCONC(spd,dlvls) "Concentrations of 9AC"
                    1               2
      1     0.0000e+00      0.0000e+00
      2     0.0000e+00      1.0515e+01
      3     0.0000e+00      1.2084e+01
      4     0.0000e+00      1.1757e+01
      5     0.0000e+00      1.0598e+01
      6     0.0000e+00      9.1688e+00
      7     0.0000e+00      7.7520e+00
      8     0.0000e+00      6.4745e+00
      9     0.0000e+00      5.3796e+00
     10     0.0000e+00      4.4685e+00
     11     0.0000e+00      3.7260e+00
     12     0.0000e+00      3.4499e+00
     13     0.0000e+00      3.4149e+00
     14     0.0000e+00      3.4610e+00
     15     0.0000e+00      3.5240e+00
     16     0.0000e+00      3.5737e+00
     17     0.0000e+00      3.5980e+00
     18     0.0000e+00      3.5946e+00
```

19	0.0000e+00	3.5658e+00
20	0.0000e+00	3.5156e+00
21	0.0000e+00	3.4484e+00
22	0.0000e+00	3.3683e+00
23	0.0000e+00	3.2790e+00
24	0.0000e+00	3.1832e+00
25	0.0000e+00	3.0834e+00
26	0.0000e+00	2.9814e+00
27	0.0000e+00	2.8785e+00
28	0.0000e+00	2.7759e+00
29	0.0000e+00	2.6742e+00
30	0.0000e+00	2.5741e+00
31	0.0000e+00	2.4760e+00
32	0.0000e+00	2.3801e+00
33	0.0000e+00	2.2868e+00
34	0.0000e+00	2.1961e+00
35	0.0000e+00	2.1081e+00
36	0.0000e+00	2.0229e+00
37	0.0000e+00	1.9405e+00
38	0.0000e+00	1.8608e+00
39	0.0000e+00	1.7840e+00
40	0.0000e+00	1.7098e+00
41	0.0000e+00	1.6384e+00
42	0.0000e+00	1.5696e+00
43	0.0000e+00	1.5034e+00
44	0.0000e+00	1.4397e+00
45	0.0000e+00	1.3784e+00
46	0.0000e+00	1.3196e+00
47	0.0000e+00	1.2630e+00
48	0.0000e+00	1.2087e+00
49	0.0000e+00	1.1566e+00
50	0.0000e+00	1.1066e+00
51	0.0000e+00	1.0586e+00
52	0.0000e+00	1.0126e+00
53	0.0000e+00	9.6846e−01
54	0.0000e+00	9.2617e−01
55	0.0000e+00	8.8564e−01
56	0.0000e+00	8.4681e−01
57	0.0000e+00	8.0961e−01
58	0.0000e+00	7.7398e−01
59	0.0000e+00	7.3987e−01
60	0.0000e+00	7.0721e−01
61	0.0000e+00	6.7595e−01
62	0.0000e+00	6.4603e−01
63	0.0000e+00	6.1740e−01
64	0.0000e+00	5.9001e−01
65	0.0000e+00	5.6380e−01
66	0.0000e+00	5.3873e−01
67	0.0000e+00	5.1475e−01
68	0.0000e+00	4.9181e−01
69	0.0000e+00	4.6988e−01
70	0.0000e+00	4.4891e−01
71	0.0000e+00	4.2886e−01
72	0.0000e+00	4.0969e−01

73	0.0000e+00	3.9137e−01
74	0.0000e+00	3.7385e−01
75	0.0000e+00	3.5711e−01
76	0.0000e+00	3.4110e−01
77	0.0000e+00	3.2581e−01
78	0.0000e+00	3.1119e−01
79	0.0000e+00	2.9723e−01
80	0.0000e+00	2.8388e−01
81	0.0000e+00	2.7113e−01
82	0.0000e+00	2.5894e−01
83	0.0000e+00	2.4730e−01
84	0.0000e+00	2.3618e−01
85	0.0000e+00	2.2555e−01
86	0.0000e+00	2.1540e−01
87	0.0000e+00	2.0571e−01
88	0.0000e+00	1.9644e−01
89	0.0000e+00	1.8759e−01
90	0.0000e+00	1.7914e−01
91	0.0000e+00	1.7107e−01
92	0.0000e+00	1.6336e−01
93	0.0000e+00	1.5599e−01
94	0.0000e+00	1.4896e−01
95	0.0000e+00	1.4224e−01
96	0.0000e+00	1.3582e−01
97	0.0000e+00	1.2969e−01
98	0.0000e+00	1.2384e−01
99	0.0000e+00	1.1825e−01
100	0.0000e+00	1.1291e−01
101	0.0000e+00	1.0782e−01
102	0.0000e+00	1.0295e−01
103	0.0000e+00	9.8299e−02
104	0.0000e+00	9.3860e−02
105	0.0000e+00	8.9620e−02
106	0.0000e+00	8.5572e−02
107	0.0000e+00	8.1706e−02
108	0.0000e+00	7.8015e−02
109	0.0000e+00	7.4489e−02
110	0.0000e+00	7.1123e−02
111	0.0000e+00	6.7909e−02
112	0.0000e+00	6.4840e−02
113	0.0000e+00	6.1909e−02
114	0.0000e+00	5.9111e−02
115	0.0000e+00	5.6439e−02
116	0.0000e+00	5.3888e−02
117	0.0000e+00	5.1451e−02
118	0.0000e+00	4.9125e−02
119	0.0000e+00	4.6904e−02
120	0.0000e+00	4.4783e−02
121	0.0000e+00	4.2758e−02
122	0.0000e+00	4.0825e−02
123	0.0000e+00	3.8979e−02
124	0.0000e+00	3.7216e−02
125	0.0000e+00	3.5533e−02
126	0.0000e+00	3.3926e−02

127	0.0000e+00	3.2391e−02
128	0.0000e+00	3.0926e−02
129	0.0000e+00	2.9528e−02
130	0.0000e+00	2.8192e−02
131	0.0000e+00	2.6917e−02
132	0.0000e+00	2.5699e−02
133	0.0000e+00	2.4537e−02
134	0.0000e+00	2.3427e−02
135	0.0000e+00	2.2367e−02
136	0.0000e+00	2.1355e−02
137	0.0000e+00	2.0389e−02
138	0.0000e+00	1.9467e−02
139	0.0000e+00	1.8586e−02
140	0.0000e+00	1.7745e−02
141	0.0000e+00	1.6943e−02
142	0.0000e+00	1.6176e−02
143	0.0000e+00	1.5444e−02
144	0.0000e+00	1.4746e−02
145	0.0000e+00	1.4078e−02
146	0.0000e+00	1.3442e−02
147	0.0000e+00	1.2833e−02
148	0.0000e+00	1.2253e−02
149	0.0000e+00	1.1698e−02
150	0.0000e+00	1.1169e−02
151	0.0000e+00	1.0664e−02
152	0.0000e+00	1.0181e−02
153	0.0000e+00	9.7206e−03
154	0.0000e+00	9.2808e−03
155	0.0000e+00	8.8609e−03
156	0.0000e+00	8.4600e−03
157	0.0000e+00	8.0772e−03
158	0.0000e+00	7.7117e−03
159	0.0000e+00	7.3628e−03
160	0.0000e+00	7.0297e−03
161	0.0000e+00	6.7116e−03
162	0.0000e+00	6.4079e−03
163	0.0000e+00	6.1180e−03
164	0.0000e+00	5.8411e−03
165	0.0000e+00	5.5768e−03
166	0.0000e+00	5.3245e−03
167	0.0000e+00	5.0836e−03
168	0.0000e+00	4.8535e−03
169	0.0000e+00	4.6339e−03
170	0.0000e+00	4.4243e−03
171	0.0000e+00	4.2241e−03
172	0.0000e+00	4.0329e−03
173	0.0000e+00	3.8504e−03
174	0.0000e+00	3.6762e−03
175	0.0000e+00	3.5099e−03
176	0.0000e+00	3.3511e−03
177	0.0000e+00	3.1994e−03
178	0.0000e+00	3.0546e−03
179	0.0000e+00	2.9164e−03
180	0.0000e+00	2.7845e−03

181	0.0000e+00	2.6585e−03
182	0.0000e+00	2.5382e−03
183	0.0000e+00	2.4233e−03
184	0.0000e+00	2.3137e−03
185	0.0000e+00	2.2090e−03
186	0.0000e+00	2.1090e−03
187	0.0000e+00	2.0136e−03
188	0.0000e+00	1.9225e−03
189	0.0000e+00	1.8355e−03
190	0.0000e+00	1.7524e−03
191	0.0000e+00	1.6731e−03
192	0.0000e+00	1.5974e−03
193	0.0000e+00	1.5251e−03
194	0.0000e+00	1.4561e−03
195	0.0000e+00	1.3902e−03
196	0.0000e+00	1.3273e−03
197	0.0000e+00	1.2673e−03
198	0.0000e+00	1.2099e−03
199	0.0000e+00	1.1552e−03
200	0.0000e+00	1.1029e−03
201	0.0000e+00	1.0530e−03
202	0.0000e+00	1.0053e−03
203	0.0000e+00	9.5985e−04
204	0.0000e+00	9.1642e−04
205	0.0000e+00	8.7495e−04
206	0.0000e+00	8.3536e−04
207	0.0000e+00	7.9756e−04
208	0.0000e+00	7.6147e−04
209	0.0000e+00	7.2701e−04
210	0.0000e+00	6.9411e−04
211	0.0000e+00	6.6271e−04
212	0.0000e+00	6.3272e−04
213	0.0000e+00	6.0409e−04
214	0.0000e+00	5.7675e−04
215	0.0000e+00	5.5065e−04
216	0.0000e+00	5.2574e−04
217	0.0000e+00	5.0195e−04
218	0.0000e+00	4.7923e−04
219	0.0000e+00	4.5755e−04
220	0.0000e+00	4.3684e−04
221	0.0000e+00	4.1708e−04
222	0.0000e+00	3.9820e−04
223	0.0000e+00	3.8018e−04
224	0.0000e+00	3.6298e−04
225	0.0000e+00	3.4656e−04
226	0.0000e+00	3.3087e−04
227	0.0000e+00	3.1590e−04
228	0.0000e+00	3.0161e−04
229	0.0000e+00	2.8796e−04
230	0.0000e+00	2.7493e−04
231	0.0000e+00	2.6249e−04
232	0.0000e+00	2.5061e−04
233	0.0000e+00	2.3927e−04
234	0.0000e+00	2.2844e−04

235	0.0000e+00	2.1811e−04
236	0.0000e+00	2.0824e−04
237	0.0000e+00	1.9881e−04
238	0.0000e+00	1.8982e−04
239	0.0000e+00	1.8123e−04
240	0.0000e+00	1.7303e−04
241	0.0000e+00	1.6520e−04
242	0.0000e+00	1.5772e−04
243	0.0000e+00	1.5059e−04
244	0.0000e+00	1.4377e−04
245	0.0000e+00	1.3727e−04
246	0.0000e+00	1.3105e−04
247	0.0000e+00	1.2512e−04
248	0.0000e+00	1.1946e−04
249	0.0000e+00	1.1406e−04
250	0.0000e+00	1.0890e−04
251	0.0000e+00	1.0397e−04
252	0.0000e+00	9.9263e−05
253	0.0000e+00	9.4771e−05
254	0.0000e+00	9.0483e−05
255	0.0000e+00	8.6389e−05
256	0.0000e+00	8.2479e−05
257	0.0000e+00	7.8747e−05
258	0.0000e+00	7.5184e−05
259	0.0000e+00	7.1782e−05
260	0.0000e+00	6.8534e−05
261	0.0000e+00	6.5432e−05
262	0.0000e+00	6.2472e−05
263	0.0000e+00	5.9645e−05
264	0.0000e+00	5.6946e−05
265	0.0000e+00	5.4369e−05
266	0.0000e+00	5.1909e−05
267	0.0000e+00	4.9560e−05
268	0.0000e+00	4.7317e−05
269	0.0000e+00	4.5176e−05
270	0.0000e+00	4.3132e−05
271	0.0000e+00	4.1180e−05
272	0.0000e+00	3.9317e−05
273	0.0000e+00	3.7538e−05
274	0.0000e+00	3.5839e−05
275	0.0000e+00	3.4217e−05
276	0.0000e+00	3.2669e−05
277	0.0000e+00	3.1191e−05
278	0.0000e+00	2.9779e−05
279	0.0000e+00	2.8432e−05
280	0.0000e+00	2.7145e−05
281	0.0000e+00	2.5917e−05
282	0.0000e+00	2.4744e−05
283	0.0000e+00	2.3624e−05
284	0.0000e+00	2.2555e−05
285	0.0000e+00	2.1535e−05
286	0.0000e+00	2.0560e−05
287	0.0000e+00	1.9630e−05
288	0.0000e+00	1.8742e−05

289	0.0000e+00	1.7894e−05;

End file: `input-dose_to_acconc.inc`

Begin file: `input-dose_to_ncconc.inc`

TABLE ALLNCCONC(spd,dlvls) "Concentrations of 9NC"

	1	2
1	0.0000e+00	0.0000e+00
2	0.0000e+00	7.5032e+01
3	0.0000e+00	8.9186e+01
4	0.0000e+00	8.7552e+01
5	0.0000e+00	7.8922e+01
6	0.0000e+00	6.7957e+01
7	0.0000e+00	5.7007e+01
8	0.0000e+00	4.7134e+01
9	0.0000e+00	3.8703e+01
10	0.0000e+00	3.1733e+01
11	0.0000e+00	2.6079e+01
12	0.0000e+00	2.1542e+01
13	0.0000e+00	1.7920e+01
14	0.0000e+00	1.5029e+01
15	0.0000e+00	1.2714e+01
16	0.0000e+00	1.0849e+01
17	0.0000e+00	9.3345e+00
18	0.0000e+00	8.0930e+00
19	0.0000e+00	7.0645e+00
20	0.0000e+00	6.2034e+00
21	0.0000e+00	5.4748e+00
22	0.0000e+00	4.8522e+00
23	0.0000e+00	4.3155e+00
24	0.0000e+00	3.8491e+00
25	0.0000e+00	3.4409e+00
26	0.0000e+00	3.0817e+00
27	0.0000e+00	2.7640e+00
28	0.0000e+00	2.4820e+00
29	0.0000e+00	2.2307e+00
30	0.0000e+00	2.0062e+00
31	0.0000e+00	1.8054e+00
32	0.0000e+00	1.6253e+00
33	0.0000e+00	1.4637e+00
34	0.0000e+00	1.3185e+00
35	0.0000e+00	1.1879e+00
36	0.0000e+00	1.0705e+00
37	0.0000e+00	9.6471e−01
38	0.0000e+00	8.6949e−01
39	0.0000e+00	7.8372e−01
40	0.0000e+00	7.0644e−01
41	0.0000e+00	6.3681e−01
42	0.0000e+00	5.7406e−01
43	0.0000e+00	5.1751e−01
44	0.0000e+00	4.6654e−01

45	0.0000e+00	4.2059e−01
46	0.0000e+00	3.7917e−01
47	0.0000e+00	3.4183e−01
48	0.0000e+00	3.0818e−01
49	0.0000e+00	2.7783e−01
50	0.0000e+00	2.5048e−01
51	0.0000e+00	2.2582e−01
52	0.0000e+00	2.0358e−01
53	0.0000e+00	1.8354e−01
54	0.0000e+00	1.6547e−01
55	0.0000e+00	1.4918e−01
56	0.0000e+00	1.3449e−01
57	0.0000e+00	1.2125e−01
58	0.0000e+00	1.0932e−01
59	0.0000e+00	9.8554e−02
60	0.0000e+00	8.8851e−02
61	0.0000e+00	8.0104e−02
62	0.0000e+00	7.2218e−02
63	0.0000e+00	6.5108e−02
64	0.0000e+00	5.8698e−02
65	0.0000e+00	5.2920e−02
66	0.0000e+00	4.7710e−02
67	0.0000e+00	4.3013e−02
68	0.0000e+00	3.8778e−02
69	0.0000e+00	3.4961e−02
70	0.0000e+00	3.1519e−02
71	0.0000e+00	2.8416e−02
72	0.0000e+00	2.5618e−02
73	0.0000e+00	2.3096e−02
74	0.0000e+00	2.0823e−02
75	0.0000e+00	1.8773e−02
76	0.0000e+00	1.6924e−02
77	0.0000e+00	1.5258e−02
78	0.0000e+00	1.3756e−02
79	0.0000e+00	1.2402e−02
80	0.0000e+00	1.1181e−02
81	0.0000e+00	1.0080e−02
82	0.0000e+00	9.0878e−03
83	0.0000e+00	8.1932e−03
84	0.0000e+00	7.3866e−03
85	0.0000e+00	6.6594e−03
86	0.0000e+00	6.0038e−03
87	0.0000e+00	5.4127e−03
88	0.0000e+00	4.8798e−03
89	0.0000e+00	4.3994e−03
90	0.0000e+00	3.9663e−03
91	0.0000e+00	3.5758e−03
92	0.0000e+00	3.2238e−03
93	0.0000e+00	2.9064e−03
94	0.0000e+00	2.6203e−03
95	0.0000e+00	2.3623e−03
96	0.0000e+00	2.1298e−03
97	0.0000e+00	1.9201e−03
98	0.0000e+00	1.7311e−03

99	0.0000e+00	1.5606e−03
100	0.0000e+00	1.4070e−03
101	0.0000e+00	1.2685e−03
102	0.0000e+00	1.1436e−03
103	0.0000e+00	1.0310e−03
104	0.0000e+00	9.2952e−04
105	0.0000e+00	8.3801e−04
106	0.0000e+00	7.5551e−04
107	0.0000e+00	6.8113e−04
108	0.0000e+00	6.1407e−04
109	0.0000e+00	5.5362e−04
110	0.0000e+00	4.9912e−04
111	0.0000e+00	4.4998e−04
112	0.0000e+00	4.0568e−04
113	0.0000e+00	3.6574e−04
114	0.0000e+00	3.2974e−04
115	0.0000e+00	2.9727e−04
116	0.0000e+00	2.6801e−04
117	0.0000e+00	2.4162e−04
118	0.0000e+00	2.1784e−04
119	0.0000e+00	1.9639e−04
120	0.0000e+00	1.7706e−04
121	0.0000e+00	1.5963e−04
122	0.0000e+00	1.4391e−04
123	0.0000e+00	1.2974e−04
124	0.0000e+00	1.1697e−04
125	0.0000e+00	1.0545e−04
126	0.0000e+00	9.5073e−05
127	0.0000e+00	8.5713e−05
128	0.0000e+00	7.7275e−05
129	0.0000e+00	6.9667e−05
130	0.0000e+00	6.2809e−05
131	0.0000e+00	5.6625e−05
132	0.0000e+00	5.1051e−05
133	0.0000e+00	4.6025e−05
134	0.0000e+00	4.1494e−05
135	0.0000e+00	3.7409e−05
136	0.0000e+00	3.3726e−05
137	0.0000e+00	3.0406e−05
138	0.0000e+00	2.7412e−05
139	0.0000e+00	2.4714e−05
140	0.0000e+00	2.2281e−05
141	0.0000e+00	2.0087e−05
142	0.0000e+00	1.8110e−05
143	0.0000e+00	1.6327e−05
144	0.0000e+00	1.4719e−05
145	0.0000e+00	1.3270e−05
146	0.0000e+00	1.1964e−05
147	0.0000e+00	1.0786e−05
148	0.0000e+00	9.7242e−06
149	0.0000e+00	8.7669e−06
150	0.0000e+00	7.9038e−06
151	0.0000e+00	7.1257e−06
152	0.0000e+00	6.4242e−06

153	0.0000e+00	5.7917e−06
154	0.0000e+00	5.2215e−06
155	0.0000e+00	4.7075e−06
156	0.0000e+00	4.2440e−06
157	0.0000e+00	3.8262e−06
158	0.0000e+00	3.4495e−06
159	0.0000e+00	3.1099e−06
160	0.0000e+00	2.8038e−06
161	0.0000e+00	2.5277e−06
162	0.0000e+00	2.2789e−06
163	0.0000e+00	2.0545e−06
164	0.0000e+00	1.8523e−06
165	0.0000e+00	1.6699e−06
166	0.0000e+00	1.5055e−06
167	0.0000e+00	1.3573e−06
168	0.0000e+00	1.2237e−06
169	0.0000e+00	1.1032e−06
170	0.0000e+00	9.9460e−07
171	0.0000e+00	8.9669e−07
172	0.0000e+00	8.0841e−07
173	0.0000e+00	7.2882e−07
174	0.0000e+00	6.5707e−07
175	0.0000e+00	5.9239e−07
176	0.0000e+00	5.3407e−07
177	0.0000e+00	4.8149e−07
178	0.0000e+00	4.3409e−07
179	0.0000e+00	3.9135e−07
180	0.0000e+00	3.5282e−07
181	0.0000e+00	3.1809e−07
182	0.0000e+00	2.8677e−07
183	0.0000e+00	2.5854e−07
184	0.0000e+00	2.3309e−07
185	0.0000e+00	2.1014e−07
186	0.0000e+00	1.8945e−07
187	0.0000e+00	1.7080e−07
188	0.0000e+00	1.5399e−07
189	0.0000e+00	1.3883e−07
190	0.0000e+00	1.2516e−07
191	0.0000e+00	1.1284e−07
192	0.0000e+00	1.0173e−07
193	0.0000e+00	9.1715e−08
194	0.0000e+00	8.2686e−08
195	0.0000e+00	7.4545e−08
196	0.0000e+00	6.7207e−08
197	0.0000e+00	6.0590e−08
198	0.0000e+00	5.4625e−08
199	0.0000e+00	4.9247e−08
200	0.0000e+00	4.4399e−08
201	0.0000e+00	4.0028e−08
202	0.0000e+00	3.6087e−08
203	0.0000e+00	3.2535e−08
204	0.0000e+00	2.9332e−08
205	0.0000e+00	2.6444e−08
206	0.0000e+00	2.3841e−08

207	0.0000e+00	2.1494e−08
208	0.0000e+00	1.9378e−08
209	0.0000e+00	1.7470e−08
210	0.0000e+00	1.5750e−08
211	0.0000e+00	1.4200e−08
212	0.0000e+00	1.2802e−08
213	0.0000e+00	1.1541e−08
214	0.0000e+00	1.0405e−08
215	0.0000e+00	9.3807e−09
216	0.0000e+00	8.4572e−09
217	0.0000e+00	7.6246e−09
218	0.0000e+00	6.8740e−09
219	0.0000e+00	6.1973e−09
220	0.0000e+00	5.5872e−09
221	0.0000e+00	5.0371e−09
222	0.0000e+00	4.5412e−09
223	0.0000e+00	4.0941e−09
224	0.0000e+00	3.6911e−09
225	0.0000e+00	3.3277e−09
226	0.0000e+00	3.0001e−09
227	0.0000e+00	2.7047e−09
228	0.0000e+00	2.4385e−09
229	0.0000e+00	2.1984e−09
230	0.0000e+00	1.9820e−09
231	0.0000e+00	1.7869e−09
232	0.0000e+00	1.6109e−09
233	0.0000e+00	1.4523e−09
234	0.0000e+00	1.3094e−09
235	0.0000e+00	1.1805e−09
236	0.0000e+00	1.0642e−09
237	0.0000e+00	9.5948e−10
238	0.0000e+00	8.6502e−10
239	0.0000e+00	7.7986e−10
240	0.0000e+00	7.0308e−10
241	0.0000e+00	6.3387e−10
242	0.0000e+00	5.7146e−10
243	0.0000e+00	5.1520e−10
244	0.0000e+00	4.6448e−10
245	0.0000e+00	4.1876e−10
246	0.0000e+00	3.7753e−10
247	0.0000e+00	3.4036e−10
248	0.0000e+00	3.0685e−10
249	0.0000e+00	2.7665e−10
250	0.0000e+00	2.4941e−10
251	0.0000e+00	2.2486e−10
252	0.0000e+00	2.0272e−10
253	0.0000e+00	1.8276e−10
254	0.0000e+00	1.6477e−10
255	0.0000e+00	1.4855e−10
256	0.0000e+00	1.3392e−10
257	0.0000e+00	1.2074e−10
258	0.0000e+00	1.0885e−10
259	0.0000e+00	9.8137e−11
260	0.0000e+00	8.8475e−11

```
261      0.0000e+00      7.9765e-11
262      0.0000e+00      7.1912e-11
263      0.0000e+00      6.4833e-11
264      0.0000e+00      5.8450e-11
265      0.0000e+00      5.2696e-11
266      0.0000e+00      4.7508e-11
267      0.0000e+00      4.2831e-11
268      0.0000e+00      3.8614e-11
269      0.0000e+00      3.4813e-11
270      0.0000e+00      3.1386e-11
271      0.0000e+00      2.8296e-11
272      0.0000e+00      2.5510e-11
273      0.0000e+00      2.2999e-11
274      0.0000e+00      2.0734e-11
275      0.0000e+00      1.8693e-11
276      0.0000e+00      1.6853e-11
277      0.0000e+00      1.5194e-11
278      0.0000e+00      1.3698e-11
279      0.0000e+00      1.2349e-11
280      0.0000e+00      1.1134e-11
281      0.0000e+00      1.0038e-11
282      0.0000e+00      9.0494e-12
283      0.0000e+00      8.1585e-12
284      0.0000e+00      7.3553e-12
285      0.0000e+00      6.6312e-12
286      0.0000e+00      5.9784e-12
287      0.0000e+00      5.3898e-12
288      0.0000e+00      4.8592e-12
289      0.0000e+00      4.3808e-12;
```

End file: `input-dose_to_ncconc.inc`

Begin file: `input-objective_function.inc`

```
obj .. z =e= + TUMOR('4032')
             + TUMOR('6048')
             + TUMOR('8064')
             + TUMOR('10080')
             + TUMOR('12096')
             + TUMOR('14112')
             + TUMOR('16128') ;
```

End file: `input-objective_function.inc`

Begin file: `input-parameters.inc`

```
*
* analysis specific
*
timestep  discretizatoin step size          /5.00000000e+00/
numsteps  number of time steps              /16128/
```

```
*
* tumor growth parameters
*
tauef     fast growth rate                  /1.94186187e+04/
taues     slow growth rate                  /1.94186187e+04/
nth       switching size                    /4.77363886e+02/
*
* nonlinear pd parameters
*
keff          rate of cell kill              /3.48501281e-05/
*
* body weight model parameters
*
tauw          rate of mouse doubling         /2.60497755e-06/
kd            effect of drug on bodyweight   /2.85795338e-05/
*
* miscalleneous parameters
*
N0            initial condition               /4.00000000e+01/
B0            initial body weight (treatment) /2.00000000e+01/
B0CYCLE       initial body weight (cycle)     /2.00000000e+01/
BMIN          minimum body weight (fraction)  /9.80000000e-01/
dose_times(q) possible dose times            /
    1       1
    2     289
    3     577
    4     865
    5    1153
    6    2017
    7    2305
    8    2593
    9    2881
   10    3169
   11    4033
   12    4321
   13    4609
   14    4897
   15    5185
   16    6049
   17    6337
   18    6625
   19    6913
   20    7201
   21    8065
   22    8353
   23    8641
   24    8929
   25    9217
   26   10081
   27   10369
   28   10657
   29   10945
   30   11233
   31   12097
```

```
   32    12385
   33    12673
   34    12961
   35    13249
   36    14113
   37    14401
   38    14689
   39    14977
   40    15265
 /
dose_levels(dlvls) possible dose levels            /
    1    1.000000e+00
 /
```

End file: `input-parameters.inc`

Begin file: `input-sets.inc`

```
k          discrete time                        /1*16128/
q          dosing time                          /1*40/
spd        steps per day                        /1*289/
dlvls      number of possible dose levels       /1*2/
```

End file: `input-sets.inc`

Begin file: `optimal_dose_profile.gms`

```
*
* SETS
*
SETS
$include "input-sets.inc"
;


*
* PARAMETERS
*
PARAMETERS
NMIN     lb on tumor volume
NMAX     ub on tumor volume
LNS      lb on slow tumor growth
UNS      ub on slow tumor growth
LNF      lb on fast tumor growth
UNF      ub on fast tumor growth
$include "input-parameters.inc"
;

$include "input-dose_to_ncconc.inc"

$include "input-dose_to_acconc.inc"
```

```
NMIN     = .1;
NMAX     = 20000;
LNS      = log(2)/tauef - log(2)/taues;
UNS      = log(2)/tauef - log(2)/taues;
LNF      = log(2)/taues - log(2)/tauef;
UNF      = log(2)/taues - log(2)/tauef;

*
* VARIABLES
*
variables
  TUMOR(k)       tumor growth
  BW(k)          body weight
  BWc(k)         corrected body weight
  CNC(k)         concentration of 9NC
  CAC(k)         concentration of 9NC
  G(k)           discontinuous tumor growth term
  BT(k)          switching variable for tumor growth
  BD(q,dlvls)    binary variable to turn on different
  z              objective function value
  ;
  free     variable  TUMOR
* positive variable  BW
  positive variable  CNC
  positive variable  CAC
  positive variable  G
  positive variable  Du
  positive variable  Dl
  binary   variable  BT
  binary   variable  BD
  free     variable  z
  ;

*
*  bounding variables
*
  TUMOR.up(k) = log(NMAX);
**BW.up(k) = 2;

*
* setting initial values
*

TUMOR.fx('1') = log(N0);
BW.fx('1')    = B0CYCLE;

*
* initial guess for variables
*
* -- no treatment
*
  CNC.l(k)       = 0;
  CAC.l(k)       = 0;
```

```
  BT.l(k)          = 0;
  BD.l(q,dlvls)    = 0;
  BD.l(q,'1')      = 1;

   TUMOR.l('1')     = log(N0);
   loop(k,
     BT.l(k)     = (1)$(TUMOR.l(k) lt log(nth));
     G.l(k)      = (log(2)/tauef)$(TUMOR.l(k) lt log(nth))
                 + (log(2)/taues)$(TUMOR.l(k) ge log(nth));
     TUMOR.l(k+1)  = TUMOR.l(k) + timestep*G.l(k) ;
*    setting the upper bound on tumor size as the size
*    of the tumor at any step 'k' if no drug were administered
     TUMOR.up(k)   = TUMOR.l(k);
   );



*
* EQUATIONS
*
EQUATIONS
   dBW(k)           "PD bodyweight"
   BWcdef(k)        "corrected body weight"
   BWcmin(k)        "minimum on bodyweight"
   odpd(q)          "one dose per day"
   CNCdef(k)        "defining CNC"
   CACdef(k)        "defining CAC"
   dTUMOR(k)        "PD tumor volume"
   swNS(k)          "active when N > nth"
   swNF(k)          "active when N < nth"
   swNLS(k)         "active when N < nth"
   swNUS(k)         "active when N < nth"
   swNLF(k)         "active when N > nth"
   swNUF(k)         "active when N > nth"
   obj              "objective function"
   ;
*
* Defining CNC and CAC
*



*
* ensuring that only one dose is selected per dosing day
*
odpd(q)   ..   sum(dlvls, BD(q,dlvls)) =e= 1;

CACdef(k)..   CAC(k) =e= sum((spd,q),
      sum(dlvls,
        BD(q,dlvls)*ALLACCONC(spd,dlvls)
        $(ord(k) eq (dose_times(q)-1+ord(spd)) )
       )
     );
```

```
CNCdef(k)..  CNC(k) =e= sum((spd,q),
       sum(dlvls,
         BD(q,dlvls)*ALLNCCONC(spd,dlvls)
         $(ord(k) eq (dose_times(q)-1+ord(spd)) )
       )
     );



*
* handling the discontinuity in N at nth
*
swNS(k)      .. TUMOR(k) - log(nth)   =l=
                (log(NMAX) - log(nth))*(1-BT(k));
swNF(k)      .. log(nth) - TUMOR(k)   =l=
                (log(nth) - log(NMIN))*BT(k);
swNLS(k)     .. LNS*BT(k)             =l=
                G(k) - log(2)/taues;
swNUS(k)     .. G(k) - log(2)/taues   =l=
                UNS*BT(k);
swNLF(k)     .. LNF*(1-BT(k))         =l=
                G(k) - log(2)/tauef;
swNUF(k)     .. G(k) - log(2)/tauef   =l=
                UNF*(1-BT(k));

*
* growth
*

 dTUMOR(k)$(ord(k) lt numsteps) .. TUMOR(k+1) =e=
 TUMOR(k) + timestep*(G(k) - keff*(CNC(k) + CAC(k)));

 dBW(k)$(ord(k) lt numsteps) .. BW(k+1) =e=
 BW(k) + timestep*( tauw*BW(k) - kd*(CNC(k) + CAC(k)));


 BWcdef(k).. BWc(k)  =e=
 BW(k)/B0  - exp(TUMOR.l(k))/(B0*1000);
 BWcmin(k) .. BWc(k) =g= BMIN;


$include "input-objective_function.inc"

  z.l = TUMOR.l('8064');

 option LIMROW   = 400000;
 option reslim   = 200000;
 option iterlim  = 200000;

Model dose /all/;

SOLVE dose minimizing z USING MIP;
```

```
display TUMOR.l;
display BW.l;
display BWc.l;
display CNC.l;
display CAC.l;
display G.l;
display BT.l;
display BD.l;
display z.l;

FILE fhdl /output-dose_levels.txt/;
put  fhdl;
fhdl.nd=10;
loop((q,dlvls),
  if(1 = BD.l(q,dlvls),
    if(ord(dlvls) > 1,
       put ord(q), @20, dose_times(q), @40,
       dose_levels(dlvls-1)    /;
    else
       put ord(q), @20, dose_times(q), @40, 0 /;
      );
    );
  );


FILE fhsv /output-state_values.txt/;
put fhsv;
fhsv.nd=10;
 loop(k,
   put (ord(k)*timestep),
       @20, CNC.l(k),
       @40, CAC.l(k),
       @60, exp(TUMOR.l(k)),
       @80, BW.l(k),
       @100, BWc.l(k)/;
 );
```

End file: `optimal_dose_profile.gms`

Begin file: `output-dose_levels-min_max.txt`

```
1.0000000000        1.0000000000        0.0000000000
2.0000000000        2.8900000E+2        0.0000000000
3.0000000000        5.7700000E+2        1.0000000000
4.0000000000        8.6500000E+2        1.0000000000
5.0000000000        1.1530000E+3        1.0000000000
6.0000000000        2.0170000E+3        1.0000000000
7.0000000000        2.3050000E+3        1.0000000000
8.0000000000        2.5930000E+3        1.0000000000
9.0000000000        2.8810000E+3        1.0000000000
1.0000000E+1        3.1690000E+3        1.0000000000
1.1000000E+1        4.0330000E+3        0.0000000000
```

1.2000000E+1	4.3210000E+3	1.0000000000
1.3000000E+1	4.6090000E+3	1.0000000000
1.4000000E+1	4.8970000E+3	1.0000000000
1.5000000E+1	5.1850000E+3	1.0000000000
1.6000000E+1	6.0490000E+3	0.0000000000
1.7000000E+1	6.3370000E+3	0.0000000000
1.8000000E+1	6.6250000E+3	1.0000000000
1.9000000E+1	6.9130000E+3	1.0000000000
2.0000000E+1	7.2010000E+3	1.0000000000
2.1000000E+1	8.0650000E+3	0.0000000000
2.2000000E+1	8.3530000E+3	0.0000000000
2.3000000E+1	8.6410000E+3	1.0000000000
2.4000000E+1	8.9290000E+3	1.0000000000
2.5000000E+1	9.2170000E+3	1.0000000000
2.6000000E+1	1.0081000E+4	0.0000000000
2.7000000E+1	1.0369000E+4	0.0000000000
2.8000000E+1	1.0657000E+4	1.0000000000
2.9000000E+1	1.0945000E+4	1.0000000000
3.0000000E+1	1.1233000E+4	1.0000000000
3.1000000E+1	1.2097000E+4	0.0000000000
3.2000000E+1	1.2385000E+4	0.0000000000
3.3000000E+1	1.2673000E+4	1.0000000000
3.4000000E+1	1.2961000E+4	1.0000000000
3.5000000E+1	1.3249000E+4	1.0000000000
3.6000000E+1	1.4113000E+4	0.0000000000
3.7000000E+1	1.4401000E+4	0.0000000000
3.8000000E+1	1.4689000E+4	1.0000000000
3.9000000E+1	1.4977000E+4	1.0000000000
4.0000000E+1	1.5265000E+4	1.0000000000

End file: `output-dose_levels-min_max.txt`

Begin file: `output-state_values-min_max.txt`

5.0000000000	0.0000000000	0.0000000000	4.0000000E+1	2.0000000E+1	0.9980000000
1.0000000E+1	0.0000000000	0.0000000000	4.0007140E+1	2.0000260E+1	0.9980126679
.	.	.	.	.	.
.	.	.	.	.	.
.	.	.	.	.	.
8.0630000E+4	0.0000000000	0.0000000000	7.6661703042	2.0503050E+1	0.9895984014
8.0635000E+4	0.0000000000	0.0000000000	7.6675386452	2.0503317E+1	0.9896054078
8.0640000E+4	0.0000000000	0.0000000000	7.6689072305	2.0503584E+1	0.9896124133

End file: `output-state_values-min_max.txt`

BIBLIOGRAPHY

[1] The American Cancer Society. Cancer facts & figures: 2005. URL: http://www.cancer.org/downloads/STT/CAFF 2005f4PWSecured.pdf, 2005.

[2] J. M. Slingerland and I. F. Tannock. *Cell Proliferation and Cell Death*, chapter 7, pages 134–165. The Basic Science of Oncology. McGraw-Hill, third edition, 1998.

[3] S. Dedhar, G. E. Hannigan, J. Rak, and R. S. Kerbel. *The Extracellular Environment and Cancer*, chapter 9, pages 197–218. The Basic Science of Oncology. McGraw-Hill, third edition, 1998.

[4] A. F. Chambers and R. P. Hill. *Tumor Progression and Metastasis*, chapter 10, pages 219–239. The Basic Science of Oncology. McGraw-Hill, third edition, 1998.

[5] R. Simon. *Clinical Trials in Cancer*, chapter 21, pages 521–538. Cancer: Principles & Practice of Oncology. Lippincott, Williams, & Wilkins, Philadelphia, PA, sixth edition, 2001.

[6] E. Horstmann, M. S. McCabe, L. Grochow, S. Yamamoto, L. Rubinstein, T. Budd, D. Shoemaker, E. J. Emanuel, and C. Grady. Risks and benefits of phase 1 oncology trials, 1991 through 2002. *N Engl J Med*, 352(9):895–932, 2005.

[7] J. H. Lee. Modeling and identification for nonlinear predictive control: Requirements, current status and future research needs. In F. Allgöwer and A. Zheng, editors, *Nonlinear Model Predictive Control: Assessment and Future Directions*. Birkhäuser, 1999.

[8] M. Morari and E. Zafiriou. *Robust Process Control*. Prentice-Hall, Englewood Cliffs, NJ, 1989.

[9] F. Allgöwer, T. A. Badgwell, J. S. Qin, J. B. Rawlings, and S. J. Wright. *Nonlinear Predictive Control and Moving Horizon Estimation – An Introductory Overview*, pages 391–449. Advances in Control – Highlights of ECC '99. Springer, London, 1999.

[10] C. Cobelli and E. Carson. *An Introduction To Modelling Methodology*, chapter 1, pages 1–44. Modelling Methodology for Physiology and Medicine. Academic Press, San Diego, CA, 2001.

[11] L. Norton. A Gompertzian model of human breast cancer growth. *Cancer Res.*, 48:7067–7071, 1988.

[12] R. Martin and K. L. Teo. *Optimal Control of Drug Administration in Cancer Chemotherapy*. World Scientific, River Edge, NJ, 1994.

[13] G. W. Swan. Cancer chemotherapy: Optimal control using the Verhulst–Pearl equation. *Bull. Math. Biol.*, 48(3/4):381–404, 1986.

[14] M. Simeoni, P. Magni, C. Cammia, G. De Nicolao, V. Croci, E. Pesenti, M. Germani, I. Poggesi, and M. Rocchetti. Predictive pharmacokinetic-pharmacodynamic modeling of tumor growth kinetics in xenograft models after administration of anticancer agents. *Cancer Res.*, 64:1094–1101, 2004.

[15] J. C. Panetta and J. Adam. A mathematical model of cycle–specific chemotherapy. *Math. Comput. Model.*, 22(2):67–82, 1995.

[16] F. L. Pereira, C. E. Pedreira, M. R. Pinho, M. H. Fernandes, and J. B. Sousa. An optimal control algorithm for multidrug cancer chemotherapy design. In *Proc. IEEE EMBS Ann. Conf.*, volume 12, pages 1021–1022, 1990.

[17] H. M. Shapiro. *Practical Flow Cytometry*. Wiley-Liss, Hoboken, New Jersey, 4th edition, 2003.

[18] J. A. Florian Jr., J. L. Eiseman, and R. S. Parker. A nonlinear model predictive control algorithm for breast cancer treatment. In *Proc. DYCOPS 7*, pages 1–12, Boston, MA, 2004.

[19] T. Teorell. Kinetics of distribution of substances administered to the body I. *Arch. Int. Pharma. Ther.*, 57:202–225, 1937.

[20] T. Teorell. Kinetics of distribution of substances administered to the body II. *Arch. Int. Pharma. Ther.*, 57:226–240, 1937.

[21] P. Vicini. *Blood-Tissue Exchange Modelling*, chapter 13, pages 373–397. Modelling Methodology for Physiology and Medicine. Academic Press, San Diego, CA, 2001.

[22] F. A. Hawtof and M. J. Egorin. Evaluation of a new program for population of PK/PD analysis applied to simulated phase I data (abstract). *Clin. Pharmacol. Ther.*, 49:153, 1991.

[23] S. L. Beal and L. B. Sheiner. *NONMEM User's Guide*. NONMEM Project Group, University of California, San Francisco, 1992.

[24] J. M. Collins. *Pharmacokinetics and Clinical Monitoring*, chapter 3, pages 37–49. Cancer Chemotherapy & Biology. Lippincott Williams & Wilkins, third edition, 2001.

[25] D. Z. D'Argenio and A. Schumitsky. *ADAPT II User's Guide*. Biomedical Simulation Resource, University of Southern California, Los Angeles, CA, 1990.

[26] B. A. Ogunnaike and W.H. Ray. *Process Dynamics, Modeling, and Control*. Oxford University Press, New York, NY, 1994.

[27] S. Skogestad and I. Postlethwaite. *Multivariable Feedback Control*. John Wiley & Sons, New York, NY, 1996.

[28] T. L. Chen, J. L. Passos-Coelho, D. A. Noe, M. J. Kennedy, K. C. Black, O. M. Colvin, and L. B. Grochow. Nonlinear pharmacokinetics of cyclophosphamide in patients with metastatic breast cancer receiving high-dose chemotherapy followed by autologous bone marrow transplantation. *Cancer Res.*, 55(4):810–816, 1995.

[29] M. Sale. Unsupervised machine learning based model selection in NONMEM. In *Advanced Methods of Pharmacokinetic & Pharmacodynamic Systems Analysis*, Marina del Rey, CA, 2001. Biomedical Simulations Resource.

[30] L. B. Sheiner and S. L. Beal. Evaluation of methods for estimating population pharmacokinetic parameters. I. Michaelis-Menten model: Routine clinical pharmacokinetic data. *J. Pharmacokinet. Biopharm.*, 8(6):553–571, 1980.

[31] L. B. Sheiner and S. L. Beal. Pharmacokinetic parameter estimates from several least squares procedures: Superiority of extended least squares. *J. Pharmacokinet. Biopharm.*, 13(2):185–201, 1985.

[32] A. Asachenkov, G. Marchuk, R. Mohler, and S. Zuev. *Disease Dynamics*. Birkhäuser, Boston, 1994.

[33] A. Caumo, M. Simeoni, and C. Cobelli. *Glucose Modeling*, chapter 12, pages 337–372. Modelling Methodology for Physiology and Medicine. Academic Press, San Diego, CA, 2001.

[34] D. R. Shopland, H. J. Eyre, and T. F. Pechacek. Smoking-attributable cancer mortality in 1991: is lung cancer now the leading cause of death among smokers in the United States? *J. Natl. Cancer Inst.*, 83(16):1142–1148, 1991.

[35] J. W. Jusko and H. C. Ko. Physiologic indirect response models characterize diverse types of pharmacodynamic effects. *Clin. Pharmacol. Ther.*, 56(4):406–419, 1994.

[36] H. D. Dawson and D. D. Taub. *Chemokine–Chemokine Receptor Database 2001: Biological, Molecular, and Pathophysiologic Properties of Chemokine–Receptor Interactions*, chapter 37, pages 1012–1127. Cancer Chemotherapy & Biology. Lippincott Williams & Wilkins, third edition, 2001.

[37] A. L. Mellott and W. J. Gradishar. *Inhibitors of Tumor Angiogenesis*, chapter 35, pages 988–997. Cancer Chemotherapy & Biology. Lippincott Williams & Wilkins, 2001.

[38] U. Ledzewicz and H. Schättler. Analysis of a class of optimal control problems arising in cancer chemotherapy. In *Proc. American Control Conf.*, pages 3460–3465, Anchorage, AK, 2002.

[39] C. H. Takimoto and S. G. Arbuck. *Topoisomerase I Targeting Agents: The Camptothecins*, chapter 20, pages 579–646. Cancer Chemotherapy & Biology. Lippincott Williams & Wilkins, 3rd edition, 2001.

[40] J. G. Liehr, N. J. Harris, J. Mendoza, and A. E. Ahmed. Pharmacology of camptothecin esters. *Ann. N.Y. Acad. Sci.*, 922:216–223, 2000.

[41] Y. Pommier, P. Pourquier, Y. Urasaki, J. Wu, and G. S. Laco. Topoisomerase I inhibitors: Selectivity and cellular resistance. *Drug Resist. Update.*, 2:307–318, 1999.

[42] E. K. Rowinsky, L. B. Grochow, and C. B. Hendricks. Phase I and pharmacologic study of topotecan: a novel topoisomerase I inhibitor. *J. Clin. Oncol.*, 10:647–656, 1992.

[43] J. M. Gallo, P. Vicini, A. Orlansky, S. Li, F. Shou, J. Ma, S. Pulfer, M. A. Bookman, and P. Guo. Pharmacokinetic model–predicted anticancer drug concentrations in human tumors. *Clinical Cancer Research*, 10:8048–8058, 2004.

[44] U. Ledzewicz and H. Schättler. Optimal bang-bang controls for a two-compartment model in cancer chemotherapy. *J. Optimization Theory Appl.*, 114(3):609–637, 2002.

[45] R. B. Martin. Optimal control drug scheduling of cancer chemotherapy. *Automatica*, 28:1113–1123, 1992.

[46] A. Swierniak and J. Smieja. Cancer chemotherapy optimization under evolving drug resistance. *Nonlinear Analysis*, 47:375–386, 2001.

[47] E. K. Afenya. Recovery of normal hemopoiesis in disseminated cancer therapy - a model. *Math. Biosci.*, 172:15–32, 2001.

[48] M. Kimmel and O. Gorlova. Stochastic models of progression of cancer and their use in controlling cancer-related mortality. In *Proc. American Control Conf.*, pages 3443–3448, Anchorage, AK, May 2002.

[49] D. Cella, A. Peterman, S. Hudgens, K. Webster, and M. A. Socinski. Measuring the side effects of taxane therapy in oncology. *Cancer*, 98(4):822–831, 2003.

[50] T. Thigpen. Maybe more is better. *J. Clin. Oncol.*, 21(13):2454–2456, 2003.

[51] R. B. Martin, M. E. Fisher, R. F. Minchin, and K. L. Teo. A mathematical model of cancer chemotherapy with an optimal selection of parameters. *Math. Biosci.*, 99:205–230, 1990.

[52] R. F. Stengel. *Optimal Control and Estimation*. Dover Publications, Inc., 31 East 2nd St., Mineola, N.Y. 11501, 1994.

[53] M. I. S. Costa, J. L. Boldrini, and R. C. Bassanezi. Drug kinetics and drug resistance in optimal chemotherapy. *Math. Biosci.*, 125:191–209, 1995.

[54] C. A. Charles, V. S. Yee, S. W. Dusza, A. A. Marghoob, S. A. Oliveria, A. Koph, D. Rigel, and A. C. Halpern. Variation in the diagnosis, treatment, and management of melanoma in situ: a survey of us dermatologists. *Arch. Dermatol.*, 141(6):723–729, 2005.

[55] L. L. Jung and W. C. Zamboni. Cellular, pharmacokinetic, and pharmacodynamic aspects of response to camptothecins: can we improve it? *Drug Resist. Update.*, 4(4):273–288, 2001.

[56] P. Pantazis, N. Harris, J. Mendoza, and B. Giovanella. Conversion of 9-nitro-camptothecin to 9-amino-camptothecin by human blood cells *in vitro*. *Eur. J. of Heamatol.*, 53(4):246–248, 1994.

[57] P. D. Allison. *Missing Data*. A Sage University Paper on Quantitative Applications in the Social Sciences, 07-136. Sage, Thousand Oaks, CA, 2002.

[58] R. Horvorka and P. Vicini. *Parameter Estimation*, chapter 5, pages 107–152. Modelling Methodology for Physiology and Medicine. Academic Press, San Diego, CA, 2001.

[59] E. K. P. Chong and S. H. Żak. *An Introduction To Optimization*. Wiley Interscience, New York, 1996.

[60] R. S. Parker. Efficient nonlinear model predictive control: Exploiting the Volterra–Laguerre model structure. In *Proceedings of CPC VI*. CACHE Corporation, AIChE Symposia Series, 2002.

[61] H. Akaike. A Bayesian extension of the minimal AIC procedures of autoregressive model fitting. *Biometrika*, 66:237, 1979.

[62] J. G. Liehr, A. E. Ahmed, and B. C. Giovanella. Pharmacokinetics of camptothecins administered orally. *Ann. N.Y. Acad. Sci.*, 803:157–163, 1996.

[63] R. B. Martin, M. E. Fisher, R. F. Minchin, and K. L. Teo. Optimal control of tumor size used to maximize survival time when cells are resistant to chemotherapy. *Math. Biosci.*, 110:221–252, 1992.

[64] R. Rajendra, M. K. Saleem, J. H. Schellens, D. D. Ross, S. E. Bates, P. Sinko, and E. H. Rubin. Differential effects of the breast cancer resistance protein on the cellular accu-

mulation and cytotoxicity of 9-aminocamptothecin and 9-nitrocamptothecin. *Cancer Res.*, 63(15):3228–33, 2003.

[65] D. Barbolosi and A. Iliadis. Optimizing drug regimens in cancer chemotherapy: A simulation study using a PK-PD model. *Comput. Biol. Med.*, pages 157–172, 2001.

[66] R. S. Parker, J. H. Ward, N. A. Peppas, and F. J. Doyle III. Robust H_∞ glucose control in diabetes using a physiological model. *AIChE Journal*, 46:2537–2549, 2000.

[67] J. Urquhart and E. De Klerk. Contending paradigms for the interpretation of data on patient compliance with therapeutic drug regimens. *Stat. Med.*, 17:251–267, 1998.

[68] C. T. Chen. *Linear System Theory and Design*. Holt, Rinehart, and Winston, Austin, TX, 1984.

[69] E. Kreyszig. *Advanced Engineering Mathematics*. John Wiley & Sons, New York, NY, 8th edition, 1999.

[70] M. L. Tyler and M. Morari. Propositional logic in control and monitoring problems. *Automatica*, 35:565–582, 1999.

[71] M. M. Thomas, B. Joseph, and J. L. Kardos. Batch chemical process quality control applied to curing of composite materials. *AIChE J.*, 43(10):2535–2545, October 1997.

[72] V. Liotta, C. Georgakis, and M. S. El-Aasser. Real-time estimation and control of particle size in semi-batch emulsion polymerization. In *Proc. of the American Control Conf.*, pages 1172–1176, Albuquerque, NM, 1997.

[73] A. Banerjee, Y. Arkun, B.A. Ogunnaike, and R.K. Pearson. Robust nonlinear control by scheduling multiple model based controllers. In *AICHE Annual Meeting, paper no. 230a*, 1994.

[74] A. B. Banerjee, Y. Arkun, B. Ogunnaike, and R. Pearson. Estimation of Nonlinear Systems Using Linear Multiple Models. *AIChE J.*, 43(5):1204–1226, 1997.

[75] B.A. Ogunnaike, R.K. Pearson, and N. Samardzija. Low order empirical modeling for nonlinear systems. In *IFAC Symposium on Advanced Control of Chemical Processes*, Kyoto, Japan, 1994.

[76] B. R. Maner, F. J. Doyle III, B. A. Ogunnaike, and R. K. Pearson. A nonlinear model predictive control scheme using second order Volterra models. In *Proc. American Control Conf.*, pages 3253–3257, Baltimore, MD, 1994.

[77] R. K. Pearson. Selecting nonlinear model structures for computer control. *J. Proc. Cont.*, 13:1–26, 2003.

[78] J. A. Florian Jr., J. L. Eiseman, and R. S. Parker. Approximating cancer tumor growth dynamics using cell-cycle models in series. In *AIChE Annual Meeting*, paper 439ab, San Francisco, CA, 2003.

[79] J. A. Florian Jr., J. L. Eiseman, and R. S. Parker. A population balance model of cell cycle-specific tumor growth. In *Proc. 2005 IFAC World Congress*, volume (accepted), Prague, Czech Republic, 2005.

[80] J. A. Florian Jr., J. L. Eiseman, and R. S. Parker. Modeling quiescent cells in tumor growth and cancer treatment. In *Proc. Foundations of Systems Biology in Engineering*, volume (submitted), Santa Barbara, CA, 2005.

[81] P. A. Andreasen, L. Kjøller, L. Christensen, and M. J. Duffy. The urokinase–type plasminogen activator system in cancer metastasis: A review. *Int. J. Cancer*, 72:1–22, 1997.

[82] A. A. Adjei and M. Hidalgo. Intracellular signal transduction pathway proteins as targets for cancer chemotherapy. *J. Clin. Oncol.*, 23(23):1–18, 2005.

[83] S. J. Cohen, R. B. Cohen, and N. J. Meropol. Targeting signal transduction pathways in colorectal cancer—more than skin deep. *J. Clin. Oncol.*, 23(23), 2005.

[84] I. M. Ghobrial, T. E. Witzig, and A. A. Adjei. Targeting apoptosis pathways in cancer therapy. *CA Cancer J. Clin.*, 55:178–194, 2005.

[85] I.-K. Hong, Y.-M. Kim, D.-I. Jeoung, K.-C. Kim, and H. Lee. Tetraspanin cd9 induces mmp-2 expression by activating p38 MAPK, JNK and c-Jun pathways in human melanoma cells. *Exp. Mol. Med.*, 37(3):230–239, 2005.

[86] E. F. Petricoin III, V. E. Bichsel, V. S. Calvert, V. Espina, M. Winters, L. Young, C. Belluco, B. J. Trok, M. Lippman, D. A. Fishman, D. C. Sgroi, P. J. Munson, L. J.

Esserman, and L. A. Liotta. Mapping molecular networks using proteomics: A vision for patient–tailored combination therapy. *J. Clin. Oncol.*, 23(15):3614–3621, 2005.

[87] L. G. Wang, X. M. Liu, W. Kreis, and D. R. Budman. The effect of antimicrotubule agents on signal transduction pathways of apoptosis: a review. *Cancer Chemoth. Pharm.*, 44:355–361.

[88] E.B. Haura, W. D. Cress, S. Chellappan, Z. Zheng, and G. Belper. Antiapoptotic signaling pathways in non-small-cell lung cancer: biology and therapeutic strategies. *Clin Lung Cancer*, 6(2):113–122, Sep 2004.

[89] A. U. Buzdar, S. E. Singletary, R. L. Theriault, and D. J. Prospective evaluation of paclitaxel versus combination chemotherapy with fluorouracil, doxorubicin and cyclophosphamide as neoadjuvant therapy in patients with operable breast cancer. *J. Clin. Oncol.*, 17(11):3412–3417, 1999.

[90] J. R. Rigas. Taxane–platinum combinations in advanced non–small cell lung cancer: A review. *The Oncologist*, 9(suppl 2):16–23, 2004.

[91] J. D. Winegarden, A. M. Mauer, G. A. Otterson, C. M. Rudin, M. A. Villalona-Calero, V. J. Lanzotti2, L. Szeto1, K. Kasza1, P. C. Hoffman1, and E. E. Vokes1. A phase ii study of oxaliplatin and paclitaxel in patients with advanced non-small-cell lung cancer. *Ann. of Oncol.*, 15:915–920, 2004.

[92] J. Han, D. H. Lee, H. Y. Kim, E. Kim, J. J. Lee, S. Y. Ju, E. H. Shin, and J. S. Lee. A phase II study of weekly irinotecan and capecitabine in patients with previously treated non-small cell lung cancer. *Clin. Cancer Res.*, 9:5909–5914, 2003.

[93] A. M. Mauer, R. H. Ansari, P. C. Hoffman, S. A. Krauss, D. Taber, S. A. Tembe, G. T. Gabrys, T. Cotter, L. P. Schumm, L. Szeto, and E. E. Vokes. Phase I/II investigation of paclitaxel, ifosfamide and carboplatin. *Ann. Oncol.*, 14:722–728, 2003.

[94] L. Loni, F. De Braud, P. L. Zinzani, and R. Danesi. Pharmacogenetics and proteomics of anticancer drugs in non-hodgkin's lymphoma. *Leuk Lymphoma*, 44(Suppl3):S115–122, 2003.

[95] L. L. Jung, R. K. Ramanathan, M. J. Egorin, R. Jin, C. P. Belani, D. M. Potter, S. Strychor, D. L. Trump, C. Walko, M. Fakih, and W. C. Zamboni. Pharmacokinetic

studies of 9-nitrocamptothecin on intermittent and continuous schedules of administration in patients with solid tumors. *Cancer Chemoth. Pharm.*, 54(6):487–96, 2004.

[96] National Research Council, editor. *Guide for the Care and Use of Laboratory Animals*. Institute of Laboratory Animal Resources Commission on Life Sciences. National Academy Press, Washington, D.C., 1996.